SCREENING OF THAI MEDICINAL PLANTS AS POTENTIAL ANTI-SARS-COV-2 AGENTS AND STUDY OF MECHANISM OF ACTION BY REVEALING THE CHANGES OF BIOMOLECULAR PROFILE IN INFECTED CELL LINES

BUSSAYARAT MAIKHUNTHOD

A Thesis Submitted in Partial Fulfillment of the Requirements for the Degree of Doctor of Philosophy in Biotechnology
Suranaree University of Technology
Academic Year 2024

การคัดเลือกสมุนไพรไทยเพื่อเป็นสารต้านเชื้อไวรัสโคโรนา SARS-CoV-2 และศึกษากลไกการออกฤทธิ์โดยติดตามการเปลี่ยนแปลงของสารชีวโมเลกุลในเซลล์ไลน์

นางสาวบุษยารัตน์ ไมขุนทด

วิทยานิพนธ์นี้เป็นส่วนหนึ่งของการศึกษาตามหลักสูตรปริญญาวิทยาศาสตรดุษฎีบัณฑิต
สาขาวิชาเทคโนโลยีชีวภาพ
มหาวิทยาลัยเทคโนโลยีสุรนารี
ปีการศึกษา 2567

SCREENING OF THAI MEDICINAL PLANTS AS POTENTIAL ANTI-SARS-COV-2 AGENTS AND STUDY OF MECHANISM OF ACTION BY REVEALING THE CHANGES OF BIOMOLECULAR PROFILE IN INFECTED CELL LINES

Suranaree University of Technology has approved this thesis submitted in partial fulfillment of the requirements for the Degree of Doctor of Philosophy.

Thesis Examining Committee

Y. Teethaisong
.....
(Dr. Yothin Teethaisong)
Chairperson

N. Tm
.....
(Prof. Dr. Neung Teaumroong)
Member (Thesis Advisor)

Gr. Eumkeb
.....
(Prof. Dr. Griangsak Eumkeb)
Member (Thesis Co-Advisor)

.....
(Assoc. Prof. Dr. Panlada Tittabutr)
Member

.....
(Asst. Prof. Dr. Pakpoom Boonchuen)
Member

Yupaporn Rukt
.....
(Assoc. Prof. Dr. Yupaporn Ruksakulpiwat)
Vice Rector for Academic Affairs
and Quality Assurance

N. Tm
.....
(Prof. Dr. Neung Teaumroong)
Dean of Institute of Agricultural
Technology

บุษยารัตน์ ไมขุนทด : การคัดเลือกสมุนไพรไทยเพื่อเป็นสารเชื้อไวรัสโคโรนา SARS-CoV-2 และศึกษากลไกการออกฤทธิ์โดยการติดตามการเปลี่ยนแปลงของสารชีวโมเลกุลในเซลล์ไลน์ (SCREENING OF THAI MEDICINAL PLANTS AS POTENTIAL ANTI-SARS-COV-2 AGENTS AND STUDY OF MECHANISM OF ACTION BY REVEALING THE CHANGES OF BIOMOLECULAR PROFILE IN INFECTED CELL LINES) อาจารย์ที่ปรึกษา : ศาสตราจารย์ ดร.หนึ่ง เตียอำรุง, 139 หน้า.

คำสำคัญ: สมุนไพร/Anti-SARS-CoV-2/LC-HRMS/Molecular docking/FTIR/หม่อน/กลไกการต้านไวรัส/โรคโควิด 19

การค้นหาสารต้านไวรัสที่มีประสิทธิภาพในการยับยั้งไวรัส SARS-CoV-2 ที่ก่อโรคโควิด 19 ยังคงเป็นสิ่งสำคัญที่ต้องศึกษา โดยเฉพาะสำหรับการมองหาการรักษาแบบทางเลือก หรือเพื่อเสริมกับการใช้ยาแผนปัจจุบัน เนื่องจากยาต้านไวรัสที่ใช้ปัจจุบันมีราคาแพงและยังไม่มียาหรือวิธีรักษาที่จำเพาะต่อไวรัสชนิดนี้ งานวิจัยนี้ได้คัดกรองพืชสมุนไพรไทย 19 ชนิดเพื่อศึกษาฤทธิ์ต้านไวรัส SARS-CoV-2 ด้วยการทดสอบความสามารถในการต้านไวรัสในระดับหลอดทดลอง พบว่าสารสกัดที่แสดงประสิทธิภาพสูงที่สุดในการต้านไวรัส SARS-CoV-2 คือ สารสกัดจากใบหม่อน (*Morus alba*) ซึ่งเป็นสารสกัดส่วนที่ละลายน้ำที่ได้จากวิธีการแยกส่วนด้วยตัวทำละลายต่างขั้ว คือ การใช้ Ethyl Acetate ร่วมกับน้ำ (WF-EtAct) จากการวิเคราะห์องค์ประกอบทางเคมีของ WF-EtAct ด้วยเทคนิค Liquid Chromatography-High Resolution Mass Spectrometry พบว่า WF-EtAct อุดมไปด้วยสารกลุ่มโพลีฟีนอลิก ได้แก่ กรดคลอโรจีนิก และไกลโคไซด์ของฟลาโวนอยด์ เช่น Rutin Isoquercitrin และ Astragalin เป็นต้น จากนั้นทำการประเมินปฏิสัมพันธ์การจับของสารเหล่านี้กับเอนไซม์ Main Protease (Mpro) ของไวรัส SARS-CoV-2 ด้วยวิธีจำลองการจับกันของโมเลกุล (Molecular Docking) เพื่อทำนายศักยภาพการต้านไวรัสจากกลไกการขัดขวางการทำงานของ Mpro ทั้งนี้พบสารหลายชนิดมีแนวโน้มการจับตัวที่ดี โดยเฉพาะ Myricetin 3-O-β-D-galactopyranoside ซึ่งมีค่าพลังงานการจับตัวสูงสุด (-9.6 kcal/mol) แสดงถึงแนวโน้มที่อาจมีประสิทธิภาพสูงกว่ายาต้านไวรัสโมลนูพิราเวียร์ (-6.21 kcal/mol)

เพื่อทำให้กระบวนการสกัดง่ายขึ้นและลดการใช้สารเคมีอันตราย ได้ทำการปรับปรุงกระบวนการสกัด โดยใช้น้ำเพียงอย่างเดียวในขั้นตอนการแยกส่วนสารสกัดหยาบใบหม่อนด้วยตัวทำละลายต่างขั้ว (WF-W) โดยจากการวิเคราะห์องค์ประกอบทางเคมียืนยันว่า WF-W มีองค์ประกอบทางเคมีที่คล้ายกับ WF-EtAct พร้อมกับมีค่าความเป็นพิษระดับเซลล์ต่ำ ซึ่งบ่งบอกด้วยค่าความเข้มข้นของสารที่ทำให้เซลล์มีชีวิตรอด 50% (CC_{50}) ที่ค่าความเข้มข้นสารสกัดสูงกว่า 500 µg/mL และยังคงมีฤทธิ์ต้านไวรัสสูง โดยเมื่อทดสอบ WF-W ที่ความเข้มข้น 100 µg/mL ทั้งในรูปแบบการยับยั้งไวรัส

ก่อนเข้ารุกรานเซลล์เจ้าบ้าน (Pre-entry mode) และการยับยั้งไวรัสหลังจากการติดเชื้อของเซลล์เจ้าบ้าน (Post-infection mode) พบว่ามีประสิทธิภาพการยับยั้งไวรัสสูงถึง 99.6% (Log Reduction Value เท่ากับ 2.448) โดยมีประสิทธิภาพดีกว่าโมลนูพิราเวียร์และ Rutin ในแบบ Pre-entry mode ซึ่งแสดงด้วยค่าความเข้มข้นของสารสกัดที่ยับยั้งการทำงานของไวรัสได้ 50% (IC_{50}) ของ WF-W เพียง 0.0011 µg/mL อย่างไรก็ตาม ผลการทดสอบการยับยั้งไวรัสในแบบ Post-infection mode พบว่า ค่า IC_{50} ของ WF-W สูงกว่ายาโมลนูพิราเวียร์ และ Rutin โดยลักษณะกราฟความสัมพันธ์ระหว่างความเข้มข้นของสารสกัดกับความสามารถในการต้านไวรัสแสดงให้เห็นว่า ที่ระดับความเข้มข้นของ WF-W ต่ำกว่า 1 µg/mL มีแนวโน้มการลดลงของประสิทธิภาพการต้านไวรัสของ WF-W เกิดขึ้นเร็วกว่าการใช้ยาโมลนูพิราเวียร์ และ Rutin นอกจากนี้เมื่อทำการศึกษากลไกการออกฤทธิ์ด้วยเทคนิค Synchrotron Radiation-Fourier Transform Infrared Microspectroscopy พบการเพิ่มขึ้นของปริมาณสารกลุ่มไขมันอย่างชัดเจน โดยเฉพาะในส่วนของหมู่ฟังก์ชัน C=O ของ Lipid head ในเซลล์เจ้าบ้าน Calu-3 ที่มีการติดเชื้อไวรัส SARS-CoV-2 แต่เมื่อภายหลังเซลล์เจ้าบ้านได้รับสารสกัด WF-W พบการลดลงในส่วน C=O นี้อย่างมีนัยสำคัญ ในขณะที่การเปลี่ยนแปลงของปริมาณสารกลุ่มโปรตีนเป็นไปในทางตรงกันข้าม ซึ่งจากการที่องค์ประกอบของ WF-W อุดมไปด้วยสารฟลาโวนอยด์ ผลการศึกษานี้ชี้ให้เห็นว่าสารสกัดใบหม่อน WF-W อาจมีบทบาทสำคัญต่อเซลล์เจ้าบ้าน ทั้งในการควบคุมเมแทบอลิซึมในระหว่างการติดเชื้อไวรัส SARS-CoV-2 และการกระตุ้นภูมิคุ้มกันซึ่งอาจช่วยในการเตรียมความพร้อมของเซลล์เพื่อต้านการติดเชื้อไวรัสในอนาคต แสดงถึงศักยภาพของการใช้สารสกัดทั้งในเชิงการป้องกันและการรักษา อย่างไรก็ตามการวิจัยในอนาคตควรมุ่งเน้นไปที่การวิเคราะห์กลไกการต้านไวรัส SARS-CoV-2 ในระดับยีน (Transcriptomics) เพื่อเข้าใจกลไกเชิงลึกให้มากขึ้น รวมถึงการศึกษาในสัตว์ทดลองและมนุษย์เพื่อประเมินศักยภาพทางคลินิกสำหรับการรักษาและป้องกันโรคโควิด 19 ต่อไป

สาขาวิชาเทคโนโลยีชีวภาพ
ปีการศึกษา 2567

ลายมือชื่อนักศึกษา _____
ลายมือชื่ออาจารย์ที่ปรึกษา _____
ลายมือชื่ออาจารย์ที่ปรึกษาร่วม _____

BUSSAYARAT MAIKHUNTHOD : SCREENING OF THAI MEDICINAL PLANTS AS POTENTIAL ANTI-SARS-COV-2 AGENTS AND STUDY OF MECHANISM OF ACTION BY REVEALING THE CHANGES OF BIOMOLECULAR PROFILE IN INFECTED CELL LINES. THESIS ADVISOR : PROF. NEUNG TEAUMROONG, Ph.D. 139 PP.

Keyword: Herb/Anti-SARS-CoV-2/LC-HRMS/Molecular docking/FTIR/Mulberry/Antiviral mechanism/COVID-19

The search for effective antiviral compounds capable of inhibiting SARS-CoV-2, the causative agent of COVID-19 disease, remains a crucial area of study, particularly for alternative treatments or as adjuncts to conventional therapies. This need arises from the high cost of currently available antiviral drugs and the lack of specific medications or definitive treatments for this virus. This study screened 19 Thai medicinal plants for antiviral activity against SARS-CoV-2 using *in vitro* assays. Among them, the water-soluble fraction obtained from the liquid-liquid fractionation of mulberry (*Morus alba*) leaf crude extract using ethyl acetate and water (WF-EtAct) showed the highest efficacy. Chemical composition analysis using Liquid Chromatography-High Resolution Mass Spectrometry revealed that WF-EtAct is rich in polyphenolic compounds, including chlorogenic acids and flavonoid glycosides, such as rutin, isoquercitrin and astragalin. Molecular docking was used to evaluate the binding interactions of these compounds with the SARS-CoV-2 main protease (Mpro) to predict their potential as Mpro inhibitors. Several compounds showed promising binding, with myricetin 3-O-β-D-galactopyranoside exhibiting the strongest affinity (-9.6 kcal/mol), suggesting greater efficacy than molnupiravir (-6.21 kcal/mol).

To simplify the extraction and reduce hazardous chemical use, the ethyl acetate–water fractionation of mulberry crude extract was modified using only water, yielding a modified water-soluble fraction (WF-W). Chemical composition analysis of WF-W confirmed that WF-W retained a similar chemical profile to the WF-EtAct while exhibiting low cytotoxicity, with a 50% cytotoxic concentration (CC_{50}) greater than 500 µg/mL. WF-W demonstrated enhanced antiviral activity, achieving a 99.6% viral reduction (Log Reduction Value = 2.448) at 100 µg/mL in both pre-entry and post-infection modes. In the pre-entry mode, WF-W exhibited the lowest half-maximal

inhibitory concentration (IC_{50}) of 0.0011 µg/mL, outperforming both molnupiravir and rutin. In contrast, WF-W showed a higher IC_{50} than molnupiravir and rutin in the post-infection mode. The antiviral dose-response curve in post-infection mode revealed that WF-W efficacy decreased more rapidly than molnupiravir and rutin at concentrations below 1 µg/mL. Mechanistic studies using Synchrotron Radiation-FTIR on SARS-CoV-2-infected Calu-3 host cells revealed significant changes in biomolecular composition, particularly an increase in lipid content, especially in the C=O functional group of lipid heads. Upon treatment with WF-W extract, a significant reduction in this C=O lipid component was observed. Conversely, protein content changes showed an opposite trend. Given its flavonoid-rich composition, WF-W of mulberry leaf extract may play a critical role in regulating metabolism during SARS-CoV-2 infection and stimulating host immune responses, potentially enhancing cellular defense against future infection. This highlights its potential for both preventive and therapeutic use. Future research should focus on investigating the antiviral mechanisms against SARS-CoV-2 at the gene level (Transcriptomics) for a deeper understanding, as well as conducting studies in animal models and humans to assess its clinical potential for the treatment and prevention of COVID-19.

School of Biotechnology
Academic Year 2024

Student's Signature B. Main
Advisor's Signature N. T W
Co-advisor's Signature G. Eumkeb

ACKNOWLEDGEMENT

I would like to express my heartfelt gratitude to all those who contributed to the success of this research. First and foremost, I extend my sincere appreciation to Suranaree University of Technology Scholarship (OROG), the Synchrotron Light Research Institute (Public Organization), and the National Research Council of Thailand (NTRC) for their financial support, which made this study possible. I am deeply grateful to the local farms that kindly provided the medicinal herbs used in this study. Their invaluable support greatly facilitated the research process.

I would like to extend my profound appreciation to my advisor, Prof. Dr. Neung Teaumroong, and his team for their invaluable guidance, support, and encouragement throughout this research. A special thanks to Assoc. Prof. Dr. Panlada Tittabutr and Asst. Prof. Dr. Pakpoom Boonchuen for their unwavering assistance and expertise. My sincere gratitude also goes to my co-advisor, Prof. Dr. Kraingsak Eumkeb, for his constructive feedback. Special thanks are also extended to Assoc. Prof. Dr. Santi Watthana (Suranaree University of Technology) for his expertise in plant identification.

I would also like to extend my sincere appreciation to Assoc. Prof. Dr. Pornsawan Leaungwutiwong and her research team from the Faculty of Tropical Medicine, Mahidol University, for their substantial collaboration in the antiviral activity experiments, which significantly contributed to this study.

A special acknowledgment goes to my incredible colleagues, Dr. Waraporn Tanthanuch and Dr. Sukanya Tastub, who have been more than colleagues—they have been like sisters, offering unwavering scientific support as well as emotional and mental encouragement. Their companionship and encouragement have made this journey both enriching and fulfilling.

Lastly, I am profoundly thankful to my beloved family for their endless love, patience, and support. Their unwavering belief in me has been my greatest motivation throughout this journey. Thank you all for being a part of this endeavor.

Bussayarat Maikhunthod

CONTENTS

Page

CONTENTS (Continued)

Page

CONTENTS (Continued)

Page

CONTENTS (Continued)

Page

CONTENTS (Continued)

Page

LIST OF TABLES

Table **Page**

LIST OF TABLES (Continued)

Table **Page**

LIST OF FIGURES

Figure **Page**

LIST OF FIGURES (Continued)

Figures **Page**

LIST OF FIGURES (Continued)

Page

LIST OF ABBREVIATIONS

ACE2	=	Angiotensin-Converting Enzyme II
CC	=	Column Chromatography
CC_{50}	=	50% Cytotoxic Concentration
CE	=	Ethanolic-Aqueous Crude Extract
COVID-19	=	A Novel Coronavirus Disease-2019
EF	=	Ethyl Acetate Fraction of Ethanolic-Aqueous Crude Extract
IC_{50}	=	Inhibitory Concentration of 50%
LC-HRMS	=	Liquid Chromatography-High Resolution Mass Spectrometer
LRV	=	Log Reduction Value
MNTC	=	Maximum Non-Cytotoxic Concentration
Mpro	=	Main Protease of SARS-CoV-2
MTT Assay	=	3,4,5-dimethylthiazol-2-yl)-2,5-diphenyltetrazolium bromide Assay
PEDV	=	Porcine Epidemic Diarrhea Virus
PLpro	=	Papain-like Proteinase
RdRp	=	RNA-dependent RNA Polymerase
SARS-CoV-2	=	Severe Acute Respiratory Syndrome Coronavirus 2
SR-FTIR	=	Synchrotron-Fourier Transform Infrared Microspectroscopy
TCID50	=	50% Tissue Culture Infective Dose
TFC	=	Total Flavonoid Content
TPC	=	Total Phenolic Content
WF	=	Water Fraction of Ethanolic-Aqueous Crude Extract
WF-MLCE	=	Water Fraction of Mulberry Leaf Crude Extract
3CLpro	=	3-Chymotrypsin-like Protease
µg/mL	=	Microgram per milliliter

CHAPTER I

INTRODUCTION

1.1 Significance of Study

The outbreak of severe acute respiratory syndrome coronavirus 2 (SARS-CoV-2) started emerging in December 2019, particularly in China, spreading rapidly worldwide. Since February 2020, the total of reported cases of coronavirus disease 2019 (COVID-19) was more than 777 million cases and over 7.1 million deaths, worldwide. In Thailand, the total number of confirmed cases as of now is 4.8 million, with 34,741 deaths(WHO, 2025b). SARS-CoV-2 infection can affect persons of all ages and genders, and has a substantial impact on both human health and emotional well-being (Zhu et al., 2020). COVID-19 disease symptoms are unspecific, a wide range of manifestations of clinical symptoms can be ranging from asymptomatic infection to severe pneumonia and death. Currently, there is no specific antiviral treatment (Huang et al., 2020; Paltiel et al., 2021). Several antiviral drugs that have previously been successful in inhibiting the SARS virus, such as malaria treatments (chloroquine) or HIV treatments (lopinavir/ritonavir) (Greenblatt et al., 2023), have been repurposed for COVID-19 remedy alongside influenza medications (oseltamivir), favipiravir and molnupiravir (Raghav et al., 2023). However, the application of these antiviral drugs has shown effective with high doses, which has most likely been associated with several side effects, especially for people in vulnerable groups. The side effects could be varied from nausea, vomiting, possibly affecting blood sugar levels when taken with certain drugs, impairment of liver function, and even potentially causing fetal abnormalities if taken during the first trimester of pregnancy, as well as drug resistance (Bangkokbiznews, 2022; NIH, 2022; Orhan & Senol Deniz, 2020; Şimşek Yavuz & Ünal, 2020). Furthermore, the drugs are costly, and during the pandemic, their limited supply created challenges in treatment accessibility for numerous patients. For patients with mild symptoms, treatment methods are similar to those for the common cold, involving symptom-based medications and the use of multiple drugs together, such as decongestants and expectorants (Rodrigues et al., 2022).

Although the infection rate has significantly decreased, there remains a necessity for monitoring and preventing potential outbreaks that may arise from the mutation of the virus. Despite the rapid development of vaccines, they do not provide a fully guaranteed efficacy, and reinfections can occur in previously infected individuals. The causes could be the mutation of the virus itself and the host-immune responsive characteristics (Nainu et al., 2020; Paltiel et al., 2021). Host immune response heavily influences the individual's COVID-19 symptoms and severity (Rabaan et al., 2021). Especially in vulnerable groups, such as pregnant women, the irregulated immunological responses almost definitely cause severe systematic damage due to the overproduction of cytokines (cytokine storm) and chemokines caused by the hyperactivation of inflammatory and immune responses following the infection (Whitehead & Walker, 2020). Hence, further research on developing a vaccination that can elicit a strong immune response and the search for alternative complementary medical treatments to support the COVID-19 remedy should still continue.

Herbal metabolites have made significant contributions to health and medicine, including fewer side effects, low potential to cause resistance, affordability, and a broad spectrum of pharmacological activities which include immune boosting, anti-inflammatory, antiviral, antibacterial, and anticancer properties. That is why research on herbal-based drugs has consistently held a pivotal position in the advancement of natural pharmaceutical development for a wide range of diseases (El Gizawy et al., 2021; Soltane et al., 2021). Certainly, to control this novel coronavirus, natural antiviral candidates have also been preferentially projected as the plausible potential anti-SARS-CoV-2, both as in the sole application (Kim, 2021; Nair et al., 2021; Nie et al., 2021; Orege et al., 2023) and in combination with western medicine (Ni et al., 2020). The researchers have purposed not only to use these alternative candidates as antiviral or virucidal agents but also to benefit from their other pharmacological properties in preventing the aggravation and serious complications in COVID-19 patients. There are several studies of various Thai herbs that showed the significance battling SARS-CoV-2 virus, such as crude extracts of *Andrographis paniculata* (Sa-ngiamsuntorn et al., 2021), and *Boesenbergia rotunda* (Kanjanasirirat et al., 2020). Despite extensive global research into effective natural extracts or compounds, to the best of our knowledge, the clinical evidence of such

candidates, both in terms of safety and effectiveness specific to COVID-19 therapy, including the study of their insight into antiviral mechanisms, is still limited. On top of that, since Thailand is well-known as one of the countries that wealth in medicinal plants and herbal medicine recipes, thus there is still a potential space to research more herbal extracts/compounds in tackling this unique coronavirus.

In this study, 19 accessible Thai medicinal plants having antiviral characteristics or that have been used in fever or flu treatment were chosen for investigation. These selected plants have never been examined for anti-SARS-CoV-2 effectiveness (or have been studied with limited information). The study was designed to test these plant extracts for antiviral potential using *in vitro* antiviral activity assays in two approaches, i.e., virucidal efficacy and viral inhibition efficacy following the infection. The most promising extracts were further insight examined for their potential antiviral lead compounds. The *in silico* molecular docking of those tentative lead compounds was also analyzed against the main protease protein of SARS-CoV-2 as the target for viral inhibition. The possible mechanisms of the promising extract in viral inhibition were also revealed by observing the biomolecular changes of the studied cell lines after the infection and once treatment with selected extract following the infection, using the Synchrotron Fourier Transform infrared microspectroscopy (SR-FTIR) technique. This study is not only useful for COVID-19 emergence, but the finding could also potentially benefit future responses to emerging infectious diseases.

1.2 Research objectives

The objective of this research was to discover potential Thai medicinal herbs that could serve as natural inhibitors of SARS-CoV-2, using an *in vitro* antiviral test as a bioassay guide. The phytochemical contents of the most promising herbal extract (the selected candidate) were further studied in order to discover the antiviral lead components. These compounds were then analyzed for interaction with the SARS-CoV-2 target protein. The mechanism of action of the chosen candidate in viral inhibition was also studied.

The specific objectives of this study were:

1. To screen for the natural antiviral candidates from nineteen accessible Thai medicinal plants using an *in vitro* antiviral test as a bioassay guide.

2. To identify the tentative chemical constituents of the extract exhibiting the most effective antiviral efficacy using a liquid chromatography-high resolution mass spectrometer and to further evaluate their potential in leading SARS-CoV-2 inhibition through *in silico* molecular docking against the main protease protein of SARS-CoV-2.

3. To simplify the herbal extraction method in order to produce a streamlined and chemically safer methodology, in conjunction with the cytotoxicity and anti-SARS-CoV-2 efficacy using human epithelial lung cells (Calu-3) as host cells.

4. To study the *in vitro* anti-SARS-CoV-2 mechanism of the most potent extract using Calu-3 as host cells by monitoring the biomolecular changes during extract treatment following SARS-CoV-2 infection using the SR-FTIR technique.

1.3 Hypothesis

This study hypothesized that the selected superior herbal extract would demonstrate comparable or greater anti-SARS-CoV-2 efficacy to the repurposed drug (molnupiravir) and the single standard compound (one of the major lead compounds found in the selected herbal extract).

1.4 Scope of the Study

The concept of this research was to explore Thai herbal extracts which demonstrated the strong potency in anti-SARS-CoV-2 efficacy using an antiviral test as the bioassay guide. The study comprised two primary components. Initially, a screening approach was employed with Vero cells as the host cells for antiviral assays. This led to the selection of the most powerful herbal extract and the identification of possible lead phytochemicals in SARS-CoV-2 suppression. Second, the extraction method of the selected herb underwent modification to produce a more streamlined and chemically safer methodology, in conjunction with the assessment of its cytotoxicity and capacity to combat SARS-CoV-2, employing human epithelial lung cells (Calu-3) as the host cells. Subsequently, this herbal extract's antiviral mechanism against SARS-CoV-2 was assessed. The schematic diagram of the study's scope is provided in **Figure 1**.

In phase 1, owing to the containment capabilities of biosafety level 3 (BSL3) facilities, the antiviral efficacies of the ethanolic-aqueous crude extract (CE) from 19

selected plants were evaluated against the porcine epidemic diarrhea virus (PEDV) as a surrogate, utilizing a plaque reduction assay. It is noteworthy that SARS-CoV-2 and PEDV are both members of the genus *Alphacoronavirus* in the Coronaviridae family, sharing a similar structure. Consequently, utilizing PEDV as a surrogate will provide substantial reliability when translating experimental results (Lin et al., 2022; Singh et al., 2021; Song et al., 2016; Su et al., 2021). Together with cytotoxicity assays, CEs demonstrating ≥70% anti-PEDV efficacy were then tested for their anti-SARS-CoV-2 activity in the Vero cells using a 50% tissue culture infectious dose (TCID50) method, based on pre-entry and post-infection modes. To enhance antiviral efficacy, the potential anti-SARS-CoV-2 crude extracts underwent a liquid-liquid fractionation to obtain their water-fractions (WF) and ethyl acetate-fractions (EF), which were subsequently evaluated for anti-SARS-CoV-2 activities. The extract fraction exhibiting the most significant antiviral efficacy was analyzed for its tentative constituent compounds using liquid chromatography-high resolution mass spectrometry (LC-HRMS). It is worth mentioning that column chromatography (CC) was used to partially separate the chosen WF or EF into various fractions prior to the LC-HRMS, in an attempt to oversimplify the LC column separation. This led to more accurate chemical identification. The tentatively identified compounds were further evaluated through *in silico* molecular docking against the SARS-CoV-2 main protease protein (Mpro) to elucidate potentially effective antiviral lead compounds.

Based on the findings from the first phase of the study, the water fraction of mulberry leaf crude extract (WF-MLCE) demonstrated the highest antiviral efficacy. This suggested that the water-soluble phytoconstituents of mulberry leaves played an important role in combating SARS-CoV-2. In phase 2 of the research, extraction modification was first carried out based on the method from phase 1 with minor alterations, mostly for the purpose of enriching water-soluble compounds. This resulted in three water-soluble mulberry leaf extracts, as shown in **Figure 2**. The three extracts were originally screened for total phenolic content (TPC), total flavonoid content (TFC), and FTIR spectral profile prior to testing for cytotoxicity and anti-SARS-CoV-2 efficacies using Calu-3 as host cells. The extract that showed the highest antiviral efficacy was then investigated for its mechanism of action against SARS-CoV-2 in post-infection mode. The SR-FTIR was utilized to track the biomolecular changes in Calu-3 after treatment with the selected mulberry leaf extract following SARS-CoV-2 infection.

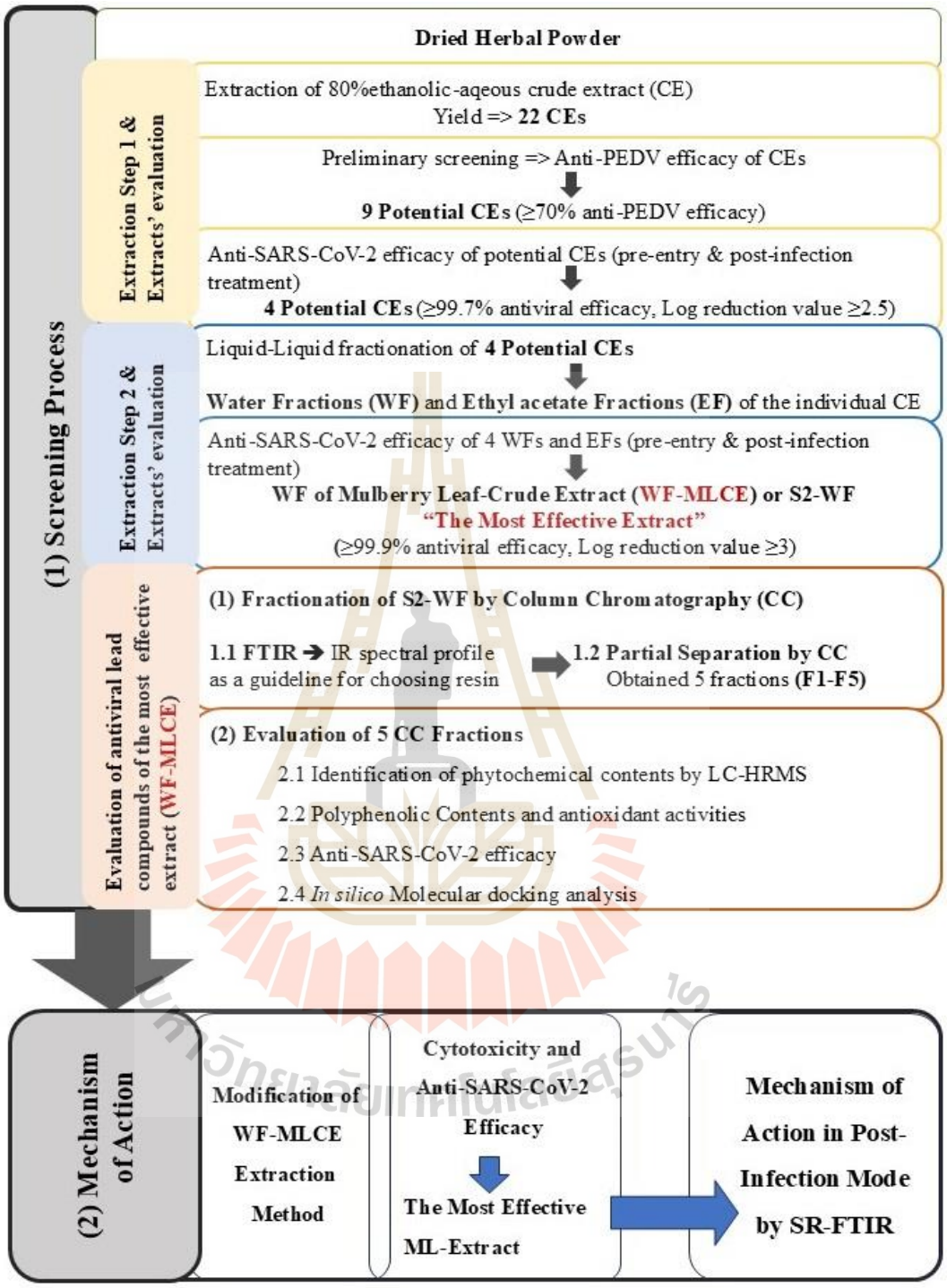

Figure 1 A Schematic diagram of an overall scope of study.

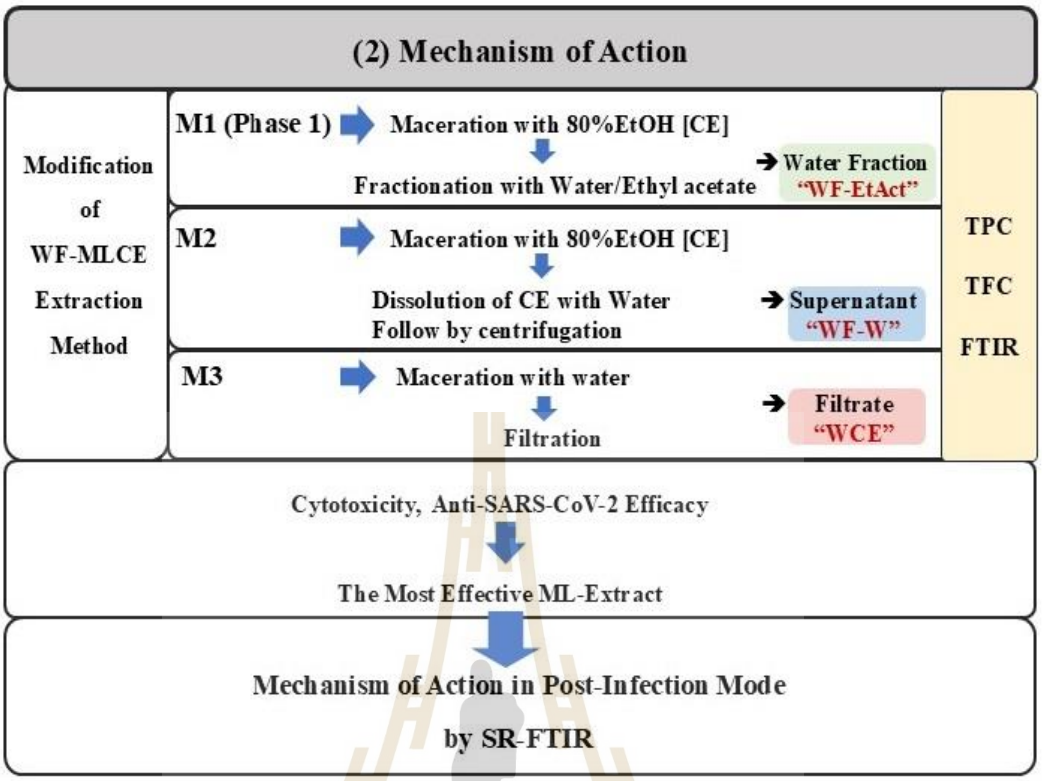

Figure 2 The schematic representation of an expanded overview of the study scope in phase 2.

CHAPTER II

LITERATURE REVIEWS

2.1 The Outbreak of COVID-19

The coronavirus disease 2019 (COVID-19) pandemic is a global outbreak of a new strain of coronavirus called severe acute respiratory syndrome coronavirus 2 (SARS-CoV-2). Cases of novel coronavirus (nCoV) were first found in China in December 2019. The virus swiftly spread to other countries across the world, with a large number of severe cases and deaths, forcing the People's Republic of China to close down the city and later the country. This prompted the World Health Organization (WHO) to declare a Public Health Emergency of International Concern (PHEIC) on January 30, 2020, and classify the epidemic as a pandemic on March 11, 2020. In Thailand, the first case of SARS-CoV-2 infection was reported on January 31, 2020 (WHO, 2025a). Over four years since the pandemic, the world cumulative number of reported cases, as of January 5, 2025, is more than 777 million cases and 7.1 million deaths. In Thailand, there are currently 4.8 million cumulative cases and 34,741 deaths, as shown in **Figure 3.**

Person-to-person transmission can occur by droplet or contact transmission, similar to flu. In addition, if there is a lack of severe infection control or sufficient personal protective equipment, first-line healthcare workers may be put at risk. COVID-19 has a mean incubation period of ~5 days, but it can range from 2 to 14 days. Symptoms frequently start with nonspecific symptoms, such as fever, dry cough, and fatigue. Multiple systems may be affected, including respiratory (cough, shortness of breath, sore throat, rhinorrhea, hemoptysis, and chest discomfort), gastrointestinal (diarrhea, nausea, and vomiting), musculoskeletal (muscle aching), and neurological (headache or disorientation). More common signs and symptoms include fever (83%-98%), cough (76%-82%), and shortness of breath (31%-55%). Those with complications may have signs in both lungs on chest X-ray, which can lead to pneumonia, renal failure, and death from severe infection. The severity of COVID-19 varies greatly among individuals. Factors influencing disease severity

include age, underlying health conditions, and the strength of the host immune response. According to the WHO, the global fatality rate from Covid-19 is expected to be around 3.4%. However, the mortality rate of Covid-19 will be higher in particular populations with concomitant conditions including cancer (5.6%), hypertension (6.0%), chronic respiratory disease (6.3%), diabetes (7.3%), and cardiovascular disease (CVD) (10.5%). Currently, there is no definitive therapy for COVID-19, while various medications are still under investigation (Amirfakhryan & safari, 2021; Wu et al., 2020).

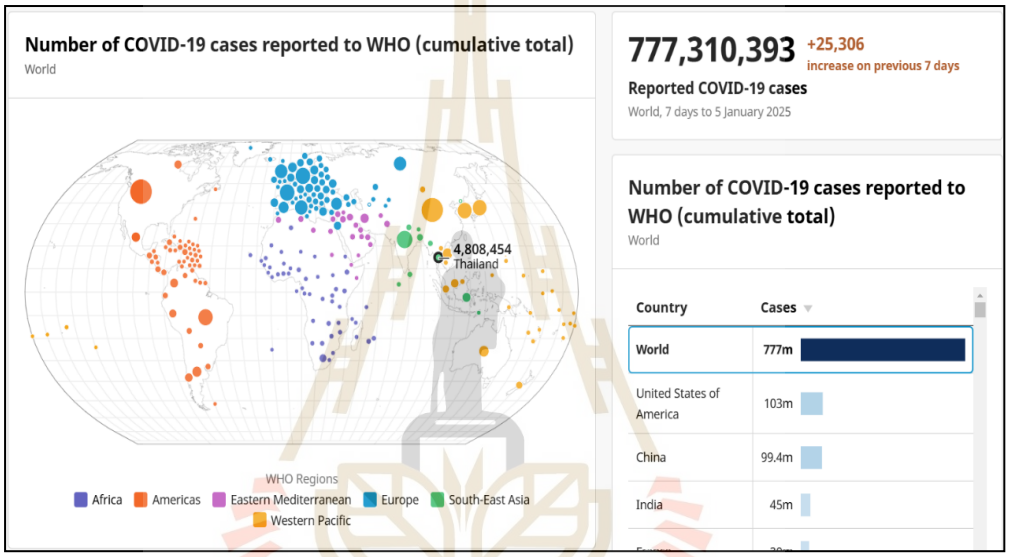

Figure 3 Number of cumulative confirmed case classified by WHO on January 5th, 2025 (WHO, 2025a).

2.2 Overview of SARS-CoV-2

Coronaviruses (family Coronaviridae) are common pathogens of humans and animals. The subfamily Coronavirinae has been divided into four genera based on genetic clustering and antigenicity: alpha, beta, gamma, and delta coronaviruses. The pandemic of COVID-19 disease pandemic was caused by a novel coronavirus (nCoV) or SARS-CoV-2 which belongs to betacoronavirus (**Figure 4**). Coronaviruses are viruses with the largest particle size in the group of RNA viruses, which are the single-stranded positive sense RNA viruses that infect a wide variety of animal species and cause respiratory, gastrointestinal, and central nervous system diseases (Rehman et al., 2020).

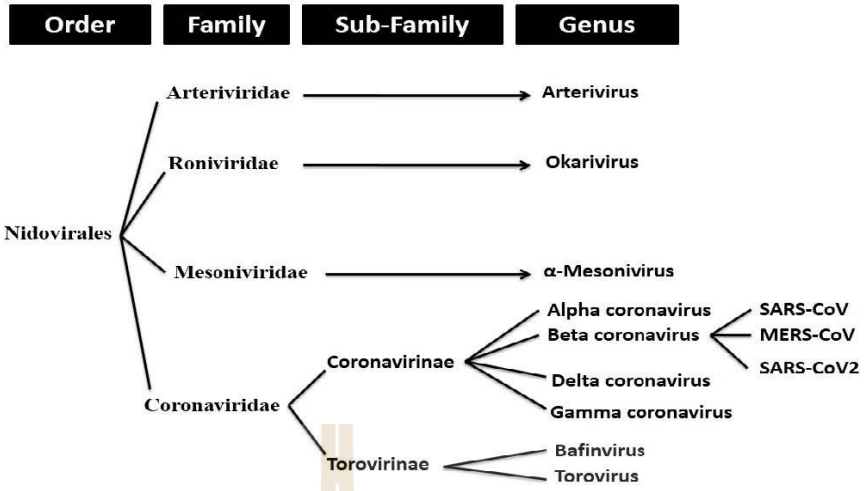

Figure 4 Classification of coronaviruses (Rehman et al., 2020).

The word "Corona" comes from the Latin word "Krone", which means the crown (Abubakar et al., 2021; Zhu et al., 2020). From the virus's view under an electron microscope, the clusters of carbohydrates can be seen as spikes protruding from the virus particle, giving it a crown-like appearance. SARS-CoV2 shares 80-96% similarity of the sequence with the bat SARS coronavirus. Since this nCOV is 79% homologous to SARS-CoV, it uses the same angiotensin-converting enzyme 2 (ACE2) as its receptor and also uses the spike (S) protein to attack the cells but ten times more powerful than that of SARS-CoV. This could be responsible for the higher infection and transmission rates (Burmer et al., 2021; Chang et al., 2014). To date, there are seven coronavirus strains that cause disease in humans. They include four strains that cause moderate illness as follows. HCoV-229E, HCoV-OC43, HCoV-NL63, and HCoV-HKU1, which typically cause upper respiratory tract infections. Three strains that cause severe disease, namely SARS-CoV-1, which caused severe acute respiratory syndrome or SARS in China and Hong Kong in 2002-2003; MERS-CoV, which caused Middle East Respiratory Syndrome (MERS) in 2012-2013; and finally, the new coronavirus type 2 or SARS-CoV-2, short for the severe acute respiratory syndrome, which causes the global pandemic of COVID-19 (Zhu et al., 2020).

The genomic structure of the 29,674 nucleotides of the SARS-CoV-2 coronavirus encodes the predicted open reading frames (ORFs) 1a and 1b. These ORFs encode nonstructural polyproteins (NSPs) and structural proteins. The NSPs include nsp1-16,

helicase, proteolytic cleavage enzymes (3-chyomotrypsin-like protease (3CLpro) or also called main protease (Mpro, Nsp5), and papain-like proteases (PLpro, Nsp3)), RNA-dependent RNA polymerase (RdRp), which have a critical role in viral RNA synthesis. The structural proteins, important for virion assembly, include spike (S), envelope (E), membrane (M), and nucleocapsid (N) structural proteins, as indicated in **Figure 5** (Abubakar et al., 2021; Chan et al., 2020).

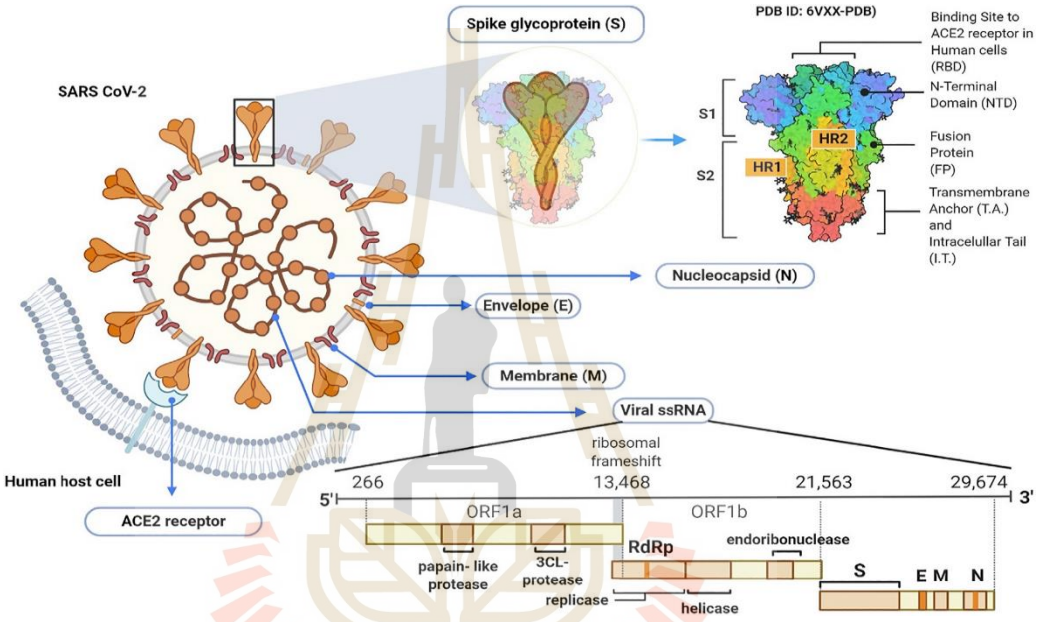

Figure 5 Schematic illustration of SARS-CoV-2 virion and its genome (Abubakar et al., 2021).

2.3 SARS-CoV-2 Life Cycle and Pathogenesis of COVID-19

As demonstrated in **Figure 6**, the life cycle of SARS-CoV-2 was described by Emrani and colleagues (2021) as follows. By attaching itself to the host cell surface's ACE2 receptor, the S-glycoprotein of SARS-CoV-2 allows the virus to enter the cell through endocytosis **(1)**. Upon release into the host cell's cytoplasm, polyproteins pp1a and pp1ab are translated which are cleaved by the PLpro and Mpro to form functional NSPs that have a critical role in viral RNA synthesis, including replicase polyproteins (RdRp and helicase) **(2 and 3).** Subgenomic transcription and RNA replication occur within the RdRp complex to synthesize negative-strand guide RNA

(gRNA) and a set of subgenomic RNAs for viral replication and transcription **(4 and 5)**. The newly produced subgenomic RNAs are translated into viral structural proteins such as the S, N, M, and E proteins **(6)**. To create viral particles, these proteins are first introduced into the rough endoplasmic reticulum (ER) membrane and subsequently transported to the ER-Golgi intermediate compartment (ERGIC), where they join the N protein-encapsidated RNA **(7 and 8)**. Virions are then released from the infected cell through exocytosis and ready to infect other cells **(9)** (Emrani et al., 2021; Trougakos et al., 2021).

The interaction between the viral spike protein and the ACE2 receptor is crucial for virus entry. Host proteases such as furin and TMPRSS2 play an essential role in preparing the spike protein for membrane fusion. Understanding the entry process is crucial for developing effective antiviral strategies, such as drugs that target the spike protein or host proteases (Essalmani et al., 2022).

The pathogenesis of SARS-CoV-2 involves a complex interplay between the virus and the host immune system. Once infection occurs, the host immune system recognizes the viral infection and initiates an innate immune response, involving the release of cytokines and the activation of immune cells. The adaptive immune system, including T cells and B cells, is activated to fight the infection (Sher et al., 2023).

Pathogenesis of COVID-19 upon the arrival of SARS-COV-2 to the host cell was summarized by Tanveer and colleagues (2022) as illustrated in **Figure 7.** The coronavirus enters host cells through ACE2 receptors, primarily found in type 2 alveolar cells in the lungs, while few in the kidney, liver, heart, intestine, and testis. This triggers innate immunity in the lungs, with dendritic cells and macrophages phagocytosing infected cells, allowing antigen presentation to T cells. The spike proteins are cleaved by the cellular proteases, transmembrane protease serine 2 (TMPRSS2), into two subunits (S1 and S2). This allows the binding between virus and host cell, and the virus-cellular membrane fusion. The immune response, initiated by T cells and plasma cells, recognizes spike proteins and produces antibodies against these proteins. This response includes protective pathways, but deregulation can lead to the hyperinflammation of COVID-19, known as a cytokine storm. The immune response is initiated by the entry of viral RNA through pattern-associated molecular

patterns (PAMPs) and pattern recognition receptors (PRRs), which are typically Toll-like receptors (TLR) 7 and 3, cytoplasmic RNA sensors (RIG-I and MDA5). These receptors translocate transcription factors NFkB and IRF3, triggering the production of pro-inflammatory cytokines like T1IFN and TNF-α. The elevated expression of pro-inflammatory mediators indicates disease severity, leading to multi-organ failure and potential death. Individuals with chronic conditions may develop the risks of lymphopenia, hyper-ferritinemia, and increased IL-6 levels. When activated by a virus, alveolar macrophages phagocytose injured cells and release pro-inflammatory mediators like IL-1, IL-6, IL-8, cytokines, and TNFα. These mediators stimulate the cough reflex and increase vascular permeability, leading to fluid outflow into interstitial spaces and alveoli, causing pulmonary edema and dyspnea. Damaged endothelial cells release prostaglandins and leukotriene, leading to bronchoconstriction and fever. Hypoxia triggers the heart to pump faster for oxygen supply, causing tachycardia and tachypnea in COVID-19 patients (Tanveer et al., 2022).

COVID-19 can disrupt the immune system in a variety of ways. Viral replication can damage the host cell leading to tissue damage and inflammation. One of the first proteins to be translated is the host shutoff factor Nsp1. This viral protein suppresses the host's innate immune response by preventing translation and accelerating host mRNA degradation (Scudellari, 2021). In some cases, an overactive immune response (cytokine storm) can lead to excessive inflammation, multiple organ damage, and acute respiratory distress syndrome (ARDS) (Ramos-Casals et al., 2021; Sher et al., 2023). An excessive inflammatory response of the host during the infection most likely develops the incidence of post-COVID-19 syndrome or so-called long COVID. This leads to the risk of new-onset autoimmune disease within the first year after COVID-19 diagnosis (Hileman et al., 2024). Understanding these immune-related complications is crucial for developing effective treatments and improving patient outcomes.

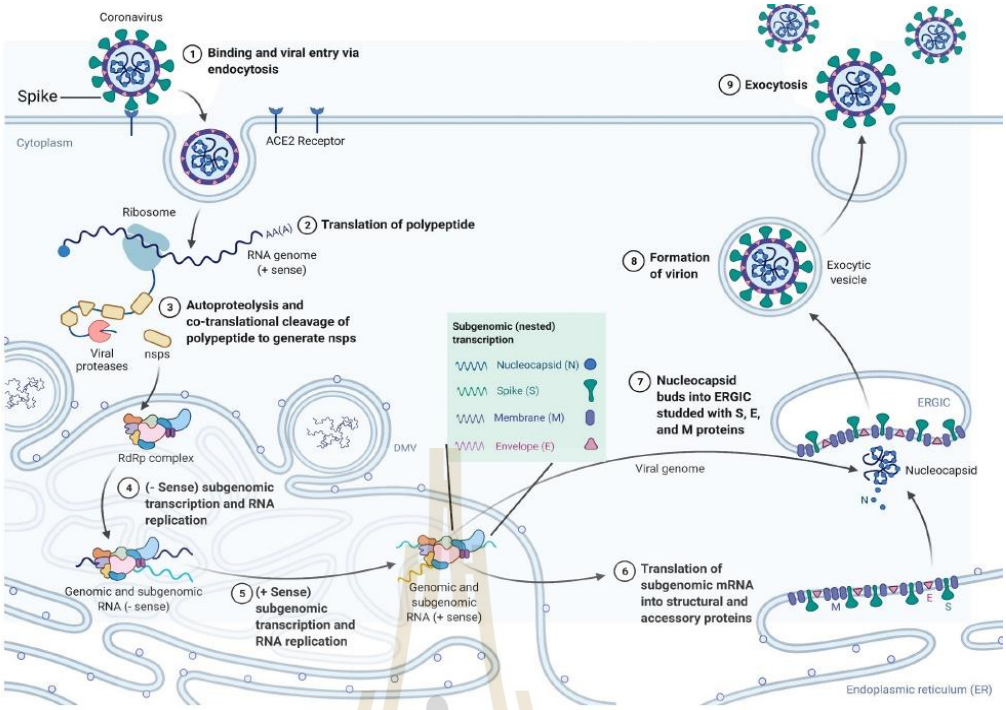

Figure 1 SARS-CoV-2 life cycle (Emrani et al., 2021).

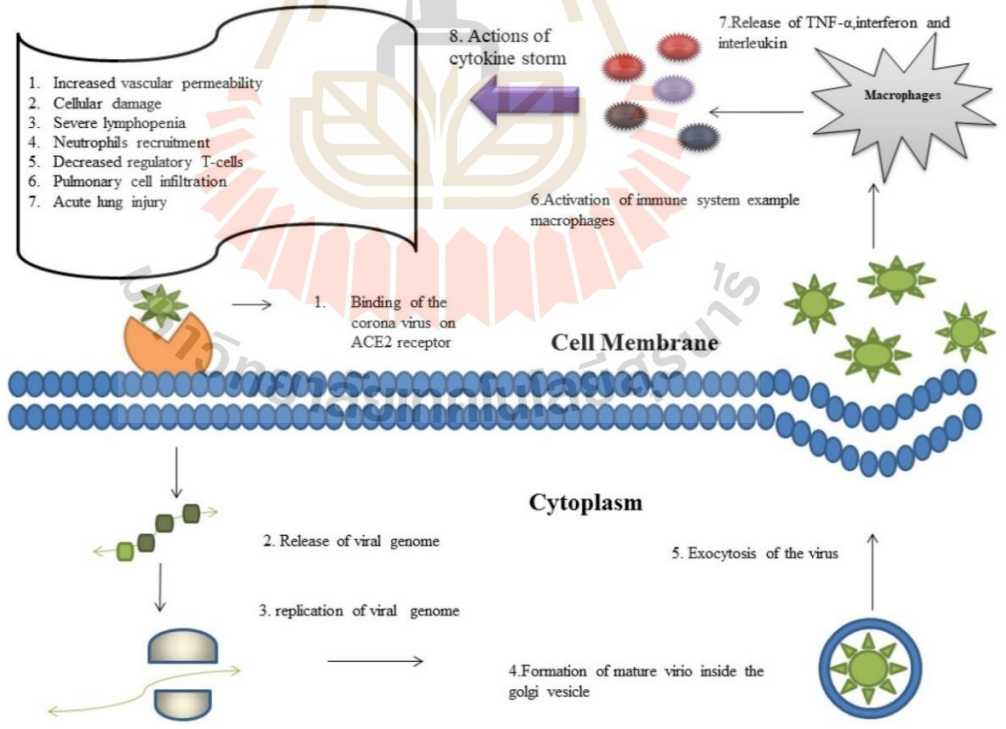

Figure 2 Pathological effects of cytokine storm upon the entry and replication of COVID-19 into host cells (Tanveer et al., 2022).

2.4 Repurposing Drugs for Treatment of COVID-19

Drugs can exert antiviral effects through several mechanisms, including the following: (1) preventing host-virus interactions; (2) interfering with the transcription or replication of the viral genome; (3) preventing the synthesis and assembly of viral proteins; or (4) altering the host's response to infection. Antiviral agents require the viral target to undergo active replication to endeavor a therapeutic effect, rendering them no harm to latent viruses. Two factors that may restrict the use of antiviral medications are drug toxicity and the development of drug resistance to the viruses. The severity of the disease determines the acceptance of the toxicity profile of a certain drug, which correlates directly with the dose used (Kimberlin, 2008).

Drug development typically takes ten years, costs $300 million to $2.8 billion, and has a 90% failure rate. The COVID-19 pandemic has accelerated drug repurposing, using previously approved drugs for new indications, to accelerate the identification and development of novel treatments, reducing morbidity, mortality, and economic costs. Drug repurposing offers three advantages over de novo drug development. First, it begins with clinically studied medicines, making repurposed drugs safer by avoiding the unknown side effect. The tolerable safety profile depends on whether the repurposed indication increases or lowers risk levels. Generally, the regulatory considerations for de novo drugs and the repurposing are similar, but more is often known about expected adverse effects. Second, investigators can use prior drug experiences to accelerate the development, reduce costs, and achieve higher success rates. Finally, extending the usage of repurposed drugs to already generic competitors can lead to lower prices and improve access to pharmaceutical innovations (Greenblatt et al., 2023).

Since particular antivirals or effective treatments are necessitated to counteract SARS-CoV-2, repurposing drugs and targeted interventions have been investigated to manage COVID-19. The efficacy of these medications is determined by their ability to target human receptors, the SARS-CoV-2 protein, or RNA. Several clinical trials and studies have been undertaken over the last few years to determine the most effective treatments.

Clinical trials have been conducted on various potential anti-SARS-CoV-2 drugs, including remdesivir, chloroquine and hydroxychloroquine, tocilizumab, favipiravir,

kaletra, and masitinib. These drugs are used in Hepatitis C treatment, malaria treatment, rheumatoid arthritis treatment, and anti-influenza drugs, respectively. The EU has approved the emergency use of Lagevrio (molnupiravir) and Paxlovid for adults with COVID-19 who do not require supplemental oxygen and are at increased risk of severe disease. These drugs are being used in HIV treatment and rheumatoid arthritis treatment (Rodrigues et al., 2022).

There were studies that investigated the use of multiple antiviral drugs at once in COVID-19 treatment, attempting to effectively inhibit SARS-CoV-2 replication and recover from the symptoms. The uses of lopinavir in combination with ritonavir (LPV/r) (Ye et al., 2020) and favipiravir in combination with hydroxychloroquine (Şimşek Yavuz & Ünal, 2020) were found to effectively inhibit viral synthesis, viral RNA polymerase/RNA synthesis, and inhibit the viral binding to host cells and also can act as an immune stimulant. It was also discovered that using lopinavir and ritonavir (LPV/r) in combination with other pneumonia-adjuvant drugs achieved evidently better results in treating COVID-19 patients in terms of quickly lowering the patient's body temperature, allowing the patient to recover quickly and without any negative side effects (Ye et al., 2020). The World Health Organization suggests that mild symptom cases, such as cough or mild fever, are not necessary for hospitalization, but rather stay home, self-isolate, and self-monitoring symptoms.

For Thailand, the treatment evaluation and drug administration sequence were based on pharmaceuticals accessible in the nation, drug efficacy in reducing severe disease and fatality rates, simplicity of drug administration, and drug pricing. According to clinical intervention data, among the therapies using molnupiravir, remdesivir, nirmatrelvir/ritonavir (Paxlovid), and favipiravir, Nirmatrelvir/Ritonavir possessed the most successful but most expensive. Favipiravir did not lower disease severity; however, it could alleviate symptoms if given on the first day of symptoms (Bangkokbiznews, 2022).

Favipiravir will be prescribed by the doctors to yellow group patients, who were either at risk of worsening symptoms such as high fever or signs of pneumonia, or patients in the groups of chronic diseases (i.e., high blood pressure, diabetes, obesity, kidney disease, and heart disease). This drug was prescribed under a doctor's supervision and depends on the doctor's discretion, as it is only taken by those with

compromised immune systems. Favipiravir is an antiviral drug that inhibits SARS-CoV-2 virus multiplication by inhibiting RdRp. Adult dosage is 9 tablets daily for the first day, then reduced to 4 tablets daily. Side effects may include nausea, vomiting, diarrhea, and changes in eyes, nails, or skin color. This symptom will disappear on its own when stopping the drug for about 14 days. Favipiravir can cause hepatitis and may potentially have a risk of affecting the fetus if it is used in pregnant women (Vichaivej-Nongkhaem, 2022).

Molnupiravir, a drug developed by Merck, has shown significant benefit in reducing hospitalization or death in mild COVID-19 patients. It is a prodrug of N4-hydroxycytidine that is converted into the active form 50-triphosphate by host kinases. The active 50-triphosphate serves as a competitive substrate for the viral RdRp and causes an antiviral effect through the accumulation of mutations after each viral replication cycle. Molnupiravir is an oral, direct-acting antiviral that reduces nasopharyngeal SARS-CoV-2 titres and has broad-spectrum antiviral activity against several coronaviruses, including SARS-CoV-2. Merck's clinical trial showed that molnupiravir reduced the risk of hospitalization and death among high-risk patients by 30%, compared to the initial estimate of 50%. The FDA has also authorized the use of molnupiravir in certain adult patients, demonstrating its potential for treating various diseases (Rodrigues et al., 2022).

Remdesivir, developed by Gilead Sciences, Inc., was initially a potential anti-Hepatitis C virus candidate. It was later repurposed for testing against Ebola and Marburg viruses. Despite its potential for COVID-19 treatment, its efficacy was questioned due to lack of evidence. The GS-441524 monophosphate prodrug inhibited RNA synthesis and replication, making it a potential candidate. Phase III clinical trials began in early 2020. However, remdesivir faced adverse side effects like hepatocellular toxicity, nausea, anemia, kidney injury, hypotension, respiratory failure, and constipation. Despite these issues, remdesivir is recommended by the EMA and the FDA for severe COVID-19 treatment (Gordon et al., 2020; Rodrigues et al., 2022). Many drugs, including paxlovid, actemra, ronapreve, nirmatrelvir, ritonavir-boosted nirmatrelvir, interferon alfa, interferon beta, interferon lambda, and ivermectin, are also used internationally (NIH, 2022).

2.5 The Potential of Using Herbs and Natural Products in Combating SARS-CoV-2

Herbal and traditional medicines have been used for decades and are recognized for their broad therapeutic spectrum and relatively low side effects compared to modern pharmaceuticals. In many countries, including China, Thailand, India, and Egypt, traditional herbal medicine has been widely applied to treat a variety of illnesses, including viral infections such as coronaviruses. Herbal metabolites have contributed significantly to medical advancements due to their affordability, low resistance potential, and diverse pharmacological properties, including anti-inflammatory, antiviral, antibacterial, and anticancer activities. This has led to a continuous interest in natural product-based drug discovery for various diseases, including COVID-19 (Hussain et al., 2017; Islam et al., 2020; Kandanur et al., 2019; Kushwaha et al., 2021; Nair et al., 2021; Orege et al., 2023; Sa-ngiamsuntorn et al., 2021).

Scientists believe that herbs with demonstrated antiviral effects against SARS-CoV may also be effective against SARS-CoV-2 due to the high genetic similarity (70% similarity) between the two viruses, particularly in their RNA genome, main protease, and ACE-2 receptor binding mechanisms. Verma and colleagues (2020) compiled a list of medicinal plants and secondary metabolites with known anti-SARS-CoV activity, identifying 83 promising compounds, including alkaloids, lycorine, lignans, and terpenoids (Verma et al., 2020). For instance, crude extracts of *Lycoris radiata*, *Artemisia annua*, *Pyrrosia lingua,* and *Lindera aggregata* exhibited anti-SARS-CoV activity at concentrations of 2.4-88.2 μg/mL (Li et al., 2005). Similarly, the water-soluble extract of *Houttuynia cordata* demonstrated antiviral activity by inhibiting the SARS-CoV 3CLpro and RdRp enzymes, while also enhancing CD4+ and CD8+ immune responses in host cells (Chiow et al., 2016; Luo et al., 2019). Extracts from *Rheum officinale* and *Polygonum multiflorum* were also reported to prevent SARS-CoV entry by blocking ACE-2 receptor binding at IC_{50} values between 1–10 μg/mL (Ho et al., 2007).

Artemisia annua L. has long been used in traditional medicine in Southeast Asia for the treatment of fever. Products derived from Artemisia have been developed for patients with respiratory distress. The study conducted by the Nie

group showed that several Artemisia extracts effectively inhibit SARS-CoV-2 and feline coronavirus (FCoV) infections (Nie et al., 2021). The study by Nair and coworkers (2021) suggests that the ability of *A. annua* extracts to inhibit SARS-CoV-2 infection is not solely due to the main component "artemisinin". Instead, it is likely due to a combination of components that work together to block viral infection in a step downstream of viral entry (Nair et al., 2021).

Thailand, with its rich biodiversity, has an abundance of medicinal plants with potential antiviral properties. Numerous Thai herbs have demonstrated efficacy against various viruses. For example, the crude extracts of *Andrographis paniculate*, turmeric (*Curcuma longa*), *Gynostemma pentaphyllum*, *Kaempferia parviflora* and guava leaves (*Psidium guajava*) showed high activity against the H5N1 avian influenza virus, where turmeric and galangal extracts stimulated the expression of TNF-α and IFN-β (mRNA expressions), resulting in the virus being unable to replicate its genetic material (Sornpet et al., 2017). In addition, *Andrographis paniculata* also has the effect of inhibiting influenza virus and simian retrovirus (Churiyah et al., 2015). It is also effective against malaria (Widyawaruyanti et al., 2014) and HIV viruses (Chen et al., 2016).

In Thailand, *Andrographis paniculate* (AP) has attracted the attention of researchers in the early stages of the COVID-19 pandemic, mainly because it is used in traditional medicine in many countries to treat diseases such as the common cold, diarrhea, and fever. Its main ingredient "andrographolide" is reputed to have a broad spectrum of antiviral properties. AP has been announced to promote its use in the treatment of mild COVID-19 patients and has received much attention from many research groups in Thailand. Sa-ngiamsuntorn and coworkers (2021) investigated the anti-SARS-CoV-2 activities of the AP extract and andrographolide compound in human lung epithelial cells, including their cytotoxicity in the cell lines of major organs, i.e., liver, kidney, intestine, lung, and brain. The post-infection treatment study showed that AP extract and andrographolide were able to significantly inhibit viral replication. The cytotoxic effects observed in the organ cell lines were within the favorable index (Sa-ngiamsuntorn et al., 2021). The clinical trial for AP treatment of patients with mild COVID-19 was evaluated. Wanaratna and coworkers (2022) investigated the efficacy and safety of AP extract (180 mg andrographolide daily for 5 days) in the early treatment of

patients with mild COVID-19 (29 patients) compared to patients treated with placebo (28 patients). The study showed promising efficacy of oral AP extract treatment with more effective pneumonia prevention compared to the placebo group, as observed by chest radiographs (Wanaratna et al., 2022). A shorter viral clearance was also observed in the AP-treated group. This study was consistent with the later study by Benjaponpitak group, which had studied a larger number of patients (Benjaponpitak et al., 2023). However, the cohort study on AP use of the Tanwettiyanont group came to the opposite conclusion that a higher percentage of patients with pneumonia occurred in the AP-treated group compared to the control group, although this was not statistically significant (Tanwettiyanont et al., 2022).

Boesenbergia rotunda (BR) was another Thai medicinal plant that is also widely used as a culinary herb in Asia and exhibited promising efficacy against SARS-CoV-2. The Kanjanasirirat group successfully discovered this promising antiviral plant candidate by screening 122 Thai natural products. They found that the extract of BR and its phytochemical compound (panduratin A) possessed potent in vitro anti-SARS-CoV-2 activity in both pre-entry and post-infection phases. In addition, the study reported their abilities to suppress viral infectivity in human airway epithelial cells. The efficacy and safety of BR-extract in clinical treatment in undergoing (Kanjanasirirat et al., 2020).

2.6 Screening for Additional Antiviral Medicinal Plants

Given the extensive historical use of medicinal plants in treating viral infections and relieving symptoms of colds, flu, and other viral diseases, it is essential to broaden the search for additional plant-derived antiviral agents. The evidence presented in this review (**Table A1** in Appendix) highlights several promising herbal candidates with anti-SARS-CoV-2 activity, particularly those from Thai traditional medicine. However, many Thai medicinal remedies remain unexplored, warranting further investigation. (Medthai, 2024; คณะเภสัชศาสตร์มหาวิทยาลัยมหิดล, 2025; คณะเภสัชศาสตร์มหาวิทยาลัยอุบลราชธานี, 2025). By systematically screening medicinal plants that have been historically used to prevent and treat viral infections-including those with immunomodulatory, anti-inflammatory, and respiratory-supportive properties-this study aims to identify novel plant-based therapeutic options against SARS-CoV-2.

Further investigations integrating ethnopharmacological knowledge, bioinformatics approaches, and experimental validation will enhance our understanding of how these natural products can contribute to antiviral drug development.

2.7 Analysis of The Biochemical Composition Using Synchrotron Radiation-Fourier Transform Infrared Microspectroscopy (SR-FTIR)

Infrared (IR) microspectroscopy is a non-destructive technology that studies chemical and structural information in samples that have a resonance frequency with infrared light. When a strong wavelength of infrared light passes through a sample, vibrations occur, resulting in the absorption of infrared light. Unabsorbed light reaches the sample and is detected by an infrared detector. The IR intensity is viewed as a relative form of IR absorption and frequencies in wavenumber units (cm^{-1}). The IR spectrum displays each molecule's distinct features, absorbing infrared light at different frequencies based on the chemical bonds and atomic weight of the functional groups in the sample. Each spectral signal of an individual group, such as proteins, lipids, carbohydrates, carbonyl groups, or aromatics, indicates their signature, also known as a "fingerprint." This technique is useful for examining the chemical structure of numerous types of samples without causing damage during measurement (Baker et al., 2014; SLRI, 2023).

The use of a synchrotron source in infrared microspectroscopy offers (SLRI, 2023) improved lateral resolution, faster acquisition time, and better spectral quality compared to a conventional infrared source due to the high brightness, the small size of the source and narrow range of emission angles. It has an improved signal-to-noise ratio in the IR spectrum without loss of spatial resolution, which is of great advantage for applications in the biological sciences (SLRI, 2023).

Biochemical composition analysis using infrared light can quickly provide information about functional groups in the chemical composition of the sample by displaying them in the form of a spectral profile. This analytical technique is becoming increasingly popular in the medical and biological sciences, for example in the analysis of plant constituents (Agatonovic-Kustrin et al., 2020; Krysa et al., 2022; Wongsa et al., 2022), the study of cellular changes (Gao et al., 2015; Portaccio et al., 2023; Wu et al., 2015), the early diagnosis of cervical cancer (Félix et al., 2024;

Sindhuphak et al., 2003), using as a tool to assess long cancer (Sulé-Suso et al., 2005), the analysis of changes in functional groups in food (Hong et al., 2017), and the study of microbial species and changes (Kassem et al., 2023). The spectral properties of biological samples provide information about the components of biochemical substances such as carbohydrates, proteins, fats, and phospholipids. The wave range of infrared light absorption, which is specific for different functional groups of biomolecules can be illustrated in **Figure 8** and explained as follows (SLRI, 2023).

1. Range 4000-3100 cm-^{1}: mainly OH (3400 cm^{-1}) and NH stretching vibration (Amide A ~ 3300 cm^{-1} and Amide B ~ 3030 cm^{-1}).

2. Range 3100-2800 cm^{-1}: CH stretching vibration of CH_3 and CH_2 from of lipid

3. Range 1800-1500 cm^{-1}: Amide I and Amide II of protein groups, enabling the indication of the secondary structure of the protein, such as alpha-helix, beta-sheet, including C=O group from ester group of lipids.

4. Range 1300-1500 cm^{-1}: CH bending vibration of CH_3 and CH_2 from lipid groups, including stretching vibration COO- from amino acid side chains.

5. Range 1230 cm^{-}1: P=O asymmetric stretching vibrations of phosphodiester, free phosphate, and monoester phosphate (mostly caused by the absorption of light by DNA/RNA Polysaccharide backbone structures).

6. Range 1200-900 cm^{-1}: PO^{2-} from nucleic acids and the -CO-C and C-O-P stretching vibrations of oligosaccharides and polysaccharides.

7. Range 1152 cm^{-1}: CO-O-C asymmetric stretching vibration of carbohydrates and sugars.

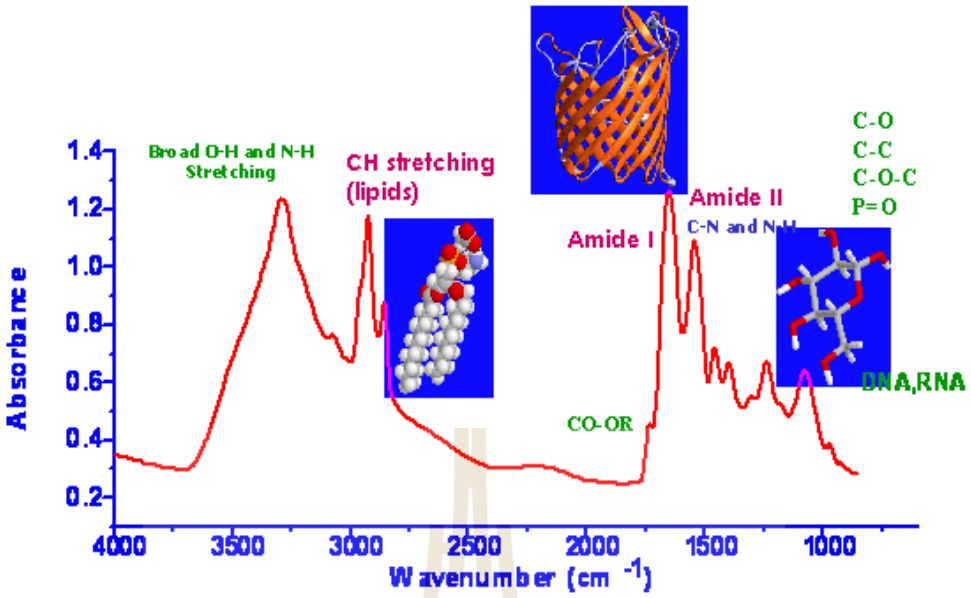

Figure 8 The mid-infrared absorption spectra of biomolecules (SLRI, 2023).

2.8 Molecular Docking Analysis as A Tool to Predict the Potential of Natural Candidates as Anti-SARS-CoV-2 Inhibitors

In silico molecular docking is a key step in the process of discovering novel drugs, including potential natural bioactive compounds. Molecular docking is a popular computer prediction technique for determining if a certain ligand (a molecule of interest) has the ability to interact with a selected target receptor. Its extensive use aids in determining the efficacy of substances and their eligibility for further research, hence promoting advances in therapeutic interventions (Stefaniu, 2019).

The development of antiviral drugs has been achieved by targeting specific proteins either in the virus, including structural or non-structural proteins in SARS-CoV-2 viruses, or in the host cells. In the case of this novel coronavirus, the main protease is a non-structural protein that plays an important role in viral replication and control of the host cell response. Simultaneously with the papain-like proteinase (PLpro), Mpro cleaves and transforms two large polyproteins (pp1a and pp1ab), which are selectively translated by lowering the viral RNA at the Leu-Gln↓ (Ser, Ala, Gly) sequence (where ↓ denotes the cleavage site), into the functional proteins responsible for viral transcription and replication. Due to its crucial role and specific

cleavage site, inhibiting the activity of the Mpro would block viral replication. Since no human proteases with similar cleavage specificity are known, it is unlikely that such inhibitors are toxic to humans. Therefore, Mpro has become one of the effective targets for the development of drugs against COVID-19 (El Gizawy et al., 2021; Maya et al., 2021; Zhang et al., 2020). Knowledge of the genetic sequence can be used to model the 3D structure of various proteins of the virus. Zhang and coworkers (2020) reported the X-ray 3D structures of the unliganded SARS-CoV-2 Mpro, as shown in **Figure 9** (Zhang et al., 2020).

In silico prediction of the ability of drugs or natural compounds to inhibit the activity of protease enzymes can be performed using the software for molecular docking analysis of protein and ligand interaction. The software simulates the binding between the active site of the target protein (viral target protein) and specific compounds (ligand). The ligand that tightly binds to the active site of the target protein is considered a potential candidate. The binding simulation randomly finds the most suitable chemical structure of the ligand-protein complex by calculating the binding energy level and using the scoring function as a scoring index. The lower the binding energy, the greater the potential interaction between the ligand and the viral target protein (Morris et al., 2009; Morris & Lim-Wilby, 2008). The program can be used to test a wide range of compounds and could help to shortlist the most promising candidates before an in vitro and in vivo bioassay is performed. This has the advantage of significantly reducing the time and cost of evaluating the potential of bioactive compounds. Based on the advantages of this technique, nelfinavir was predicted as a potential inhibitor of SARS-CoV-2 through interaction with the viral Mpro, for example (Xu et al., 2020).

Protomer of the dimer is shown in light blue, the other one in orange. Domains are labeled by Roman numerals. Amino acid residues of the catalytic site are indicated as yellow spheres for Cys145 and blue spheres for His41. Asterisks mark residues from protomer B (orange). Black spheres indicate the positions of Ala285 for each of the two domains III (see text). Chain termini are labeled N and C for molecule A (light blue) and N* and C* for molecule B (orange) (Zhang et al., 2020).

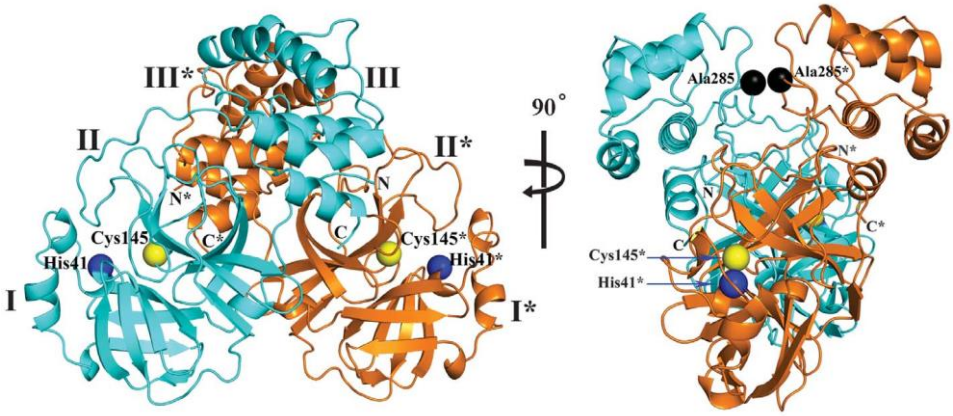

Figure 9 Three-dimensional structure of SARS-CoV-2 Mpro in two different views.

CHAPTER III

RESEARCH METHODOLOGY

3.1 Conceptual Framework of the Research Methodology

The study aimed to identify Thai herbal extracts with potent anti-SARS-CoV-2 activity using antiviral assays as bioassay guides, as outlined in Section 1.4 (Scope of the Study) and illustrated in **Figure 1**. The research was conducted in two experimental phases. **Phase 1** involved screening extracts using Vero cells to identify the most effective extract and its potential lead phytochemicals. **Phase 2** focused on refining the extraction process to develop a safer and more efficient method, including evaluations of cytotoxicity and antiviral efficacy in human lung epithelial cells (Calu-3). The mechanism of SARS-CoV-2 suppression by the selected extract was subsequently analyzed (**Figure 2**). The experimental methodology is detailed below.

3.2 Plant Materials

This study focused on 19 medicinal plants, commonly used Thai herbs, which were sourced from agricultural sites in Thailand. Taxonomic identification was conducted by Associate Professor Dr. Santi Watthana from the Institute of Science, Suranaree University of Technology. Voucher specimens of these plants were deposited in the Thai Traditional Medicine Herbarium, accompanied by their respective specimen numbers, plant parts utilized for extraction, and harvesting locations, as detailed in **Table A2** (Appendix). Since different plant parts often contain distinct phytochemicals, a total of 22 parts were analyzed. The preparation process involved shredding the herbs, drying them in an oven at 40°C, and grinding them into a fine powder prior to further use.

3.3 Research Methodology of Phase 1 Study

3.3.1 Preparation of herbal extract

3.3.1.1 Preparation of crude extract (CE)

The experiment followed previous studies with minor modifications (Abubakar & Haque, 2020; Rattanamaneerusmee et al., 2018). Plant powder was macerated in an 80% ethanolic-aqueous solution (1:10 ratio) and incubated in a shaking incubator (NB-205VL, N-BIOTEK, Korea) at 25°C, 175 rpm for 24 h. The liquid extract was separated from the plant residue (marc) using Whatman No. 1 filter paper (GE Health Care, UK) and a vacuum pump, yielding CE micelles. The marc underwent two additional extractions using the same method, and the micelles were combined. Ethanol was removed using a rotary evaporator (RV 10 digital, IKA, Germany), and the concentrated micelles were dried in a freeze dryer (Chris Alpha 2–4 LSCplus, Martin Christ Gefriertrocknungsanlagen GmbH, Germany). The resulting crude extract (CE) was evaluated for antiviral properties.

3.3.1.2 Liquid-liquid fractionation of potential crude extract

CEs demonstrating ≥ 2.5 log reduction value (LRV) in viral count (≥ 99.7% efficacy) were subjected to liquid-liquid fractionation using water (a highly polar solvent) and ethyl acetate (a less polar solvent) in a 1:10:10 (w/v/v) ratio (Minh et al., 2019). The CE was initially dissolved in water and transferred to a separating funnel. Ethyl acetate was subsequently added, and the mixture was gently agitated before being allowed to separate into two distinct phases. The upper ethyl acetate-soluble fraction was then separated from the lower water-soluble fraction. The water-soluble fraction was further extracted with fresh ethyl acetate in two additional rounds. All ethyl acetate-soluble fractions were combined according to standard procedures. Both the ethyl acetate-soluble fraction (EF) and water-soluble fraction (WF) were dried using a speed vacuum centrifuge and a freeze dryer, respectively. These fractions were then evaluated for anti-SARS-CoV-2 activity, with the most potent fraction further analyzed for its chemical constituents.

3.3.2 Cell culture

In the preliminary screening of 22 CEs using PEDV (clinically isolated) as a surrogate, Vero cells (CCL-81, ATCC, USA) were used for PEDV propagation and the anti-PEDV assay. For anti-SARS-CoV-2 activity, Vero E6 cells (CRL-1586, ATCC, USA)

served as the host for SARS-CoV-2 propagation, cytotoxicity, and anti-SARS-CoV-2 assays. Vero cells were maintained and subcultured in Dulbecco's modified Eagle's medium (DMEM), while Vero E6 cells were cultured in minimum essential medium (MEM), both supplemented with 10% fetal bovine serum, 100 U/mL penicillin-streptomycin, and 1% GlutaMAX. Cells were incubated at 37°C with 5% CO_2.

3.3.2.1 Preparation of PEDV

PEDV was propagated in Vero cells using serum-free DMEM, supplemented with 10 µg/µL TPCK-treated trypsin (Trypsin 1:250, Gibco) and 0.3% Tryptose Phosphate Broth (TPB) (Sigma-Aldrich). When the cytopathic effect (CPE) reached 70-80% (18–24 h post-infection), the cells underwent three freeze-thaw cycles. The supernatant was collected, aliquoted, and stored at −80°C. Viral titer was determined by plaque assay (Wang et al., 2005). PEDV stock was serially diluted, inoculated into Vero cells, and incubated at 37°C for 4–5 days. After fixation with 0.5% agar and crystal violet staining, plaques were counted, and the titer was expressed as plaque-forming units per mL (pfu/mL).

3.3.2.2 Preparation of SARS-CoV-2

The Delta B.1.617.2 variant of SARS-CoV-2 was isolated from nasopharyngeal swabs of a confirmed COVID-19 patient in Thailand and verified by the Tropical Medicine Diagnostic Reference Laboratory at the Faculty of Tropical Medicine, Mahidol University. The virus strain report can be found in Figure A1 (Appendix). The virus was subsequently propagated in Vero E6 cells (CRL-1586) at a density of 2.5×10^5 cells/mL in MEM supplemented with 2% fetal calf serum and 1% penicillin-streptomycin. To establish a high-titer viral stock, the virus was cultured at 37°C in a 5% CO_2 humidified incubator for 72 h. The viral titer was quantified using the TCID50 method, following the Reed-Muench approach (Baeshen et al., 2022; Reed & Muench, 1938), and expressed as TCID50/mL. All experiments involving live SARS-CoV-2 were conducted in a certified BSL3 facility at the Faculty of Veterinary Science (Approval No. MU2023-038), Mahidol University.

3.3.3 Cytotoxicity assay

Cytotoxicity of extracts/drugs was evaluated using the 3-(4,5-dimethylthiazol-2-yl)-2,5-diphenyltetrazolium bromide (MTT) assay. The extracts/drugs were diluted in 0.5% DMSO and serially diluted in a culture medium (1–1,000

μg/mL). Vero cells were seeded in 96-well plates (2×10^5 cells/mL) and incubated at 37°C for 24–48 h to form confluent monolayers. Cells were treated with extracts/drugs at various concentrations for 1 h (pre-entry antiviral assay) or 48 h (post-infection antiviral assay). The MTT solution (0.5 mg/mL) was added, and after 2 h of incubation, formazan crystals were dissolved in DMSO, and absorbance at 595 nm was measured (Bajrai et al., 2021; Sa-ngiamsuntorn et al., 2021). Cell viability was normalized to the negative control, and the 50% cytotoxic concentration (CC_{50}) was determined. Concentrations yielding > 70% viability were considered maximum noncytotoxic concentrations (MNTCs) (Astiti et al., 2021). CEs were tested at MNTCs for PEDV (single dose) and at three concentrations (MNTC and two consecutive twofold dilution concentrations) for anti-SARS-CoV-2 activity (Vlietinck et al., 1995).

3.3.4 Antiviral assay

Cytotoxicity of extracts/drugs was evaluated using the 3-(4,5-dimethylthiazol-2-yl)-2,5-diphenyltetrazolium bromide (MTT) assay. The extracts/drugs were diluted in 0.5% DMSO and serially diluted in a culture medium (1–1,000 μg/mL). Vero cells were seeded in 96-well plates (2×10^5 cells/mL) and incubated at 37 °C for 24–48 h to form confluent monolayers. Cells were treated with extracts/drugs at various concentrations for 1 h (pre-entry antiviral assay) or 48 h (post-infection antiviral assay). The MTT solution (0.5 mg/mL) was added, and after 2 h of incubation, formazan crystals were dissolved in DMSO, and absorbance at 595 nm was measured (Bajrai et al., 2021; Sa-ngiamsuntorn et al., 2021). Cell viability was normalized to the negative control, and the 50% cytotoxic concentration (CC_{50}) was determined. Concentrations yielding > 70% viability were considered maximum noncytotoxic concentrations (MNTCs) (Astiti et al., 2021). CEs were tested at MNTCs for PEDV (single dose) and at three concentrations (MNTC and two consecutive twofold dilution concentrations) for anti-SARS-CoV-2 activity (Vlietinck et al., 1995).

3.3.4.1 Anti-PEDV assay

A preliminary screening of 22 CEs was conducted to evaluate their antiviral activity against PEDV. A single-dose concentration corresponding to the defined MNTC for each CE was used in the plaque reduction neutralization test (PRNT) (Wang et al., 2005). PEDV was incubated with the crude extracts for 5 mins at 37°C, and the remaining infectious virus was detected in Vero cells (CCL-81). The viral

solution was serially diluted, inoculated into Vero cells, and incubated at 37°C for 3 days, allowing for plaque formation. Cells were then fixed, and stained with crystal violet, and plaque numbers were counted. Viral titer was quantified in plaque-forming units per mL (pfu/mL). The virucidal activity was determined by the reduction in plaque formation relative to the untreated PEDV control, with efficacy reported as the percentage of viral reduction. CEs demonstrating ≥ 70% anti-PEDV efficacy were selected for subsequent in vitro anti-SARS-CoV-2 activity assays.

3.3.4.2 Anti-SARS-CoV-2 assay

Two modes of action for the anti-SARS-CoV-2 activity of herbal extracts were assessed in Vero E6 cells, following several studies with modifications (Abd-Alla et al., 2022; Bajrai et al., 2021; Kanjanasirirat et al., 2020). **The pre-entry** study involved directly exposing SARS-CoV-2 to extracts/drugs to assess virucidal activity (% virucidal). **Post-infection study** involved infecting host cells with SARS-CoV-2, followed by treatment with extracts/drugs to evaluate viral replication inhibition (% inhibition) (Abd-Alla et al., 2022; Kanjanasirirat et al., 2020). Extracts were tested at three concentrations: MNTC and two consecutive twofold dilutions. All experiments were conducted in triplicate, with results presented as the mean ± SD. Prior to the antiviral assay, Vero E6 cells were seeded at 2×10^5 cells/well in a 96-well plate, incubated at 37°C for 24 h to form a monolayer, and washed with PBS before the test. Molnupiravir (EIDD-2801, Selleckchem, USA) served as a positive control, and extract-free MEM as a negative control.

1) Pre-entry mode: The virucidal activity of extracts/drugs against SARS-CoV-2 was evaluated following ASTM method no. ASTM E1053-20 (ASTM, 2020), at three concentrations based on cytotoxicity results, using a 1-h exposure. SARS-CoV-2 (1×10^5 TCID50/mL) was incubated with the extracts/drugs at 37°C for 1 h. The virus suspension was then cultured on Vero E6 cell monolayers in MEM (2% FBS) in a 96-well plate for 2 h to allow viral absorption. After washing with PBS, a fresh medium was added, and cells were cultured for 48 h before assessing cytopathic effects (CPE). The anti-SARS-CoV-2 efficacy was determined by viral reduction at each concentration, expressed as % virucidal and log reduction value (LRV) relative to the negative control. LRV values of 2, 3, and 4 corresponded to viral

reductions of 99%, 99.9%, and 99.99%, respectively. Calculations are described by Bullen et al. (Bullen et al., 2022) in the Appendix A1 (**Table A3**).

2) Post-infection treatment mode: Vero E6 cell monolayers were infected with SARS-CoV-2 (1×10^5 TCID50/mL) and incubated at 37°C for 2 h for viral absorption. The culture supernatant was then removed, and the cells were washed with PBS before being treated with various concentrations of herbal extracts/drugs in fresh MEM (2% FBS). The culture was maintained at 37°C for 48 h, and cytopathic effects (CPE) were observed. The anti-SARS-CoV-2 activity was quantified as % inhibition and expressed as log reduction value (LRV), with the negative control exhibiting the most significant CPE.

3) Half-maximal inhibitory concentration (IC_{50}) evaluation: IC_{50} values for molnupiravir and the most potent antiviral extract were determined using the TCID50 method, following the modified Reed–Muench method (Reed & Muench, 1938). The herbal extract and molnupiravir were evaluated at their MNTCs and four twofold serial dilution concentrations in both modes of action. After observing CPE, TCID50 was assessed, and IC_{50} concentrations were calculated.

3.3.5 Evaluation of antiviral lead compounds from the most effective extract

To identify antiviral lead compounds from the most effective extract, liquid chromatography–high-resolution mass spectrometry (LC-HRMS) and molecular docking studies were conducted. Due to challenges in phytochemical separation on the LC column, the workflow was divided into four steps: ***(1)*** simplifying the complexity of the most effective extract (WF-MLCE) by partially separating it into major fractions using column chromatography (CC), ***(2)*** identifying small molecules in each fraction *via* LC–HRMS, ***(3)*** refining antiviral leads based on anti-SARS-CoV-2 efficacy and total phenolic/flavonoid content, and ***(4)*** performing molecular docking on compounds with the highest efficacy against SARS-CoV-2 Mpro.

3.3.5.1 Phytochemical profiling of the most effective extract using Fourier-transform infrared spectroscopy (FTIR)

FTIR spectroscopy was used to determine the phytochemical profile of the most effective extract before partial separation by CC. The spectra were obtained in the mid-infrared region (MIR) region (4000–400 cm^{-1}) using a Bruker

Tensor 27 FTIR spectrometer with an attenuated total reflectance (ATR) accessory and diamond crystal (Bruker Optics Ltd., Ettlingen, Germany). Data were collected over 64 scans at a resolution of 4 cm^{-1}, and baseline correction and spectral averaging were performed using OPUS 7.5 software. A reference air spectrum was recorded before sample measurement (Abbas et al., 2017; Walkowiak-Bródka et al., 2022).

3.3.5.2 Partial separation of the effective extract using column chromatography

Following FTIR analysis, Sephadex-LH20 resin (Cytiva, USA) was selected for column chromatography (CC) separation, using an AKTA prime system (Amersham Biosciences, UK). The extract (250 mg/mL in water) was loaded onto the column, and sequential elution was performed with slight modifications from previous studies (Arfan et al., 2007; Mottaghipisheh & Iriti, 2020; Paje et al., 2022; Riihinen et al., 2012) in three steps: (1) 250 mL of water, (2) 250 mL of 50% ethanol aqueous solution, and (3) 150 mL of 100% ethanol, at a flow rate of 2 mL/min. Fractions (10 mL each) were collected based on absorbance at 280 nm, pooled into major fractions, and freeze-dried for subsequent LC–HRMS analysis.

3.3.5.3 Identification of tentative small molecules of CC fractions (CCFs) using LC–HRMS technique

LC–HRMS was employed to identify potential phytoconstituents in CC fractions (CCFs), with modifications from prior studies (Ali et al., 2021; Ruan et al., 2019). Analysis was performed on an Ultimate 3000 RSLC system coupled with a Q Orbitrap mass spectrometer (Thermo Fisher Scientific, Germany). LC separation occurred on an XSelect HSS T3 column (2.1 × 100 mm, 2.5 µm, Waters, USA) at 30°C, using mobile phase A (0.1% formic acid in water) and mobile phase B (0.1% formic acid in acetonitrile). The gradient started at 1% B and increased to 95% B over 52 min at 0.3 mL/min. The mass spectrometer operated in positive/negative ion modes with heated electrospray ionization. Full-scan MS (100–1500 m/z, resolution 140,000) was followed by data-dependent MS2 (35 NCE, resolution 35,000). Data were processed using Xcalibur and Compound Discoverer software (Thermo Fisher Scientific). Tentative compounds were identified by comparing MS2 fragments with mzCloud and precursor ions with ChemSpider, using ≥ 50% and ≥ 70% match criteria,

respectively. Compounds were identified with their estimated abundances, based on the peak area of the predominant adduct intensity.

3.3.5.4 Refinement of antiviral lead identification: Anti-SARS-CoV-2 assay and total phenolic/flavonoid content analysis

1) Anti-SARS-Cov-2 assay: CC fractions (CCFs) were evaluated for anti-SARS-CoV-2 activity using established protocols (Section 3.3.4.2). The total phenolic content (TPC) and total flavonoid content (TFC) were quantified as detailed below.

2) Quantification of total phenolic and flavonoid contents

Total phenolic content (TPC) was determined using the Folin–Ciocalteu assay with gallic acid (GA) as the standard. In a 96-well plate, 25 µL of the Folin–Ciocalteu reagent (diluted 1:3 with water) was mixed with 25 µL of the sample and 200 µL of water. After 5 min of incubation at room temperature, 25 µL of 10% (w/v) Na_2CO_3 was added, and the mixture was incubated in the dark for 60 min. Absorbance was measured at 765 nm using a microplate reader. TPC was calculated from a GA calibration curve (0–250 µg/mL) and expressed as mg gallic acid equivalents per gram of dried extract (mg GAE/g extract) (Ali et al., 2021; Tang et al., 2020).

Total flavonoid content (TFC) was assessed using the aluminum chloride method with quercetin (Q) as the standard. In a 96-well plate, 25 µL of the sample was combined with 100 µL of water and 10 µL of 10 g/L $NaNO_2$, followed by a 5 min incubation at room temperature. Next, 15 µL of 100 g/L $AlCl_3$ was added, and the mixture was incubated for 6 min before adding 50 µL of water and 50 µL of 1 M NaOH. After shaking for 30 sec, absorbance was recorded at 415 nm. TFC was quantified using a quercetin calibration curve (50–1,000 µg/mL) and reported as mg quercetin equivalents per gram of dried extract (mg QE/g extract) (Ali et al., 2021; Tang et al., 2020).

To further identify potential antiviral leads, only the phytochemical constituents of CCF(s) demonstrating significant anti-SARS-CoV-2 activity were selected for molecular docking analysis.

3.3.5.5 *In Silico* molecular docking: Identification of potential SARS-CoV-2 Mpro inhibitors

Molecular docking of small molecules from the target CC fractions (CCFs) against SARS-CoV-2 Mpro was conducted using AutoDockTools (ADT 1.5.6) (Morris et al., 2009), with three repurposed drugs (lopinavir, hydroxychloroquine, and molnupiravir) as references. The crystal structure of SARS-CoV-2 Mpro (PDB ID: 6LU7) (Jin et al., 2020) was retrieved from the Protein Data Bank, while ligand structures were sourced from NCBI PubChem and MolView databases (Kim et al., 2022). Ligands were prepared as 3D conformers in SDF or MOL format, converted to PDB using Open Babel GUI (O'Boyle et al., 2011), and optimized in ADT with rotatable bonds (Berman et al., 2000).

The docking grid was defined with dimensions of 66 Å × 70 Å × 48 Å, centered at X = −10.357 Å, Y = 18.601 Å, Z = 67.669 Å, encompassing key residues (His-41, Asn-142, Gly-143, Ser-144, Cys-145, His-163, Met-165, Glu-166) (Liang et al., 2020; Rafi et al., 2022). Binding energies (kcal/mol) were calculated, with more negative values indicating stronger interactions, and inhibition constants (Ki, μM) were estimated to assess inhibitory activity. Lower Ki values indicated the higher potential for viral protein inhibition. Compounds with favorable docking scores underwent further evaluation of their 3D interactions with Mpro active site residues using PyMOL (Lill & Danielson, 2011).

3.4 Research Methodology of Phase 2 Study

3.4.1 Modification of WF-MLCE extraction method

Based on the Phase 1 results, the water fraction of the mulberry leaf crude extract (WF-MLCE) was identified as the most effective extract, emphasizing the key role of water-soluble phytoconstituents in combating SARS-CoV-2. Consequently, in Phase 2, the WF-MLCE extraction method was refined with minor modifications to enhance the enrichment of water-soluble compounds, as outlined in Section 1.4. (Figure 2).

3.4.1.1 Preparation of water-soluble extract of mulberry leaves

1) Method 1: As illustrated in **Figure 2 (M1)**, the process began with the preparation of a crude extract via maceration using an 80%

ethanol-aqueous solution. This was followed by liquid-liquid fractionation with water and ethyl acetate, as described in Section 3.3.1. The resulting extract was designated as "WF-EtAc."

2) Method 2: As illustrated in **Figure 2 (M2)**, the process commenced with the preparation of a crude extract (CE) via maceration using an 80% ethanol-aqueous solution, following the same protocol as M1. However, the water-soluble fraction was obtained by dissolving the CE in water alone (1:10 w/v). The resulting CE-water suspension was centrifuged at 25,000 × g for 30 min, and the supernatant was separated and freeze-dried to produce the second type of water-soluble extract, designated as "WF-W."

3) Method 3: As depicted in **Figure 2 (M3)**, finely ground mulberry leaf powder was extracted by maceration with water at a 1:10 (w/v) ratio in a shaking incubator (NB-205VL, N-BIOTEK, Gyeonggi-do, Korea) at 175 rpm and 25°C for 24 h. The mixture was filtered through Whatman No. 1 filter paper, and the residue was subjected to two additional rounds of water extraction. The filtered solutions from all three extractions were combined and freeze-dried, resulting in the water-soluble extract, designated as "WCE".

3.4.1.2 Chemical constituent analysis of extracts: Preliminary selection of target mulberry leaf extract(s)

The chemical profiles of the three extracts-WF-EtAct, WF-W, and WCE-were analyzed using FTIR (as outlined in Section 3.3.5.1), total phenolic content (TPC), and total flavonoid content (TFC) determination (described in Section 3.3.5.4). Additionally, a tentative phytochemical analysis was performed using LC-HRMS (detailed in Section 3.3.5.3). The mass spectral analysis allowed for the statistical differentiation of the extracts based on mass spectral data.

The results revealed that WF-W exhibited a chemical pattern closely resembling that of WF-EtAct. Consequently, these two extracts were selected for the anti-SARS-CoV-2 assay using Calu-3 cells as the host.

3.4.2 Cell culture

Calu-3 cells (HTB-55, ATCC), a human epithelial lung cell line, were used as the host system in the Phase 2 experiment to better reflect human physiological interactions in the evaluation of antiviral activity and mechanism of

action, providing a notable improvement over the use of Vero cells. The cells were cultured in RPMI 1640 medium supplemented with 10% fetal bovine serum (FBS), 100 U/mL penicillin-streptomycin, and 1% GlutaMAX. Calu-3 cells were seeded at a density of 2.0×10^5 cells/mL in 96-well plates, with 100 µL of cell suspension per well, and incubated at 37°C in a humidified atmosphere containing 5% CO_2 for 24–48 h to form a confluent monolayer before experimental assays.

3.4.3 Cytotoxicity of mulberry leaf extract

The Calu-3 cell monolayers were tested at contact periods of 1 h and 48 h. The cytotoxic effects of the extracts on Calu-3 cells were determined by evaluating cell viability relative to the negative control group, which was treated with extract-free RPMI 1640 medium. In addition to WF-EtAct and WF-W extracts, rutin (CFN99642, ChemFaces Biochemical, China), a predominant compound in mulberry leaf extract, and molnupiravir (EIDD-2801, MK-4482, Selleckchem, USA), a reference repurposed drug, were also tested. Serial 2-fold dilutions were performed, resulting in a test concentration range of 1–1000 µg/mL. The cytotoxicity assessment was performed using the MTT assay, and the CC_{50} values for each sample were calculated as described previously in Section 3.3.3.

3.4.4 Anti-SARS-CoV-2 assay

Anti-SARS-CoV-2 assays of the extracts were conducted in pre-entry and post-infection modes, as detailed in Section 3.3.4.2. The IC_{50} values were determined using the AAT Bioquest calculator with a 4-parameter logistic regression model. Extracts and drugs were tested in concentrations ranging from 0.001 to 1000 µg/mL through serial 10-fold dilution in RPMI 1640 medium (2% FBS).

3.4.5 Analysis of the anti-SARS-CoV-2 mechanism of action in post-infection treatment mode using SR-FTIR

The experiment was divided into two groups: (1) a test group to evaluate the effect of the extract on Calu-3 cells under normal conditions, and (2) a test group to assess the effect of the extract on virus-infected cells, as detailed in Table 1. Both groups were seeded with 6×10^5 Calu-3 cells, and the WF-W extract was applied at a concentration of 100 µg/Ml. In the normal cell group, WF-W was administered to the Calu-3 monolayer for 1, 24, and 48 h prior to cell collection. For

the infected cell group, the post-infection treatment protocol, as outlined in Section 3.3.4.2, was followed. Three independent cultures were grown for each condition.

Before harvesting the cells, the medium was removed, and the cell monolayer was detached from the culture support by means of a 5-min treatment with 0.5% trypsin-EDTA. The reaction was inactivated by adding RPMI 1640 medium. The cells were pelleted by 5-min centrifugation (1500 rpm) and washed in isotonic solution (0.85% NaCl), followed by centrifugation, to ensure complete removal of trypsin and culture medium. In the case of infected samples, a 70% ethanol solution was added to the pellets for 15 min to ensure virus inactivation prior to washing with isotonic solution. The pellets were resuspended in ~10 µL of water before dropping onto BaF_2 windows for FTIR measurement (Derenne et al., 2013).

All measurements were carried out using SR-FTIR imaging microspectroscopy in transmission mode. Spectra were recorded over 64 scans at a resolution of 2 cm^{-1}. All spectra were processed as follows: Water and air contribution were subtracted, the baseline corrected and normalized before spectral averaging performed using OPUS 7.5 software (Bruker Optics Ltd, Ettlingen, Germany), and the Unscrambler 10.3 was used to calculate the differences in the main components of the extracts using the Principal Component Analysis (PCA) technique.

Table 1 Samples for the mechanism of action study of WF-W by SR-FTIR technique.

Host cells	**Cell experiment test**	**Category of sample**
Test group 1: Normal cells (non-infected host cells)	(1) Calu-3 + Media	Control group
	(2) Calu-3 + WF-W_1 h contact	Treatment 1
	(3) Calu-3 + WF-W_24 h contact	Treatment 2
	(4) Calu-3 + WF-W_48 h contact	Treatment 3
Test group 2: Virus infected-host cells	(1) Calu-3 + Media	Control group
	(2) SARS-CoV-2 infected-Calu-3	Treatment 1
	(3) SARS-CoV-2 infected-Calu-3+ WF-W_48 h contact	Treatment 2

3.5 Statistical Analysis

All experiments were performed in triplicate, and the results are expressed as mean ± SD. Statistical analysis across three or more groups was conducted using a one-way ANOVA followed by Tukey's HSD post-hoc test at a significance level of $p < 0.05$. For comparisons between two groups, a t-test was employed with a significance level of $p < 0.05$ (SPSS Statistics version 26, IBM Corporation, 2019).

CHAPTER IV
RESULTS

4.1 Phase 1: Screening of Potential Anti-SARS-CoV-2 Agents Through *In Vitro* Antiviral Testing

4.1.1 Initial evaluation of potential antiviral CEs using PEDV as a surrogate

To identify a potential anti-SARS-CoV-2 agent, 22 ethanolic-aqueous crude extracts (CEs) from 19 Thai medicinal plants were screened for antiviral activity against PEDV. A single dose (MNTC) of each CE was tested, revealing eight extracts with ≥ 70% virucidal efficacy, as shown in **Table 2**. The effective CEs were derived from *Colubrina asiatica* (S1), *Morus alba* (leaves) (S2), *Gynostemma pentaphyllum* (S3), *Artemisia annua* (S4), *Centella asiatica* (S5), *Justicia gendarussa* (S6), *Helicteres isora* (S7), and *Phyllanthus niruri* (S8). These eight CEs were selected for further antiviral evaluation against SARS-CoV-2 using Vero E6 cells.

Table 2 Anti-PEDV efficacy as %virucidal of twenty-two crude extracts tested at their individual maximum non-cytotoxicity concentration (70% cell viability).

Sample Code	Thai common name	Tested conc. (µg/mL)	Efficacy (%)
S1	Khan song	1000.0	89
S2	Mon	125.0	89
S3	Jiaogulan	500.0	87
S4	Kot chula lampha	1000.0	91
S5	Bua bok	500.0	70
S6	San phra mon	1000.0	70
S7	Po bid	125.0	70
S8*	Lok tai bai	125.0	95
S9	Ya nuat maew	125.0	62
S10	Ya lin ngu	250.0	67
S11	Som khaek	1000.0	62

Table 1 (continued).

Sample Code	Thai common name	Tested conc. (µg/mL)	Efficacy (%)
S12	Phutha raksa	750.0	66
S13	Nam nom ratchasi lek	62.5	54
S14	Ngueak pla mo	125.0	57
S15	Phaya plong thong	500.0	64
S16	Pattawia (flower)	125.0	68
S17	Pattawia (leaves)	125.0	57
S18	Pattawia (stem)	250.0	54
S19	Thapthim (leaves)	62.5.0	50
S20	Mara kee nok	125.0	62
S21	Plub plueng tin pade (root)	62.5	61
S22	Plub plueng tin pade (leaves)	62.5	61

*****After ethanol evaporation using a rotary vacuum evaporator, S8-CE is separated into two components: a light soluble fraction (S8-L) and a dark, gummy fraction (S8-D). During the initial rapid anti-PEDV screening, these two components were combined in a 1:1 ratio for testing, including cytotoxicity assessments. In subsequent studies, the two components were tested separately, resulting in the evaluation of nine CEs for their anti-SARS-CoV-2 activity.

4.1.2 Cytotoxicity and anti-SARS-CoV-2 activity of potential CEs

The cytotoxicity of nine crude extracts (CEs) in Vero E6 cells and their respective CC_{50} values are shown in **Figure 10**. In the 1-h contact period assay (pre-entry study), the results indicated moderate cytotoxicity across most extracts, with CC_{50} values ranging from 0.24 to 0.40 mg/mL. However, *Gynostemma pentaphyllum* (S3) and *Phyllanthus niruri* (S8-D) demonstrated the lowest cytotoxicity, with CC_{50} values above 1 mg/mL (**Figure 10a**). A similar pattern was observed in the 48-h contact period assay (post-infection treatment study), with CC_{50} values ranging from 0.30 to 0.71 mg/mL (**Figure 10b**).

In the pre-entry mode, most CEs exhibited significant anti-SARS-CoV-2 efficacy, with a Log Reduction Value (LRV) of 2 (~99% virucidal activity) as shown in **Table 3.** The highest efficacy was recorded for S8-D, which achieved an LRV of 2.56 (99.68% virucidal) at a concentration of 0.0625 mg/mL. In the post-infection treatment mode, four CEs (S1, S2, S8-L, and S8-D) showed significant antiviral activity with an LRV of approximately 2.5 (99.7% viral inhibition). The strongest inhibition was observed in S8-D at 0.1250 mg/mL (2.94 LRV, 99.89% inhibition), followed by S2 at 0.0313 mg/mL (2.60 LRV, 99.75% inhibition).

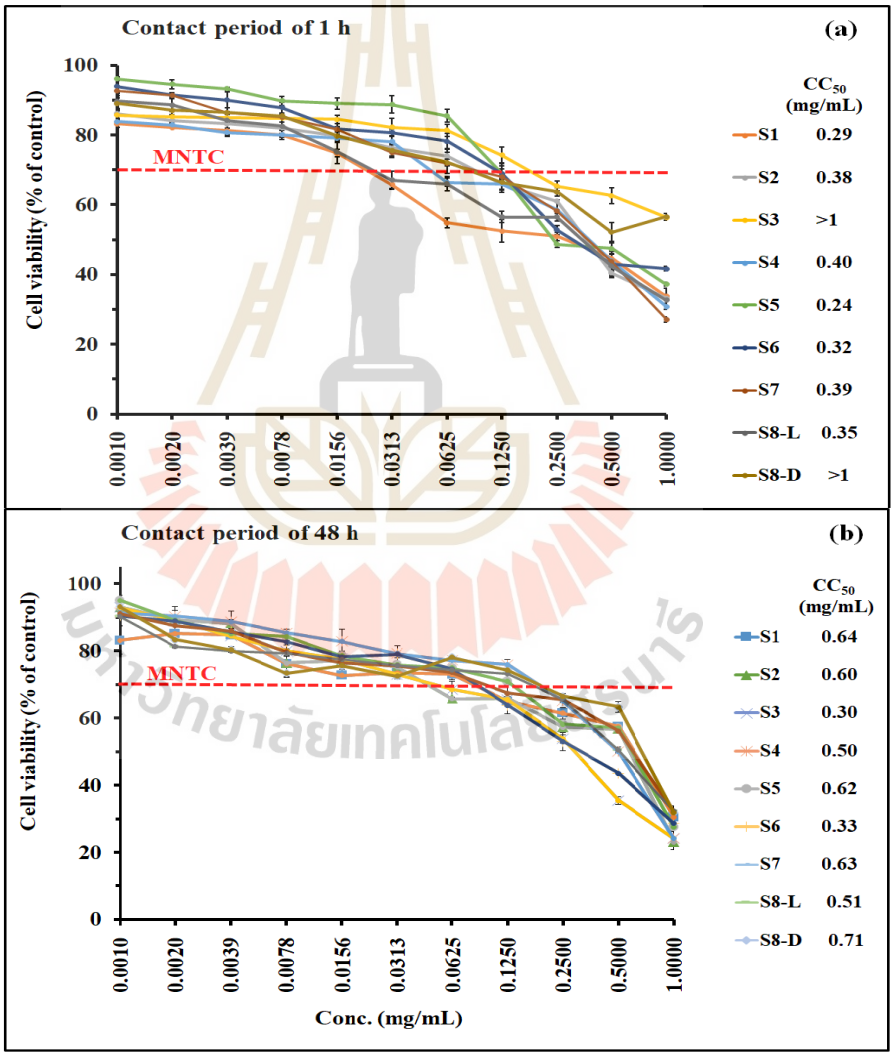

Figure 10 Cytotoxicity of the nine crude extracts (S1–S8) with CC_{50}, evaluated in Vero E6 cells. (a) Cytotoxicity after 1 h of treatment with crude extracts, and (b) cytotoxicity after 48 h of treatment. Results are expressed as %

cell viability at various extract concentrations (mean ± SD). The red dot line indicates the minimum non-toxic concentration (MNTC), defined as the concentration where cell viability is ≥ 70% for each individual crude extract.

4.1.3 Cytotoxicity and anti-SARS-CoV-2 efficacy of liquid-liquid separation fractions from four promising CEs

The four most promising CEs (S1, S2, S8-L, and S8-D) were subjected to liquid-liquid fractionation using a water and ethyl acetate solvent system. Cytotoxicity assessment of the resulting water fractions (WFs) and ethyl acetate fractions (EFs) showed that WFs exhibited significantly lower toxicity to Vero E6 cells compared to EFs (**Figure 11**). Notably, S1-WF and S2-WF demonstrated minimal cytotoxicity, with a CC_{50} ≥ 0.72 mg/mL across both 1-h and 48-h contact periods, showing 2–4 times less toxicity than molnupiravir.

Regarding anti-SARS-CoV-2 efficacy, molnupiravir exhibited 99.81% virucidal activity (LRV of 2.76) in the pre-entry phase and 99.08% inhibition of viral replication (LRV of 2.05) in the post-infection treatment phase at a concentration of 0.0625 mg/mL for both stages (**Table 4**). The anti-SARS-CoV-2 activity of WFs and EFs followed a pattern similar to molnupiravir, with higher efficacy in the pre-entry phase than in the post-infection phase, contrasting with the CE results (**Table 5**). The fractions showed slightly better virucidal activity than the original CEs. Among them, S2-WF exhibited the highest virucidal effect, achieving an LRV of 3.06 (99.9% virucidal) at 0.250 mg/mL and 2.90 (99.8% inhibition) in the post-infection phase at 0.1250 and 0.250 mg/mL. The IC_{50} of S2-WF was below 0.0156 mg/mL for both phases, while molnupiravir's IC_{50} was under 0.0039 mg/mL (**Figure 12)**. Despite limitations in determining S2-WF's IC_{50}, it appears comparable to molnupiravir. As the most promising anti-SARS-CoV-2 agent, S2-WF (WF-MLCE) was selected for further evaluation of its antiviral compounds and potential interactions with the SARS-CoV-2 Mpro.

Table 3 Anti-SARS-CoV-2 efficacy of nine crude extracts in pre-entry and post-infection modes using Vero E6 cells as the host.

Crude Extract	Pre-entry study			Post-infection treatment study		
	Conc.	Anti-SARS-CoV-2 efficiency		Conc.	Anti-SARS-CoV-2 efficiency	
	(mg/mL)	Log Reduction	% Virucidal	(mg/mL)	Log Reduction	% Inhibition
S1	0.0156	2.10 ± 0.22	99.21 ± 0.26	0.0625	2.52 ± 0.22	99.69 ± 0.13
	0.0078	2.10 ± 0.22	99.21 ± 0.26	0.0313	2.35 ± 0.14	99.56 ± 0.17
	0.0039	1.98 ± 0.14	98.96 ± 0.32	0.0156	2.27 ± 0.21	99.46 ± 0.18
S2	0.0625	2.10 ± 0.22	99.21 ± 0.26	0.0313	2.60 ± 0.21	99.75 ± 0.08
	0.0313	2.02 ± 0.12	99.08 ± 0.16	0.0156	2.40 ± 0.30	99.54 ± 0.36
	0.0156	1.98 ± 0.07	99.00 ± 0.00	0.0078	2.52 ± 0.44	99.62 ± 0.26
S3	0.1250	2.06 ±0.14	99.16 ± 0.18	0.0313	2.52 ± 0.22	99.69 ± 0.13
	0.0625	2.02 ±0.02	99.08 ± 0.16	0.0156	2.31 ± 0.38	99.45 ± 0.27
	0.0313	1.94 ±0.15	98.88 ± 0.23	0.0078	2.35 ± 0.30	99.53 ± 0.24
S4	0.0313	1.98 ± 0.07	99.00 ± 0.00	0.1250	2.10 ± 0.22	99.21 ± 0.26
	0.0156	1.94 ± 0.15	98.88 ± 0.23	0.0625	2.02 ± 0.02	99.08 ± 0.16
	0.0078	1.94 ± 0.15	98.88 ± 0.23	0.0313	1.94 ± 0.15	98.88 ± 0.23
S5	0.0625	2.06 ± 0.22	99.13 ± 0.27	0.1250	2.12 ± 0.14	99.37 ± 0.11
	0.0313	1.98 ± 0.07	99.00 ± 0.00	0.0625	1.98 ± 0.07	98.96 ± 0.32
	0.0156	1.98 ± 0.07	99.00 ± 0.00	0.0313	1.85 ± 0.12	98.65 ± 0.23

Table 3 (continued).

Crude Extract	Pre-entry study			Post-infection treatment study		
	Conc.	Anti-SARS-CoV-2 efficiency		Conc.	Anti-SARS-CoV-2 efficiency	
	(mg/mL)	Log Reduction	% Virucidal	(mg/mL)	Log Reduction	% Inhibition
S6	0.0625	2.10 ± 0.22	99.21 ± 0.26	0.0625	2.44 ± 0.07	99.65 ± 0.07
	0.0313	2.06 ± 0.14	99.12 ± 0.39	0.0313	2.19 ± 0.14	99.37 ± 0.11
	0.0156	2.02 ± 0.12	99.04 ± 0.37	0.0156	1.94 ± 0.07	98.88 ± 0.23
S7	0.0625	2.06 ± 0.22	99.13 ± 0.27	0.0625	1.94 ± 0.07	98.88 ± 0.23
	0.0313	2.02 ± 0.17	99.04 ± 0.37	0.0313	1.98 ± 0.07	99.00 ± 0.00
	0.0156	1.94 ± 0.07	98.88 ± 0.23	0.0156	1.85 ± 0.12	98.65 ± 0.23
S8-L (Light-water soluble)	0.0156	2.27 ± 0.21	99.46 ± 0.18	0.1250	2.56 ± 0.30	99.68 ± 0.25
	0.0078	2.35 ± 0.49	99.31 ± 0.66	0.0625	2.31 ± 0.38	99.45 ± 0.27
	0.0039	2.27 ± 0.43	99.27 ± 0.61	0.0313	2.06 ± 0.14	99.16 ± 0.18
S8-D (Dark-gummy)	0.0625	2.56 ± 0.30	99.68 ± 0.25	0.1250	2.94 ± 0.07	99.89 ± 0.02
	0.0313	2.44 ± 0.28	99.60 ± 0.23	0.0625	2.65 ± 0.25	99.77 ± 0.10
	0.0156	2.31 ± 0.38	99.45 ± 0.27	0.0313	2.56 ± 0.22	99.73 ± 0.08

Data are presented as mean ± SD from quadruplicate experiments. Log reduction represents the decrease in viral titer following treatment, calculated in a logarithmic scale. % Virucidal or % Inhibition denotes the percentage reduction in viral titer relative to the initial viral load. The herbal names for S1-S8 are provided in Table A1.

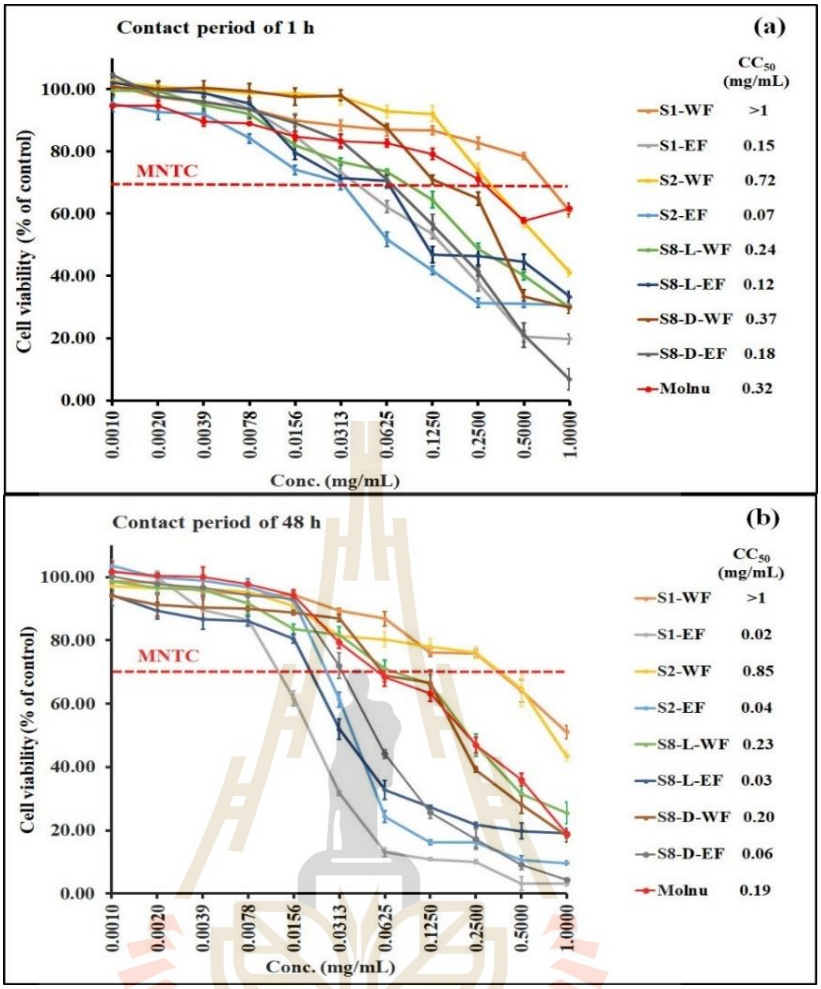

Figure 11 Cytotoxicity of water fractions (WF) and ethyl acetate fractions (EF) from the selected four crude extracts and molnupiravir (Molnu) evaluated in Vero E6 cells. (a) Cytotoxicity after 1 h of treatment with fractions/drugs, and (b) after 48 h of treatment with fractions/drugs. Results are presented as % cell viability (mean ± SD) at various extract concentrations, with CC50 values. The red dotted line represents the minimum non-toxic concentration (MNTC), defined as the concentration achieving ≥ 70% cell viability for each fraction. Sample (S) full names are provided in Table A2.

Table 4 Anti-SARS-CoV-2 efficacy of molnupiravir using Vero E6 cells as the host.

Pre-entry study			Post-infection treatment study		
[Molnupiravir]	Anti-SARS-CoV-2 efficacy		[Molnupiravir]	Anti-SARS-CoV-2 efficacy	
(mg/mL)	Log Reduction	% Virucidal	(mg/mL)	Log Reduction	% Inhibition
0.0625	2.76 ± 0.21	99.81 ± 0.09	0.0625	2.05 ± 0.08	99.08 ± 0.16
0.0313	2.55 ± 0.20	99.69 ± 0.13	0.0313	1.93 ± 0.09	98.77 ± 0.27
0.0156	2.22 ± 0.26	99.30 ± 0.36	0.0156	1.84 ± 0.12	98.48 ± 0.48
0.0078	2.05 ± 0.23	99.02 ± 0.41	0.0078	1.55 ± 0.20	96.89 ± 1.30
0.0039	1.76 ± 0.18	98.11 ± 0.85	0.0039	1.47 ± 0.06	96.47 ± 0.74

Data are presented as mean ± SD from quadruplicate experiments. Log reduction represents the decrease in viral titer following treatment, calculated in a logarithmic scale. % Virucidal or % Inhibition denotes the percentage reduction in viral titer relative to the initial viral load.

Table 5 Anti-SARS-CoV-2 efficacy of water fraction and ethyl acetate fraction obtained from liquid–liquid fractionation of the four crude extracts using Vero E6 cells as the host.

Extract	Pre-entry study			Post-infection treatment study		
	Conc.	Anti-SARS-CoV-2 efficacy		Conc.	Anti-SARS-CoV-2 efficacy	
	(mg/mL)	Log Reduction	% Virucidal	(mg/mL)	Log Reduction	% Inhibition
S1-WF	0.5000	2.52 ± 0.14	99.71 ± 0.05	0.500	1.64 ±0.27	97.63 ± 1.03
	0.250	2.35 ± 0.30	99.53 ± 0.24	0.2500	1.73 ±0.20	98.05 ± 0.94
	0.1250	2.27 ± 0.30	99.44 ± 0.23	0.1250	1.98 ±0.69	98.28 ± 1.29
S1-EF	0.0313	2.69 ± 0.22	99.79 ± 0.08	0.0313	2.31 ± 0.38	99.45 ± 0.27
	0.0156	2.44 ± 0.23	99.62 ± 0.20	0.0156	2.40 ± 0.33	99.54 ± 0.27
	0.0078	2.35 ± 0.14	99.56 ± 0.17	0.0078	2.44 ± 0.07	99.65 ± 0.07
S2-WF	0.250	3.06 ± 0.14	99.92 ± 0.02	0.2500	2.90 ± 0.07	99.88 ± 0.03
	0.1250	2.65 ± 0.25	99.77 ± 0.10	0.1250	2.90 ± 0.07	99.88 ± 0.03
	0.0625	2.44 ± 0.07	99.65 ± 0.07	0.0625	2.48 ± 0.30	99.63 ± 0.23
S2-EF	0.0313	2.44 ± 0.07	99.65 ±0.07	0.0313	2.02 ± 0.12	99.04 ± 0.37
	0.0156	2.35 ± 0.47	99.04 ±0.59	0.0156	2.10 ± 0.18	99.17 ± 0.34
	0.0078	2.10 ± 0.22	99.21 ±0.26	0.0078	2.35 ± 0.35	99.46 ± 0.38

Table 5 (continued).

Extract	Pre-entry study			Post-infection treatment study		
	Conc. (mg/mL)	Anti-SARS-CoV-2 efficacy		Conc. (mg/mL)	Anti-SARS-CoV-2 efficacy	
		Log Reduction	% Virucidal		Log Reduction	% Inhibition
S8-L-WF	0.0625	2.44 ± 0.07	99.65 ±0.07	0.0625	2.19 ± 0.14	99.37 ± 0.11
	0.0313	2.35 ± 0.30	99.53 ±0.24	0.0313	1.85 ± 0.12	98.65 ± 0.23
	0.0156	2.10 ± 0.22	99.21 ±0.26	0.0156	1.81 ± 0.25	98.34 ± 1.03
S8-L-EF	0.0625	2.44 ± 0.48	99.51 ± 0.42	0.0625	2.02 ± 0.12	99.04 ± 0.37
	0.0313	2.31 ± 0.38	99.45 ± 0.27	0.0313	1.94 ± 0.21	98.85 ± 0.38
	0.0156	2.44 ± 0.07	99.53 ± 0.24	0.0156	1.85 ± 0.14	98.65 ± 0.23
S8-D-WF	0.1250	1.94 ± 0.10	98.85 ± 0.38	0.1250	1.56 ± 0.22	97.26 ± 0.85
	0.0625	2.69 ± 0.22	99.79 ± 0.08	0.0625	1.52 ± 0.22	96.89 ± 1.30
	0.0313	2.65 ± 0.25	99.77 ± 0.10	0.0313	1.44 ± 0.07	96.47 ± 0.74
S8-D-EF	0.0625	2.85 ± 0.14	99.86 ± 0.02	0.0625	2.31 ± 0.38	99.45 ± 0.27
	0.0313	2.52 ± 0.14	99.71 ± 0.05	0.0313	2.27 ± 0.30	99.44 ± 0.23
	0.0156	2.35 ± 0.30	99.53 ± 0.24	0.0156	2.19 ± 0.14	99.37 ± 0.11

Data are presented as mean ± SD from quadruplicate experiments. WF, water fraction; EF, ethyl acetate fraction; Conc., tested extract concentration; Log reduction represents the decrease in viral titer following treatment, calculated in logarithmic scale. % Virucidal or % Inhibition denotes the percentage reduction in viral titer relative to the initial viral load.

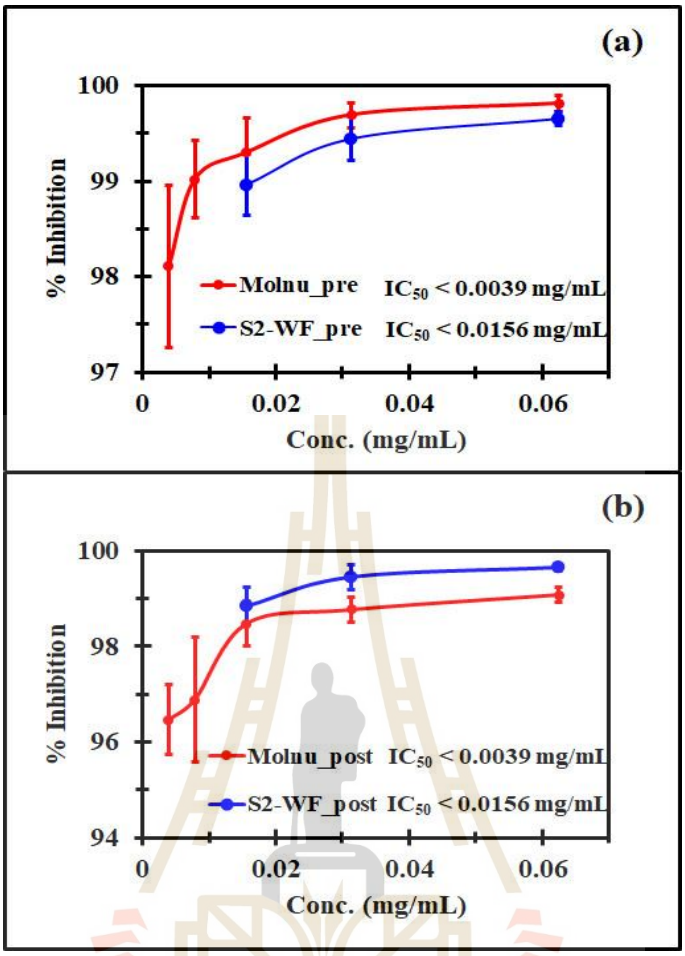

Figure 12 Anti-SARS-CoV-2 activity and IC50 values of molnupiravir (Molnu) and S2-WF evaluated in Vero E6 cells. (a) Antiviral activity and IC50 in the pre-entry mode; (b) Antiviral activity and IC50 in the post-infection treatment mode.

4.1.4 Evaluation of antiviral lead compounds in the most promising extract: Water fraction of mulberry leaf crude extract (WF-MLCE)

4.1.4.1 FTIR spectral profile of WF-MLCE

Figure 13 presents the FTIR spectrum of WF-MLCE, with six regions identified for classifying compound classes. Spectral band assignments are detailed in **Table A4** ((Abbas et al., 2017; Hssaini et al., 2022; Krysa et al., 2022; Wongsa et al., 2022; Zolkefali & Noh, 2017)). Regions 1, 2, and 6 include general functional groups that, while not specific for classification, contribute to the structure of polyphenolics, carbohydrates, and lipids.

Regions 3–5 are recognized as fingerprint regions for polyphenolics. Peaks at 1573 cm^{-1} and 1500–1450 cm^{-1} correspond to the C=C–C skeleton and C–H bonds of aromatic rings, including phenols. Coabsorbances at 1540–1140 cm^{-1} are characteristic of flavonoids, involving C=O and C=C bonds of phenol groups, as well as –C–OH, C–H, and O–H deformations in aromatic rings. Distinct bands at 1041 cm^{-1}, 990 cm^{-1}, and a smaller band at 1103 cm^{-1} indicate sugar content. Bands in the 1100–1075 cm^{-1} range, attributed to the C–H of Ring B in flavonoids, were also observed. The FTIR profile of WF-MLCE suggests a dominance of flavonoids, particularly flavonols and flavonoid glycosides, alongside moderate levels of phenolic and carboxylic acid compounds.

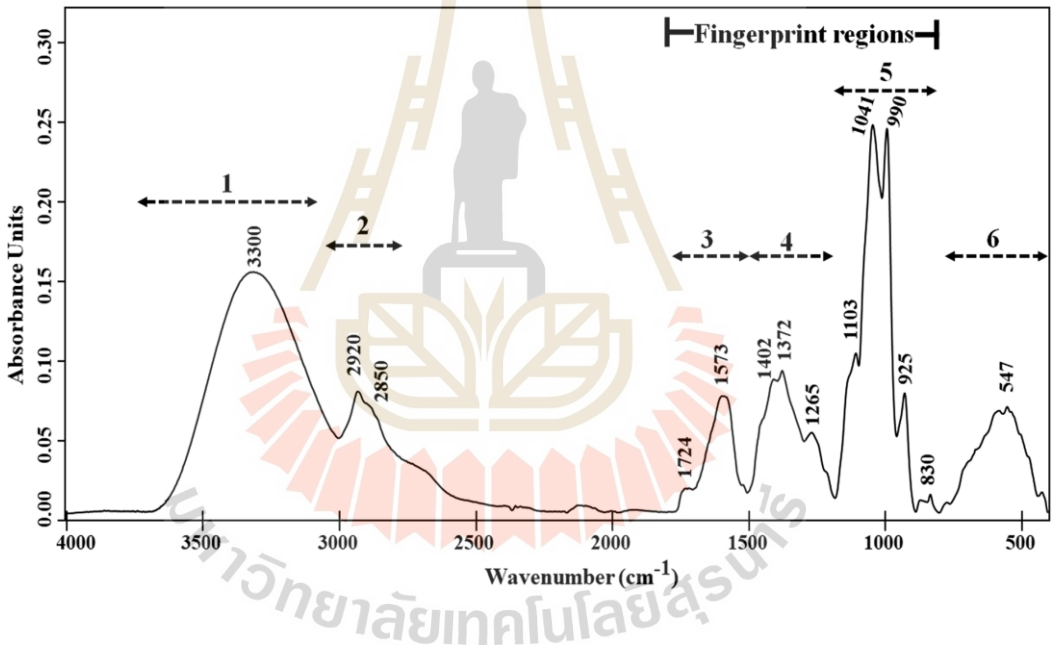

Figure 13 FTIR spectrum of water fraction of mulberry leaf crude extract (S2-WF).

4.1.4.2 Partial separation of WF-MLCE by CC

Five chromatographic fractions (F1–F5) were obtained from the CC of WF-MLCE, with F1–F4 eluted using water and F5 using 50% aqueous ethanol (**Figure 14**). No absorbance peaks were detected with absolute ethanol elution. F1–F5 were subsequently analyzed for antiviral lead compounds, including anti-SARS-

CoV-2 efficacy testing, antioxidant activity, LC–HRMS profiling, and molecular docking analysis.

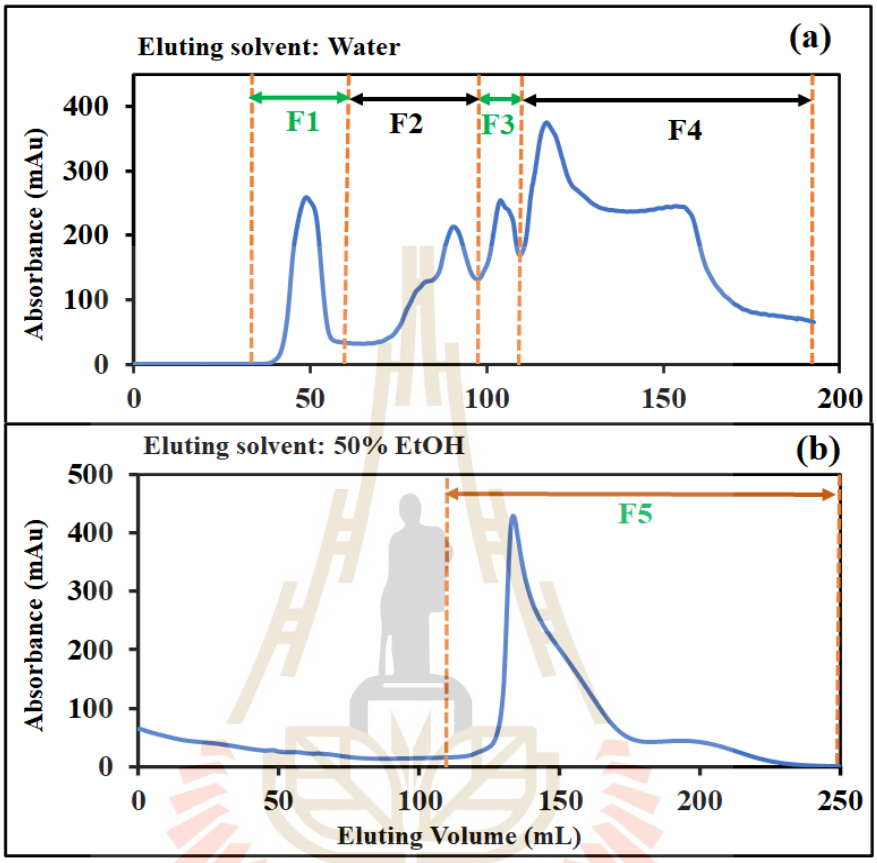

Figure 14 Fractionation of WF-MLCE (S2-WF) using Sephadex LH-20 column chromatography: (a) fractions eluted with water and (b) fractions eluted with 50% ethanolic aqueous.

4.1.4.3 Identification of tentative phytochemicals in CC fractions of WF-MLCE using LC-HRMS technique

The five fractions were analyzed using LC–HRMS to identify their chemical constituents. A total of 213 putative compounds were detected, including polyphenolics, sugars and derivatives, amino/organic acids, and peptides. **Table 6** lists the 18 compounds found in F1, with 4-O-caffeoylquinic acid and trans-5-O-caffeoylquinic acid as the most prevalent polyphenolics. Benzoyl derivatives and amino acids/amino-sugar groups were also observed. **Table 7** shows the 29

compounds in F5, with 1-deoxynojirimycin (DNJ) as the main compound. F5 also contained flavonoids and flavonoid glycosides, such as quercetin, rutin, isoquercetrin, 3,7-di-O-glucoside, astragalin, and kaempferol 3-O-rutinoside-7-O-rhamnoside. The tentative compounds for F2–F4 are listed in **Tables A5–A7**, respectively, with predominant classes including amino acids, phenolic acids, and carboxylic acids. The chemical profiles from LC–HRMS align with the FTIR spectrum of WF-MLCE.

4.1.4.4 Optimization of antiviral lead identification: Evaluation of anti- SARS-CoV-2 efficacy, TPC, and TFC of CC fractions of WF-MLCE

The antiviral activities of the five CC fractions are summarized in **Table 8**, with their cytotoxicity shown in Figure A2. Fractions F1 and F5 demonstrated strong virucidal activity, achieving LRVs > 3 (99.9% virucidal). F5 also exhibited the highest total polyphenolic content and antioxidant activity. However, no significant differences in viral inhibition efficiency were observed among the fractions in the post-infection treatment study, with LRVs ranging from 2.0 to 2.8. No clear correlation was found between total phenolic content, total flavonoid content, or antioxidant activity (**Table A8**) and anti-SARS-CoV-2 efficacy. Thus, the virucidal efficacy of the CC fractions was the sole criterion for selecting the antiviral lead fractions for further molecular docking analysis. Consequently, the tentative compounds identified in F1 and F5 were subjected to molecular docking.

4.1.4.5 *In Silico* molecular docking: Potential lead compounds as SARS-CoV-2 Mpro inhibitors

The binding affinities of tentative compounds from F1 and F5, along with repurposed drugs, against the SARS-CoV-2 Mpro are detailed in **Table 9**, expressed as binding energy (kcal/mol) and inhibition constant (Ki; μM). Hydroxychloroquine and molnupiravir showed similar binding energies (−6.09 and −6.21 kcal/mol, respectively), while lopinavir demonstrated the lowest potency (−5.65 kcal/mol). Inhibition constants aligned with these values. Among the 47 docked phytocompounds, notable F1 compounds included 5-O-caffeoylquinic acid (−6.93 kcal/mol, Ki 8.30 μM), and 4-O-caffeoylquinic acid (−6.79 kcal/mol, Ki 10.59 μM. However, their docking scores were not markedly better than those of the reference drugs.

Table 6 LC–HRMS analysis of tentative phytochemical contents of Fraction 1 (F1) of WF-MLCE (S2-WF).

No.	Tentative phytocompound	Formula	Theoretical MW	Reference ion	Average Peak Area (Most Common Adduct)
1	Adenine	$C_5H_5N_5$	135.0545	$[M+H]^+$	1.17E+08
2	UDP-N-acetylglucosamine	$C_{17}H_{27}N_3O_{17}P_2$	607.0816	$[M-H]^-$	1.03E+08
3	5-O-Caffeoylquinic acid	$C_{16}H_{18}O_9$	354.0951	$[M-H]^-$	8.53E+07
4	4-O-Caffeoylquinic acid	$C_{16}H_{18}O_9$	354.0951	$[M-H]^-$	3.36E+07
5	L-Pyroglutamic acid	$C_5H_7NO_3$	129.0426	$[M+H]^+$	4.90E+07
6	Proline	$C_5H_9NO_2$	115.0633	$[M+H]^+$	3.70E+07
7	Acetylcholine	$C_7H_{15}NO_2$	145.1103	$[M+H]^+$	3.61E+07
8	Y-L-Glutamyl-L-glutamic acid	$C_{10}H_{16}N_2O_7$	276.0958	$[M+H]^+$	2.59E+07
9	1-Stearoylglycerol	$C_{21}H_{42}O_4$	358.3083	$[M+H]^+$	2.37E+07
10	2,6-Di-tert-butyl-1,4-benzoquinone	$C_{14}H_{20}O_2$	220.1463	$[M+H]^+$	1.65E+07
11	9-Oxo-10(E),12(E)-octadecadienoic acid	$C_{18}H_{30}O_3$	294.2195	$[M+H]^+$	1.47E+07
12	12-oxo Phytodienoic Acid	$C_{18}H_{28}O_3$	292.2038	$[M+H]^+$	1.35E+07
13	4-Hydroxybenzaldehyde	$C_7H_6O_2$	122.0368	$[M+H]^+$	1.12E+07

Table 6 (continued).

No.	Tentative phytocompound	Formula	Theoretical MW	Reference ion	Average Peak Area (Most Common Adduct)
14	L-Glutathione (reduced)	$C_{10}H_{17}N_3O_6S$	307.0838	$[M+H]^+$	6.47E+06
	(2R,5R,6R)-3-[(1E,3E)-hepta-1,3-dien-1-yl]-				5.43E+06
15	5,6-dihydroxy-2-	$C_{14}H_{22}O_4$	254.1518	$[M+H]^+$	
	(hydroxymethyl)cyclohexan-1-one				
16	Jasmonic acid	$C_{12}H_{18}O_3$	210.1256	$[M-H]^-$	7.20E+06
17	Gentisic acid 5-O-β-D-glucoside	C13H16O9	316.0794	[M-H]-	4.80E+06
18	NP-014604	C19H34O10	422.2152	[M-H]-	3.17E+06

Table 7 LC–HRMS analysis of tentative phytochemical contents of Fraction 5 (F5) of WF-MLCE (S2-WF).

No.	Tentative phytocompound	Formula	Theoretical MW	Reference ion	Average Peak Area (Most Common Adduct)
1	1-deoxynorijimycin	$C_6H_{13}NO_4$	163.0845	$[M+H]^+$	5.95E+09
2	Quercetin 3-O-rutinoside [Rutin]	$C_{27}H_{30}O_{16}$	610.1534	$[M-H]^-$	5.34E+09
3	Kaempferol 3-O-neohesperidoside	$C_{27}H_{30}O_{15}$	594.1585	[M-H]-	4.25E+09
4	Quercetin 3,7-di-O-glucoside	$C_{27}H_{30}O_{17}$	626.1483	[M-H]-	3.73E+09
5	Quercetin-3β-D-glucoside [Isoquercetrin]	$C_{21}H_{20}O_{12}$	464.0955	[M-H]-	3.58E+09
6	Quercetin 3-O-rutinoside-7-O-rhamnoside [Morkotin B]	$C_{33}H_{40}O_{20}$	756.21129	[M-H]-	3.33E+09
7	Kaempferol 3-O-rutinoside	$C_{27}H_{30}O_{15}$	594.1585	[M-H]-	3.12E+09
8	Quercetin 3-O-robinobioside [Bioquercetrin]	$C_{27}H_{30}O_{16}$	610.1534	[M-H]-	2.75E+09
9	Kaempferol 3,7-di-O-glucoside	$C_{27}H_{30}O_{16}$	610.1534	[M-H]-	2.70E+09
10.1*	Kaempferol 3-O-galactoside [Trifolin]	$C_{21}H_{20}O_{11}$	448.1006	[M-H]-	2.23E+09
10.2*	Kaempferol 3-O-glucoside [Astragalin]	$C_{21}H_{20}O_{11}$	448.1006		
11	Kaempferol 3-O-rhamninoside	C33H40O19	740.2164	[M-H]-	2.18E+09
12	Kaempferol 3-O-β-D-glucosylgalactoside	$C_{27}H_{30}O_{16}$	610.1534	[M+H]+	1.47E+09

Table 7 (continued).

No.	Tentative phytocompound	Formula	Theoretical MW	Reference ion	Average Peak Area (Most Common Adduct)
13.1**	Robinin	$C_{33}H_{40}O_{19}$	740.2164	[M+H]+	1.43E+09
13.2**	Kaempferol3-O-rutinoside-7-O-rhamnoside [Marakrol B]	$C_{33}H_{40}O_{19}$	740.2164		
14	Quercetin	$C_{15}H_{10}O_7$	302.0422	[M+H]+	1.41E+09
15	Kaempferol	$C_{15}H_{10}O_6$	286.0477	[M+H]+	1.28E+09
16	Methyl cinnamate	$C_{10}H_{10}O_2$	162.0681	[M+H]+	6.51E+07
17	Luteolin-4'-glucoside	$C_{21}H_{20}O_{11}$	448.1006	$[M+H]^+$	5.18E+07
18	Luteolin-7-glucoside [Cynaroside]	$C_{21}H_{20}O_{11}$	448.1006	$[M-H]^-$	2.05E+07
19	Myricetin 3-O- β -D-galactopyranoside	$C_{21}H_{20}O_{13}$	480.0904	$[M-H]^-$	2.03E+07
20	Thiamine	C12H16N4OS	264.1045	[M+H]+	1.53E+07
21	Myricetin	C15H10O8	318.0371	[M+H]+	1.36E+07
22	1-[4-hydroxy-3-(3-methylbut-2-en-1-yl) phenyl]ethan-1-one	$C_{13}H_{16}O_2$	204.1150	$[M+H]^+$	1.15E+07
23	1,4-dihydroxyheptadec-16-en-2-yl acetate	$C_{19}H_{36}O_4$	328.26076	$[M+H]^+$	1.06E+07
24	Formonetin	$C_{16}H_{12}O_4$	268.0736	$[M+H]^+$	8.06E+06

Table 7 (continued).

No.	Tentative phytocompound	Formula	Theoretical MW	Reference ion	Average Peak Area (Most Common Adduct)
25	4-((3S)-7-hydroxy-8-(3-methylbut-2-en-1-yl)-3,4-dihydro-2H-1-benzopyran-3-yl) benzene-1,3-diol	$C_{20}H_{22}O_4$	326.1518	$[M+H]^+$	7.00E+06
26	Resveratrol	$C_{14}H_{12}O_3$	228.0786	$[M-H]^-$	5.20E+06
27	Apigetrin	$C_{21}H_{20}O_{10}$	432.1057	$[M-H]^-$	4.65E+06
28	Bayin	$C_{21}H_{20}O_9$	416.1107	$[M-H]^-$	4.24E+06
29	2-(2-Oxo-8,9-dihydro-2H-furo(2,3-h) chromen-8-yl)-2-propanyl beta-D-glucopyranoside	$C_{20}H_{24}O_9$	408.1420	$[M-H]^-$	3.20E+06

Table 8 Anti-SARS-CoV-2 efficacy of the five fractions (F1-F5) obtained from column chromatography of WF-MLCE.

Fraction	Pre-entry study			Postinfection treatment study		
	Conc. (mg/mL)	Anti-SARS-CoV-2 efficacy		Conc. (mg/mL)	Anti-SARS-CoV-2 efficacy	
		Log Reduction	% Virucidal		Log Reduction	% Inhibition
F1	1.00	3.31 ± 0.22	99.95 ± 0.03	0.0156	2.44 ± 0.07	99.65 ± 0.07
	0.50	3.19 ± 0.30	99.93 ± 0.04	0.0078	2.65 ± 0.27	99.74 ± 0.17
	0.25	3.02 ± 0.27	99.90 ± 0.04	0.0039	2.65 ± 0.27	99.74 ± 0.17
F2	1.00	2.69 ± 0.30	99.78 ± 0.11	0.0625	2.69 ± 0.30	99.78 ± 0.11
	0.50	2.56 ± 0.22	99.73 ± 0.08	0.0313	2.69 ± 0.30	99.78 ± 0.11
	0.25	2.44 ± 0.07	99.65 ± 0.07	0.0156	2.69 ± 0.30	99.78 ± 0.11
F3	1.00	2.78 ± 0.18	99.82 ± 0.10	0.0625	2.77 ± 0.18	99.82 ± 0.10
	0.50	2.52 ± 0.14	99.71 ± 0.05	0.0313	2.60 ± 0.21	99.75 ± 0.08
	0.25	2.10 ± 0.22	99.21 ± 0.26	0.0156	2.52 ± 0.14	99.71 ± 0.05
F4	1.00	2.81 ± 0.22	99.83 ± 0.01	0.1250	2.56 ± 0.30	99.70 ± 0.15
	0.50	2.44 ± 0.07	99.65 ± 0.07	0.0625	2.56 ± 0.30	99.70 ± 0.15
	0.25	2.27 ± 0.30	99.36 ± 0.56	0.0313	2.52 ± 0.22	99.69 ± 0.13

Table 8 (continued).

Fraction	Pre-entry study			Postinfection treatment study		
	Conc. (mg/mL)	Anti-SARS-CoV-2 efficacy		Conc. (mg/mL)	Anti-SARS-CoV-2 efficacy	
		Log Reduction	% Virucidal		Log Reduction	% Inhibition
F5	1.00	3.73 ± 0.38	99.97 ± 0.03	0.1250	1.94 ± 0.07	98.88 ± 0.23
	0.50	3.15 ± 0.38	99.92 ± 0.04	0.0625	2.35 ± 0.38	99.46 ± 0.38
	0.25	2.77 ± 0.07	99.84 ± 0.03	0.0313	2.81 ± 0.07	99.85 ± 0.00

Results are expressed as mean ± SD of quadruplicate experiments; Conc., tested concentration of fraction; Log reduction, the reduction of viral titer after experimental treatment in logarithmic function; % Inhibition or % Virucidal, % viral titer reduction by comparing with the initial viral load.

F5 contained promising compounds, particularly glycoside derivatives of flavonoids, with strong binding affinities for Mpro. The top three compounds were myricetin 3-O-β-D-galactopyranoside (−9.66 kcal/mol, Ki 0.08 μM), maragrol B (−9.01 kcal/mol, Ki 0.25 μM), and quercetin 3-O-robinobioside (−8.68 kcal/mol, Ki 0.43 μM). Rutin, a major compound in F5, also showed notable docking performance (−7.89 kcal/mol, Ki 1.65 μM). Other flavonoids, including isoquercetrin, trifolin, and kaempferol, demonstrated favorable scores as well.

Docking analysis revealed that flavonoids and their conjugates efficiently bind to the active site of SARS-CoV-2 Mpro via hydrogen bonds. Examples of 3D binding interactions for molnupiravir, rutin, and myricetin 3-O-β-D-galactopyranoside are shown in **Figure 15**. Molnupiravir formed two hydrogen bonds with Thr-54 and Glu-166 (**Figure 15a**). Rutin established five hydrogen bonds with Thr-26 (1.714 Å, 2.174 Å), Asn-142 (1.97 Å), Gly-143 (2.07 Å), and Ser-144 (1.738 Å) (**Figure 15b**). Myricetin 3-O-β-D-galactopyranoside also formed five hydrogen bonds with Thr-26 (2.134 Å), Phe-140 (2.08 Å), Leu-141 (2.046 Å), Gly-143 (2.108 Å), and His-163 (2.196 Å) (**Figure 15c**).

Table 9 Molecular docking scores of drugs and tentative phytochemical constituents from F1 and F5 with SARS-CoV-2 main protease (Mpro, PDB: 6LU7).

No.	Drug/	Docking Score	
		Binding energy (kcal/mol)	Inhibition constant [Ki] (μM)
Drugs			
1	Lopinavir	-5.65	72.57
2	Hydroxychloroquine	-6.09	34.14
3	Molnupiravir	-6.21	28.19
Fraction 1			
1	Adenine	-3.85	1510.00
2	UDP-N-acetylglucosamine	-4.84	285.00
3	trans-5-*O*-Caffeoylquinic acid	-6.93	8.30
4	4-*O*-Caffeoylquinic acid	-6.79	10.59
5	L-Pyroglutamic acid	-4.37	624.24

Table 9 (continued).

No.	Drug/	Docking Score	
		Binding energy (kcal/mol)	Inhibition constant [Ki] (μM)
6	Proline	-4.89	261.92
7	Acetylcholine	-3.65	2090.00
8	γ-L-Glutamyl-L-glutamic acid	-4.54	470.12
9	1-Stearoylglycerol	-5.58	81.76
10	2,6-Di-tert-butyl-1,4-benzoquinone	-5.37	116.65
11	9-Oxo-10(E),12(E)-octadecadienoic acid	-4.52	484.03
12	12-oxo Phytodienoic Acid	-5.14	171.92
13	4-Hydroxybenzaldehyde	-4.03	1120.00
14	L-Glutathione (reduced)	-5.28	135.89
15	(2R,5R,6R)-3-((1E,3E)-hepta-1,3-dien-1-yl)-5,6-dihydroxy-2-(hydroxymethyl) cyclohexan-1-one	-6.74	11.52
16	Jasmonic acid	-5.13	173.67
17	Gentisic acid 5-O-β-D-glucoside	-5.84	52.46
Fraction 5			
1	1-deoxynorijimycin	-4.57	444.76
2	Quercetin 3-*O*-rutinoside [Rutin]	-7.89	1.65
3	Kaempferol 3-*O*-neohesperidoside	-6.36	21.82
4	Quercetin 3,7-di-*O*-glucoside	-7.50	3.19
5	Quercetin-3β-D-glucoside [Isoquercetrin]	-7.62	2.59
6	Quercetin 3-*O*-rutinoside-7-*O*-rhamnoside [Morkotin B]	-6.10	33.81
7	Kaempferol 3-O-rutinoside [Nicotiflorin]	-7.04	6.91

Table 9 (continued).

No.	Drug/Compound	Docking Score	
		Binding energy (kcal/mol)	Inhibition constant [Ki] (μM)
Fraction 5 (Continued)			
8	Quercetin 3-*O*-robinobioside [Bioquercetrin]	-8.68	0.43
9	Kaempferol 3,7-di-*O*-glucoside	-7.86	1.73
10	Kaempferol 3-*O*-galactoside [Trifolin]	-8.10	1.15
11	Kaempferol 3-*O*-glucoside [Astragalin]	-7.41	3.68
12	Kaempferol 3-*O*-rhamninoside	-5.24	143.24
13	Kaempferol 3-*O*-β-D-glucosylgalactoside	-6.04	37.27
14	Kaempferol 3-*O*-robioside-7-*O*-rhamnoside [Robinin]	-5.43	105.35
15	Kaempferol 3-*O*-rutinoside-7-*O*-rhamnoside [Maragrol B]	-9.01	0.25
16	Quercetin	-6.91	8.61
17	Kaempferol	-7.38	3.89
18	Methyl cinnamate	-4.64	394.66
19	Luteolin-4'-glucoside	-7.54	2.99
20	Luteolin-7-glucoside [Cynaroside]	-7.51	3.11
21	Myricetin 3-*O*- β -D-galactopyranoside	-9.66	0.08
22	Thiamine	-5.82	54.60
23	Myricetin	-6.93	8.35
24	1-(4-hydroxy-3-(3-methylbut-2-en-1-yl) phenyl) ethan-1-one	-6.23	27.35
25	1,4-dihydroxyheptadec-16-en-2-yl acetate	-5.74	62.50
26	Formonetin	-6.96	7.97

Table 9 (Continued).

No.	Drug/Compound	Docking Score	
		Binding energy (kcal/mol)	Inhibition constant [Ki] (μM)
Fraction 5 (Continued)			
27	4-((3S)-7-hydroxy-8-(3-methylbut-2-en-1-yl)-3,4-dihydro-2H-1-benzopyran-3-yl) benzene-1,3-diol	-6.91	8.56
28	Resveratrol	-6.51	16.99
29	Apigetrin	-7.82	1.84
30	Bayin	-8.65	0.46
31	2-(2-Oxo-8,9-dihydro-2H-furo(2,3-h) chromen-8-yl)-2-propanyl beta-D-glucopyranoside	-8.38	0.72

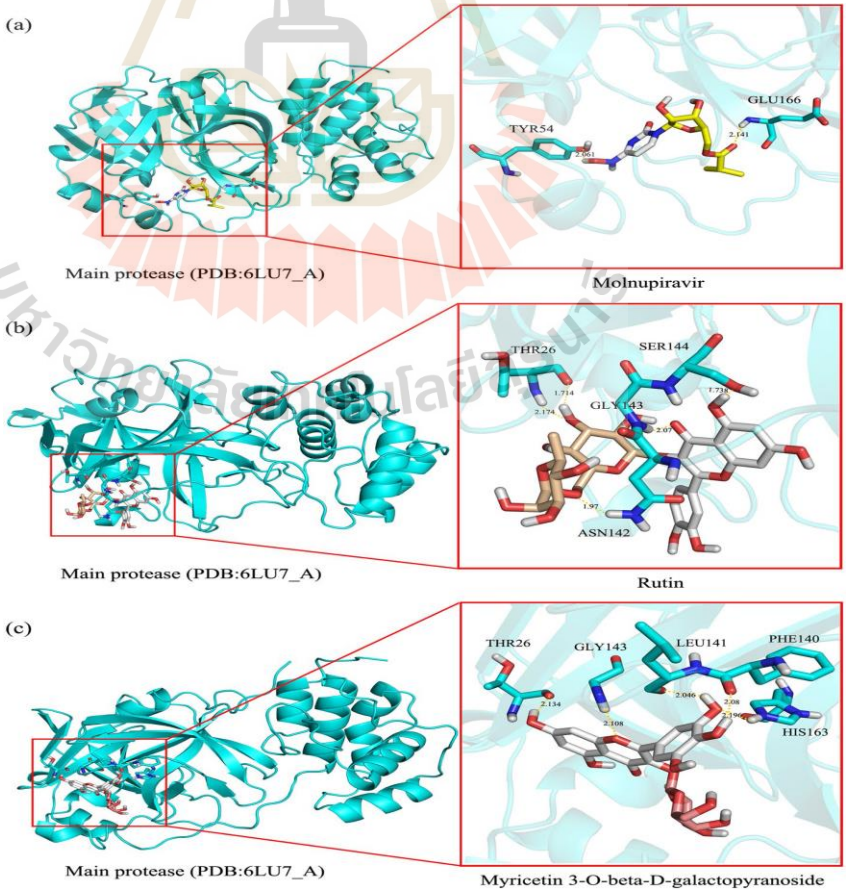

Figure 15 Three-dimensional molecular docking of key bioactive compounds with the active site of SARS-CoV-2 main protease (Mpro). Zoomed views of interaction patterns are shown in the right panels. Panels (a), (b), and (c) illustrate molecular interactions of molnupiravir, rutin, and myricetin 3-O-β-D-galactoside, respectively, with Mpro amino acid residues. The cyan ribbon represents the 3D structure of Mpro (PDB code: 6lu7_A). Color coding: cyan for carbon in Mpro, yellow for carbon in molnupiravir, wheat for carbon in rutin, deep salmon for carbon in myricetin 3-O-β-D-galactoside, gray for hydrogen, blue for nitrogen, and red for oxygen. Binding residues are marked according to Mpro sequence numbering, with hydrogen bonds depicted as yellow dashed lines and distances provided in Å.

4.2 Phase 2: Mechanism of Action Study

4.2.1 Modification of WF-MLCE extraction method

4.2.1.1 Chemical profile of water-soluble extracts of mulberry (*Morus alba*) leaves SARS-CoV-2 Mpro inhibitors

Based on Phase 1 results, the water-soluble fraction of mulberry leaf crude extract (WF-MLCE) exhibited the highest anti-SARS-CoV-2 efficacy. Consequently, the modification of the mulberry leaf extract was simplified, focusing on water-soluble compounds as the key active constituents against SARS-CoV-2. Method 1, derived from Phase 1 (WF-EtAct), was modified in Method 2 by using water alone for liquid fractionation to isolate water-soluble components from crude extract (WF-W), while Method 3 involved macerating leaf powder with water during the initial crude extraction (WCE). The chemical compositions of the resulting extracts were analyzed using FTIR spectra (**Figure 16**) and determination of total phenolic content (TPC) and total flavonoid content (TFC) (**Table 10**).

As illustrated in **Figure 16**, Region 1 (3600–3000 cm^{-1}) corresponds to the stretching vibration of polymeric hydroxyl groups (-OH) and hydrogen bond vibrations. Region 2 (3000–2800 cm^{-1}) is attributed to CH_2 and CH_3 stretching vibrations, with absorptions around 2925 cm^{-1} and 2850 cm^{-1} from CH_3 and CH_2 groups, respectively. Region 3 features a peak at 1724 cm^{-1}, indicating ester

carbonyl groups (C=O) in carboxylic acids, while absorptions between 1670–1520 cm^{-1} are due to CH and C=C vibrations in aromatic rings. Region 4 (1500–1450 cm^{-1}) shows CH stretching and overlapping vibrations of various functional groups like phenolics and flavonoids, with deformation of OH, CO, CH, and C=C bonds between 1540–1140 cm^{-1}. Region 5 (1041–990 cm^{-1}) corresponds to C–O–C vibrations in sugar and carbohydrate molecules, with additional peaks at 1103 cm^{-1} and 925 cm^{-1}, indicative of flavonoids and flavonoid glycosides. Region 6 (900–400 cm^{-1}) includes out-of-plane CH bending, typical for terpenoids, aromatics, and flavonoids, but this range has weaker absorption signals (Hssaini et al., 2022; Nangare et al., 2021).

Overall, functional groups in regions 1 and 2 suggest polyphenolics, carbohydrates (monosaccharides, disaccharides), amino acids, and carboxylic acids. The CH_2 and CH_3 vibrations (3000–2700 cm^{-1}) are associated with fatty acids or hydrocarbons (Hssaini et al., 2022; Krysa et al., 2022; Walkowiak-Bródka et al., 2022; Wongsa et al., 2022). WCE (water-crude extract) exhibited significantly lower absorption in this range, possibly due to its inability to extract non-polar or slightly polar compounds, such as terpenoids.

The FTIR spectral profile of the WCE extract differs from other extracts in regions 3, 4, and 5, which correspond to the main functional groups of polyphenolics and cyclic compounds commonly found in secondary metabolites with biological activity. These compounds typically have neutral to slightly polar properties. The 80EtOH-Crude extract, WF-EtAct, and WF-W extracts show similar FTIR profiles, particularly in region 5, with overlapping peaks that align with their higher TPC and TFC values. In contrast, the WCE extract has fewer overlapping peaks, indicating a less complex chemical composition, likely due to the use of water as the sole solvent. This results in a more polar and less diverse extract, which may explain its lower phenolic content and potentially weaker antiviral activity. FTIR and TPC/TFC analysis confirm that WCE has the lowest polyphenolic content (**Table 10**).

Statistical analysis of LC-HRMS mass spectral data corroborated the findings, showing that the chemical profile of WF-EtAct closely resembled that of WF-W but differed significantly from WCE. Principal component analysis (PCA) clearly separated WCE from WF-EtAct and WF-W, with PC1(+) accounting for 42.5% of the variance (**Figure 17**). No distinct separation between WF-EtAct and WF-W was observed,

as their score distributions were closely grouped along the y-axis of PC2. The volcano plot of metabolite abundance fold change and t-tests (X-axis: log2(fold change, FC); Y-axis: −log10 (adjusted for false discovery rate)) confirmed a similar phytochemical profile between WF-EtAct and WF-W, with most Log2FC ratios clustering near zero (**Figure 18**). Some compounds, significantly more abundant in WF-EtAct, are highlighted in the yellow zone. Tentative identifications indicated these compounds were acyl long-chain acids and polyhydroxy fatty acids, such as 9,12,13-Trihydroxy-10,15-octadecadienoic acid and hexadecanedioic acid (data not shown). Despite similar chemical profiles between WF-EtAct and WF-W, further testing of WF-W against SARS-CoV-2 is needed to evaluate its antiviral efficacy compared to WF-EtAct.

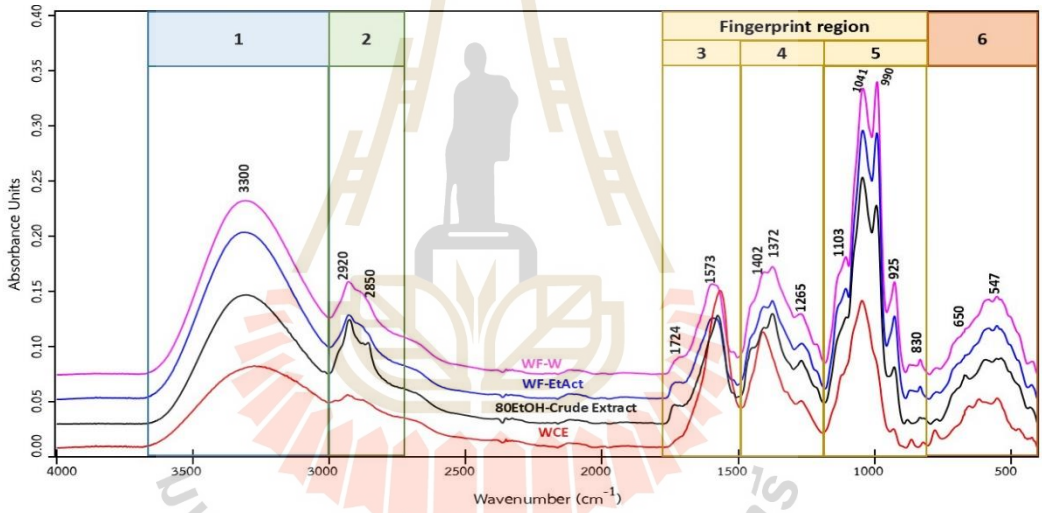

Figure 16 FTIR spectral profiles of mulberry leaf extracts obtained from different preparation methods. 80Et-OH-Crude Extract, mulberry leaf crude extract; WF-EtAct, resulted extract obtained from Method 1 (Phase 1 method); WF-W, resulted extract obtained from Method 2; WCE, resulted extract obtained from Method 3.

Table 10 The yield of the extracts by different methods and the total polyphenolic content (mean ± SD).

Extract	% yield[A] in dried ML powder	% yield* in crude extract	TPC* (mg GAE/g extract)	TFC* (mg QE/g extract)
1) 80EtOH-Crude Extract (Phase 1-CE)	20.9 ± 0.6	-	39.6 ± 2.3b	38.5 ± 0.8c
2) WF-EtAct (Method 1)	17.0 ± 0.5	79.6 ± 0.4[a]	44.9 ± 1.8[a]	57.2 ± 2.5[b]
3) WF-W (Method 2)	13.8 ± 1.1	62.9 ± 1.7[b]	45.8 ± 0.4[a]	60.3 ± 1.6[a]
4) WCE (Method 3)	21.5 ± 0.9	-	22.1 ± 0.7[c]	27.6 ± 1.0[d]

ML, Mulberry leaves; TPC, Total Phenolic Content; TFC, Total Flavonoid Content; mg GAE, milligram equivalent of gallic acid; mg QE, milligram equivalent of quercetin; [A], no statistical comparison; * indicates significant differences ($p<0.05$) when comparing different mulberry leaf extracts within the same column, with different superscript letters representing significant differences.

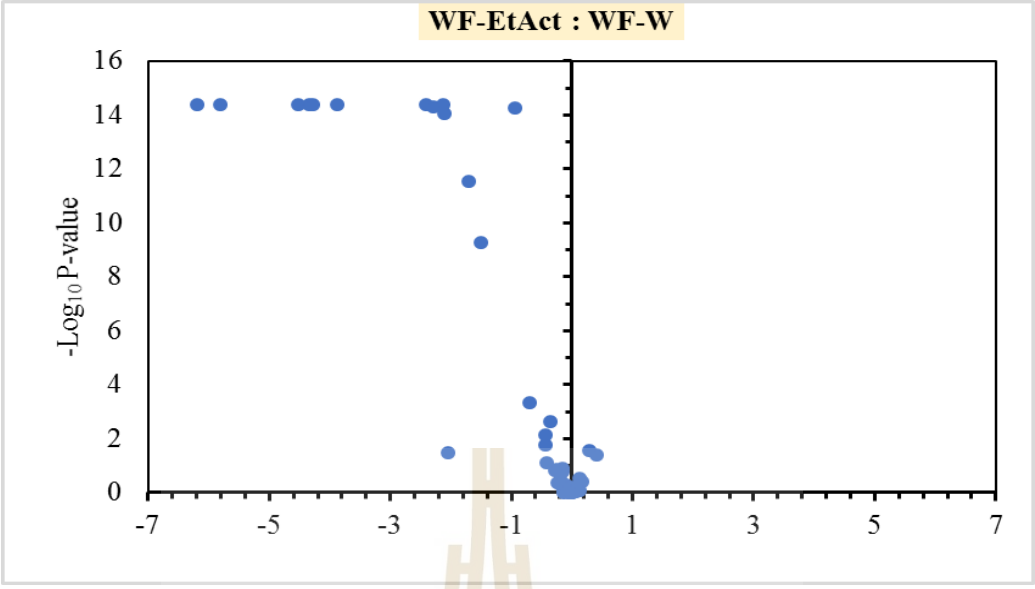

Figure 17 Volcano plot of differential metabolites between WF-EtAct and WF-W extracts. Dots in the yellow zone represent metabolites with significantly higher abundance in WF-EtAct, while dots near zero indicate metabolites with no significant difference in abundance between the two extracts (-1 <Log_2FC <1).

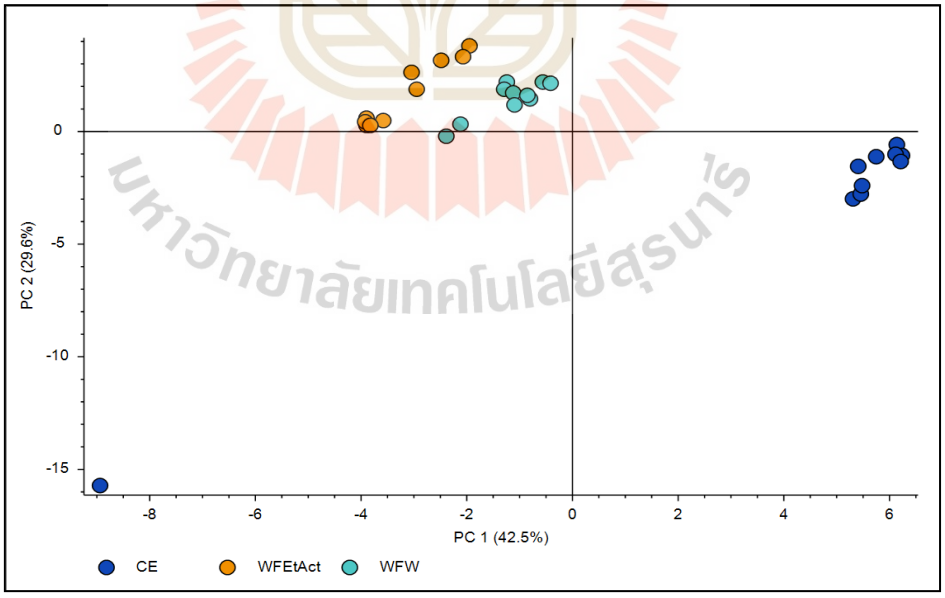

Figure 18 Score plot of principal component analysis (PCA) based on LC-MS spectra of three mulberry leaf extracts.

4.2.1.2 Cytotoxicity and anti-SARS-CoV-2 efficacy of water-soluble extracts of mulberry leaves

Cytotoxicity testing of WF-EtAct, WF-W, molnupiravir, and rutin over a 1-h exposure showed that all four substances were relatively safe, with Calu-3 cell viability at MNTC >1 mg/mL, except for WF-W, which had an MNTC of 0.5 mg/mL. All test substances exhibited CC_{50} values > 1 mg/mL (**Figure 19**). After 48 hs, WF-EtAct demonstrated the highest cellular safety (MNTC of 1 mg/mL, 78.9% viability), followed by WF-W (MNTC of 0.5 mg/mL, 85.6% viability). Rutin and molnupiravir showed higher cytotoxicity, with MNTC values of 0.25 mg/mL and 0.0625 mg/mL, respectively. All compounds had CC_{50} values > 0.5 mg/mL (**Figure 20**).

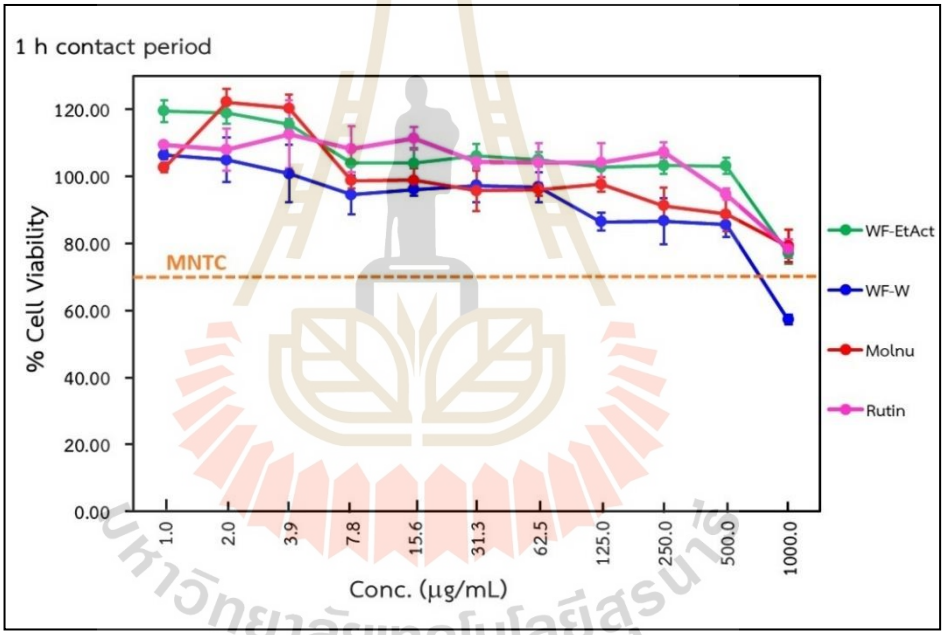

Figure 19 The cytotoxicity (expressed as % cell viability) of extracts (WF-EtAct and WF-W), molnupiravir (Molnu), and standard rutin on Calu-3 cells at different concentrations after a 1-h contact period.

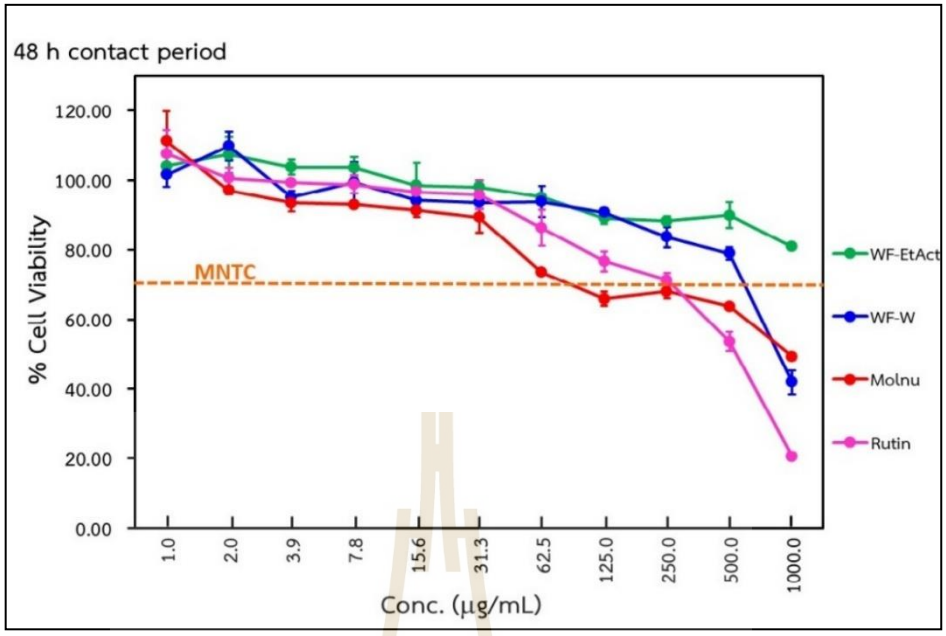

Figure 20 The cytotoxicity (expressed as % cell viability) of extracts (WF-EtAct and WF-W), molnupiravir (Molnu), and standard rutin on Calu-3 cells at different concentrations after a 48-h contact period.

In the pre-entry antiviral efficacy test (**Table 11**), using a 100 µg/mL concentration for safety (with >90% cell viability, Figure 19), WF-W demonstrated the highest SARS-CoV-2 inhibition, achieving an LRV of 2.448 (99.6% inhibition), followed by WF-EtAct with an LRV of 2.240 (99.4% inhibition). Molnupiravir and rutin exhibited similar antiviral activity, with LRVs of 2.115 (99.2% inhibition) and 2.177 (99.3% inhibition), respectively. At 10 µg/mL, WF-W maintained 99.1% inhibition, while the efficacy of the other substances significantly decreased (<99% inhibition). The IC_{50} values (**Figure 21**) confirmed that WF-W was the most effective, with the lowest IC_{50} of 0.0011 µg/mL, surpassing WF-EtAct, rutin, and molnupiravir in pre-entry mode.

The anti-SARS-CoV-2 efficacy of the four substances in post-infection mode is presented in **Table 12.** At a concentration of 100 µg/mL, WF-W exhibited superior viral inhibition (LRV 2.458, 99.6% inhibition) compared to WF-EtAct (LRV 2.052, 99.1% inhibition), outperforming both molnupiravir and rutin. However, IC_{50} values (**Figure 22**) showed that WF-W (IC_{50} 0.0100 µg/mL) and WF-EtAct (IC_{50}

0.0117 µg/mL) had higher values than rutin (IC_{50} 0.0008 µg/mL) and molnupiravir (IC_{50} 0.0025 µg/mL). The dose-response curves indicated that viral inhibition by WF-W and WF-EtAct dropped sharply below 1 µg/mL, while molnupiravir and rutin exhibited a gradual decrease in efficacy until concentrations fell below 0.01 µg/mL. These results suggest that rutin and molnupiravir may be more effective at lower concentrations, which is crucial for determining optimal dosing for viral inhibition.

Based on the cytotoxicity, antiviral activity data against SARS-CoV-2, and total polyphenolic content, the WF-W extract at a concentration of 100 µg/mL was selected for further testing in post-infection treatment mode to investigate the mechanism of antiviral activity.

Table 11 Anti-SARS-CoV-2 efficacy of WF-EtAct, WF-W, molnupiravir and rutin, expressed in log reduction value (LRV) and % inhibition, using Calu-3 cells as the host in a pre-entry mode (contact period of 1 h).

Test substance	Conc. (µg/mL)	LRV (Ave ± SD)	% Inhibition (Ave ± SD)
WF-EtAct	1000	2.760 ± 0.161	99.82 ± 0.07
	100	2.240 ± 0.086	99.42 ± 0.12
	10	1.521 ± 0.072	96.95 ± 0.50
	1	1.083 ± 0.118	91.53 ±2.07
	0.1	0.573 ± 0.086	72.86 ± 5.55
	0.01	0.271 ± 0.042	46.22 ± 4.91
	0.001	0.021 ± 0.042	4.36 ± 8.73
WF-W	1000	3.187 ± 0.125	99.93 ± 0.02
	100	2.448 ± 0.052	99.64 ± 0.04
	10	2.094 ± 0.063	99.19 ± 0.13
	1	1.573 ± 0.086	97.29 ± 0.55
	0.1	0.979 ± 0.042	89.47 ± 1.06
	0.01	0.531 ± 0.062	70.34 ± 4.31
	0.001	0.146 ± 0.042	28.28 ± 6.55

Table 11 (Continue).

Test substance	Conc. (µg/mL)	LRV (Ave ± SD)	% Inhibition (Ave ± SD)
Molnupiravir	1000	2.417 ± 0.048	99.62 ± 0.04
	100	2.115 ± 0.021	99.23 ± 0.04
	10	1.958 ± 0.048	98.89 ± 0.12
	1	1.302 ± 0.120	94.86 ± 1.58
	0.1	0.896 ± 0.219	85.88 ± 8.14
	0.01	0.333 ± 0.102	52.64 ± 10.68
	0.001	0.115 ± 0.086	22.03 ± 15.93
Rutin	1000	2.927 ± 0.098	99.88 ± 0.03
	100	2.177 ± 0.062	99.33 ± 0.09
	10	1.469 ± 0.171	96.39 ± 1.46
	1	0.927 ± 0.052	88.11 ± 1.39
	0.1	0.510 ± 0.052	68.96 ± 3.62
	0.01	0.302 ± 0.062	49.74 ± 7.11
	0.001	0.083 ± 0.059	16.87 ± 11.80

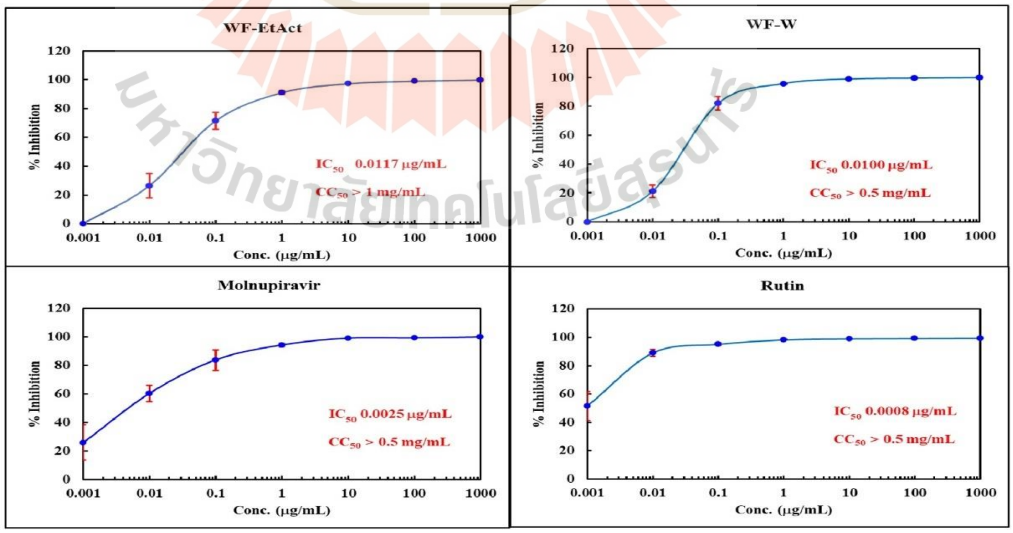

Figure 21 Anti-SARS-CoV-2 efficacy (% viral inhibition) and IC_{50} of WF-EtAct, WF-W, molnupiravir and rutin in post-infection mode (viral replication inhibition) using Calu-3 as the host.

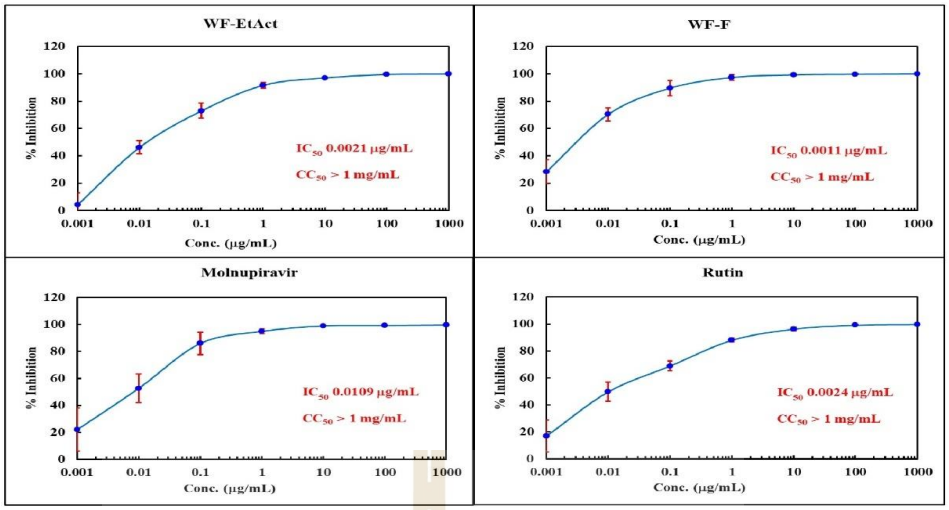

Figure 22 Anti-SARS-CoV-2 efficacy (% viral inhibition) and IC_{50} of WF-EtAct, WF-W, molnupiravir and rutin in pre-entry mode (Virucidal mode) using Calu-3 as the host.

Table 12 Anti-SARS-CoV-2 efficacy of WF-EtAct, WF-W, molnupiravir and rutin, expressed in log reduction value (LRV) and % inhibition, using Calu-3 cells as the host in a post-infection treatment mode (contact period of 48 h).

Test substance	Conc. (µg/mL)	LRV (Ave ± SD)	% Inhibition (Ave ± SD)
WF-EtAct	1000	3.031 ± 0.063	99.91 ± 0.01
	100	2.052 ± 0.063	99.11 ± 0.13
	10	1.573 ± 0.086	97.29 ± 0.55
	1	1.052 ± 0.063	91.06 ± 1.26
	0.1	0.552 ± 0.092	71.48 ± 5.88
	0.01	0.135 ± 0.052	26.40 ± 8.58
	0.001	0.000 ± 0.000	0.00 ± 0.00
WF-W	1000	3.229 ± 0.146	99.94 ± 0.02
	100	2.458 ± 0.170	99.63 ± 0.14
	10	2.021 ± 0.080	99.03 ± 0.18
	1	1.385 ± 0.052	95.86 ± 0.48
	0.1	0.760 ± 0.120	82.16 ± 4.58
	0.01	0.104 ± 0.024	21.24 ± 4.36
	0.001	0.000 ± 0.000	0.00 ± 0.00

Table 22 (Continue).

Test substance	Conc. (µg/mL)	LRV (Ave ± SD)	% Inhibition (Ave ± SD)
WF-W	1000	3.229 ± 0.146	99.94 ± 0.02
	100	2.458 ± 0.170	99.63 ± 0.14
	10	2.021 ± 0.080	99.03 ± 0.18
	1	1.385 ± 0.052	95.86 ± 0.48
	0.1	0.760 ± 0.120	82.16 ± 4.58
	0.01	0.104 ± 0.024	21.24 ± 4.36
	0.001	0.000 ± 0.000	0.00 ± 0.00
Molnupiravir	1000	4.167 ± 0.076	99.99 ± 0.00
	100	2.167 ± 0.076	99.31 ± 0.12
	10	2.052 ± 0.063	99.11 ± 0.13
	1	1.260 ± 0.098	94.40 ± 1.35
	0.1	0.823 ± 0.181	83.91 ± 7.14
	0.01	0.406 ± 0.063	60.45 ± 5.74
	0.001	0.135 ± 0.079	25.92 ± 12.42
Rutin	1000	2.198 ± 0.052	99.36 ± 0.08
	100	2.073 ± 0.052	99.15 ± 0.11
	10	1.969 ± 0.062	98.92 ± 0.17
	1	1.760 ± 0.120	98.22 ± 0.46
	0.1	1.323 ± 0.098	95.16 ± 1.02
	0.01	0.969 ± 0.092	89.07 ± 2.25
	0.001	0.323 ± 0.098	51.58 ± 10.19

4.2.2 Anti-SARS-CoV-2 mechanism of action of water-soluble extract of mulberry leaves (WF-W) in post-infection treatment mode using SR-FTIR technique

SR-FTIR imaging spectroscopy was employed to investigate the mechanism of action of the WF-W extract in post-infection treatment. Molecular insights into the interaction between the extract and viral components were

provided, revealing biomolecular changes during infection and treatment. Potential targets or pathways involved in its antiviral activity were discussed.

4.2.2.1 Impact of WF-W on biomolecular alterations in uninfected Calu-3 cells

The effect of WF-W on uninfected Calu-3 cells was evaluated by treating the cells for 1, 24, and 48 h, with SR-FTIR imaging employed to assess biomolecular changes. Untreated Calu-3 cells were used as controls. Normalized and averaged SR-FTIR spectra (n=80) for each group are shown in **Figure 23**. Notable spectral variations were observed in the wavenumber ranges of 3000–2800 cm^{-1} (CH_2 and CH_3 stretching in fatty acids of triacylglycerides), 1760–1720 cm^{-1} (C=O stretching in ester/lipid head groups), 1700–1480 cm^{-1} (Amide I and II of proteins), and 1200–1000 cm^{-1} (carbohydrates). Peak areas in these regions, expressed as percentages of total absorbance (peak area), are depicted in **Figure 24**. After 1 h of WF-W treatment, a significant increase in the peak areas for CH_2/CH_3 (3000–2800 cm^{-1}) and C=O (1740 cm^{-1}) suggested elevated lipid content, which subsequently returned to similar levels of that of control after 24 and 48 h. Protein content demonstrated an inverse trend compared to lipid content, showing a significant reduction following 1 h of WF-W treatment, followed by an increase at 24 h. A significantly notable rise in protein levels was observed at 48 h, suggesting potential stimulation of protein synthesis pathways with prolonged exposure. Conversely, carbohydrate content significantly decreased following WF-W treatment.

Figure 23 Average SR-FTIR spectra of uninfected Calu-3 cell groups treated with WF-W for various durations. Control: untreated Calu-3 cells; Calu3 WFW 1H: Calu-3 cells treated with WF-W for 1 h; Calu3 WFW 24H: Calu-3 cells treated with WF-W for 24 h; Calu3 WFW 48H: Calu-3 cells treated with WF-W for 48 h. Treated concentration of WF-W was 100 µg/mL.

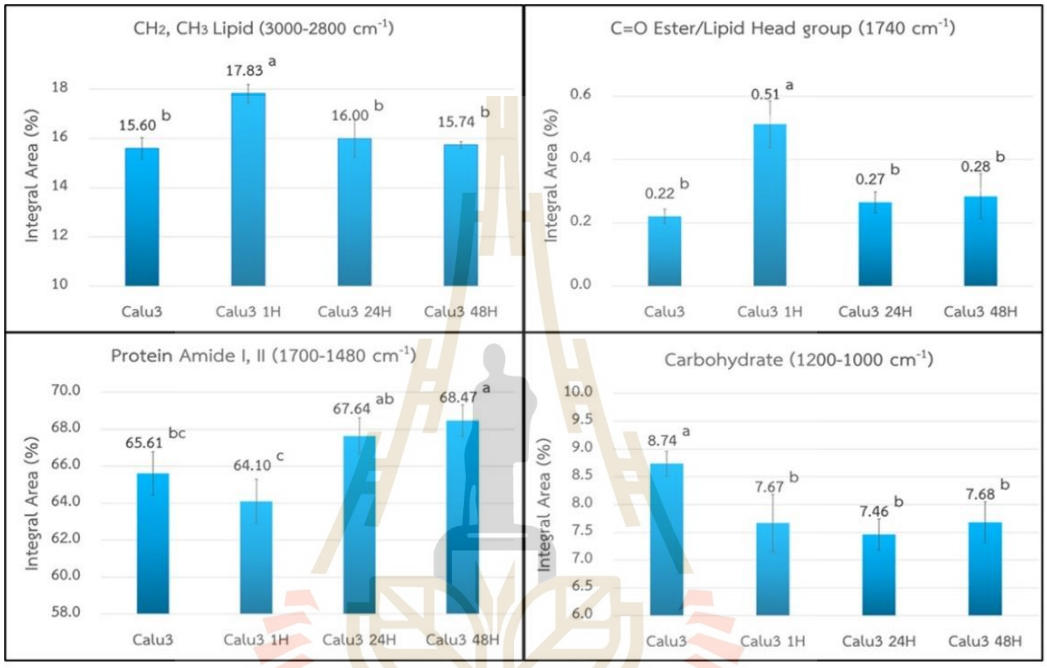

Figure 24 Peak area illustration of individual characteristic IR spectra derived from the average SR-FTIR spectra of the uninfected Calu-3 cell group treated with WF-W for various durations. Control: untreated Calu-3 cells; Calu3 WFW 1H: Calu-3 cells treated with WF-W for 1 h; Calu3 WFW 24H: Calu-3 cells treated with WF-W for 24 h; Calu3 WFW 48H: Calu-3 cells treated with WF-W for 48 h. Data are expressed by mean ± S.D. Means that those sharing the same superscript are not significantly different from each other (Tukey's HSD, $P < 0.05$).

4.2.2.2 Impact of WF-W on biomolecular alterations in SARS-CoV 2-infected Calu-3 cells: A post-infection study

The post-infection antiviral mechanisms of WF-W were investigated using SR-FTIR imaging to analyze differences in chemical composition

and functional group patterns among cell groups. The samples included uninfected Calu-3 cells (Control; **Calu3**), SARS-CoV-2-infected Calu-3 cells (**Calu3CoV2**), and infected Calu-3 cells treated with WF-W for 48 h post-infection (**Calu3CoV2WFW**). Principal component analysis (PCA) was utilized to differentiate among sample groups (n=80), ensuring that the spectral changes reflected genuine differences. FTIR spectral data underwent second-derivative processing with 13 smoothing points and EMSC correction. The PCA score plot revealed that PC1(+) distinguished normal Calu-3 cells from SARS-CoV-2-infected cells, accounting for 62% of data variance. The corresponding loading plot identified key discriminatory wavenumbers at 2921 and 2852 cm^{-1} (CH_2 and CH_3 stretching of lipid acyl chains) and 1743 and 1710 cm^{-1} (C=O stretching of ester and lipid head groups) (**Figure 25**). The PC5 score plot distinguished the viral-infected cell group with minimal variance (2%). Along the PC5 y-axis, most Calu3CoV2 samples scored below zero, while Calu3CoV2WFW samples predominantly scored above zero, with some overlap. The PC5 loading plot revealed that chemical differences between the two groups corresponded to similar wavenumbers identified in PC1. The average spectra comparison (**Figure 26**) revealed distinct differences among groups at 3000–2800 cm^{-1} (CH_2/ CH_3 in fatty acid acyl chains) and 1760–1720 cm^{-1} (C=O ester). Control Calu-3 cells exhibited the lowest lipid content based on CH_2/ CH_3 and C=O ester peak areas (**Figure 27**). Notably, the C=O ester band at 1740 cm^{-1} exhibited an increase following SARS-CoV-2 infection, but decreased after 48 hs of WF-W treatment, while still remaining higher compared to control cells.

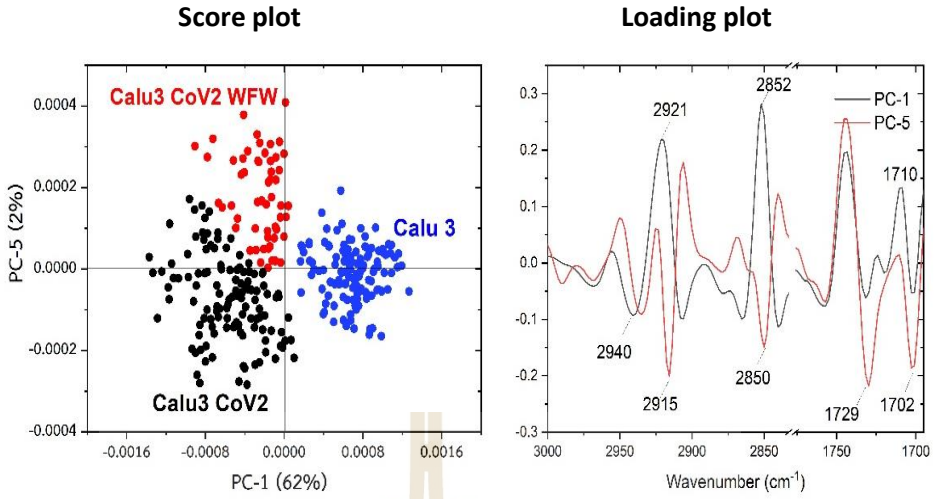

Figure 25 Principal Component Analysis (PCA) score plot (PC1 vs. PC5) of SR-FTIR data from the SARS-CoV-2-infected Calu-3 cell group, with the corresponding loading plot in the wavenumber region of 3000–1700 cm^{-1}. Groups include: **Calu3** (control as untreated, uninfected Calu-3 cells), **Calu3CoV2** (SARS-CoV-2-infected Calu-3 cells), and **Calu3CoV2WFW** (SARS-CoV-2-infected Calu-3 cells treated with 100 µg/mL WF-W for 48 h).

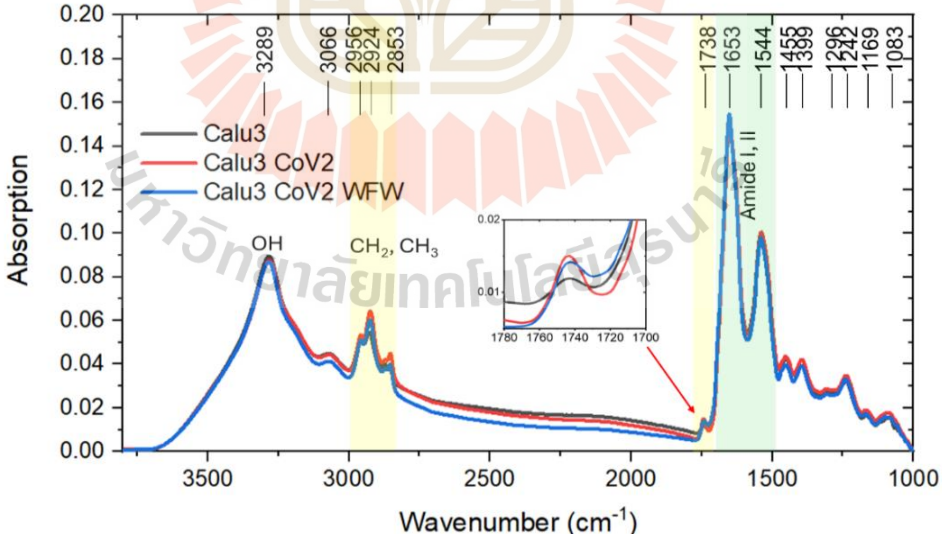

Figure 26 Average SR-FTIR spectra of the SARS-CoV-2-infected Calu-3 cell group. The groups analyzed include: Calu3 Control (untreated, uninfected Calu-3 cells), Calu3CoV2 (SARS-CoV-2-infected Calu-3 cells), and Calu3CoV2WFW (SARS-CoV-2-infected Calu-3 cells treated with 100 µg/mL WF-W for 48 h).

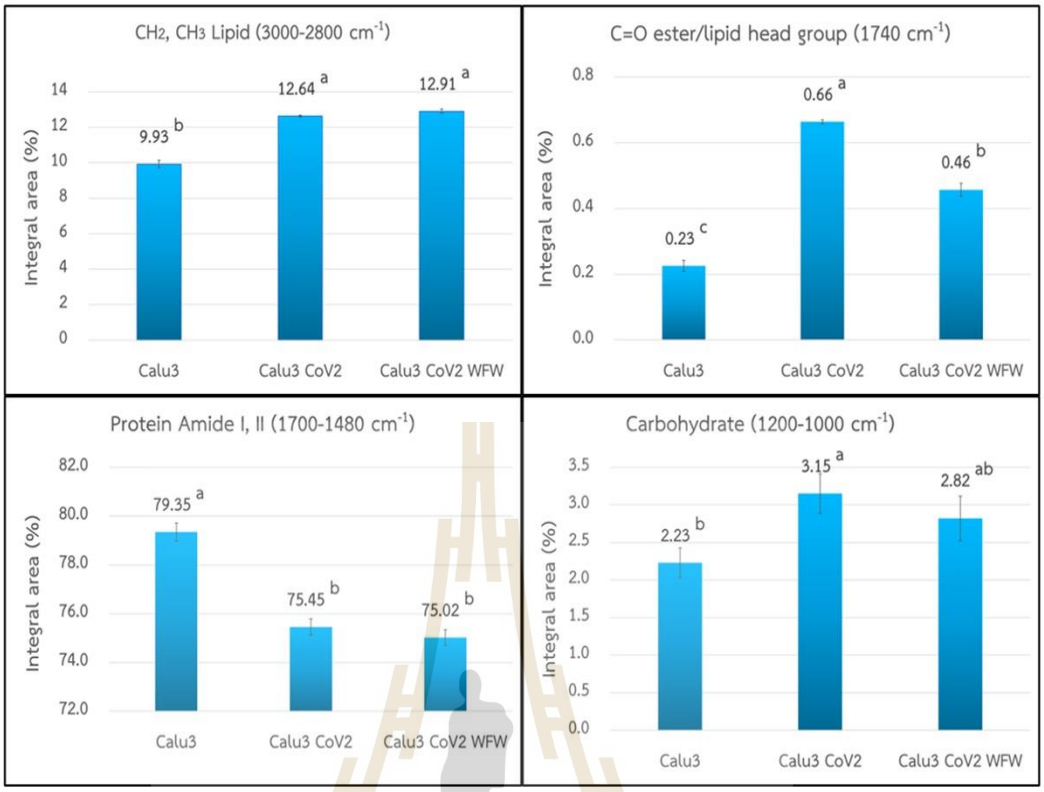

Figure 27 Peak area illustration of individual characteristic IR spectra derived from the average SR-FTIR spectra of the SARS-CoV-2-infected Calu-3 cell group. The groups include: **Calu3** Control (untreated, uninfected Calu-3 cells), **Calu3CoV2** (SARS-CoV-2-infected Calu-3 cells), and **Calu3CoV2WFW** (SARS-CoV-2-infected Calu-3 cells treated with 100 µg/mL WF-W for 48 h). Data are expressed by mean ± S.D. Means that those sharing the same superscript are not significantly different from each other (Tukey's HSD, $P < 0.05$).

CHAPTER V
DISCUSSION

5.1 Screening of Anti-SARS-CoV-2 Candidates and Identification of Lead Phytochemicals

Medicinal plants, with their diverse phytochemical profiles, have garnered significant attention as potential candidates for combating SARS-CoV-2. Their extracts exhibit antiviral properties that can inhibit SARS-CoV-2 infection during both the pre-entry and post-infection stages (Hafez Ghoran et al., 2021; Matveeva et al., 2020). Beyond the antiviral activity, phytochemicals demonstrate antioxidant, anti-inflammatory, antibacterial, and immunomodulatory effects, which can help mitigate hyperinflammatory and dysregulated immune responses associated with severe COVID-19 (Orhan & Senol Deniz, 2020; Rabaan et al., 2021). In this study, the *in vitro* antiviral assay was employed as a bioassay-guided screening approach using Vero E6 cells as the host to evaluate antiviral efficacy, focusing on two mechanisms: virucidal efficacy (pre-entry phase) and inhibition of viral replication (post-infection phase). Promising crude extracts were fractionated using a water/ethyl acetate system to separate highly polar compounds (water fraction, WF) from mid-to-nonpolar compounds (ethyl acetate fraction, EF), thereby enhancing antiviral efficacy. Among the fractions, WF-MLCE (S2-WF) demonstrated superior potency with low cytotoxicity (CC_{50} > 0.7 mg/mL; **Figure 11**) and high antiviral activity (IC_{50} < 15.6 µg/mL; **Figure 12**). compared to its original crude extract and EF. Notably, WF-MLCE also outperformed *Andrographis paniculata* extract (AP), which exhibited an IC_{50} of 68 µg/mL and CC_{50} > 0.1 mg/mL from the study in Vero E6 cells by Sa-ngiamsuntorn et al (Sa-ngiamsuntorn et al., 2021). WF-MLCE achieved ≥99.9% inhibition (LRV ≥ 3; **Table 5**), making it the most promising candidate in this study. Its efficacy also surpassed that of molnupiravir and other extracts, underscoring the effectiveness of the water/ethyl acetate fractionation approach applied to MLCE.

Phytochemical analysis of WF-MLCE using FTIR (**Figure 13**) and LC–HRMS (**Tables 6, 7, and A5–A7**) identified flavonoids and phenolic acids as the principal constituents, with rutin and chlorogenic acids being the most abundant. This aligns with the findings by Guo et al. (2023), who reported high concentrations of polyphenolics, particularly flavonoids and flavonoid glycosides, in mulberry leaves, with the dominant metabolites exhibiting strong polarity characteristics (Guo et al., 2023). These polyphenolics are proposed to play a pivotal role in the remarkable anti-SARS-CoV-2 efficacy of WF-MLCE. Flavonoids, including quercetin, myricetin, and rutin, have gained significant attention for their potential anti-SARS-CoV-2 properties. Their structural configuration-two benzene rings (A and B) connected by a pyrene ring (C) with varying hydroxylation levels is fundamental to their biological activity. Computational studies have identified several flavonoids capable of inhibiting SARS-CoV-2 through viral interaction mechanisms (Li et al., 2022; Solnier & Fladerer, 2021).

Molecular docking of WF-MLCE phytocompounds identified promising SARS-CoV-2 Mpro inhibitors, particularly sugar-conjugated flavonoids such as myricetin-3-O-D-galactopyranoside, kaempferol-3-O-rutinoside-7-O-rhamnoside (maragrol B), and quercetin-3-O-robinobioside. These compounds exhibited significantly lower binding energies (<−7 kcal/mol) and inhibition constants (<4 μM) compared to their aglycone forms (e.g., myricetin, kaempferol, and quercetin), suggesting enhanced interactions with the Mpro active site (**Table 9**). The integration of in silico molecular docking with in vitro biochemical assays provided a cost- and time-efficient approach to shortlist lead phytochemical candidates (Mahmud et al., 2021; Maya et al., 2021; Vincent et al., 2020)

The structural dependence of flavonoids' efficacy as Mpro inhibitors has been widely studied. Nguyen et al. (2021) reported that myricetin exhibited the strongest inhibition, followed by quercetin, rutin, and kaempferol, with efficacy linked to hydroxyl substitutions in the B-ring. For instance, myricetin's multiple hydroxyl groups enhanced its inhibitory power, while kaempferol's single hydroxyl substitution at C4′ reduced activity. Rutin (quercetin-3-O-rutinose) displayed reduced inhibition due to steric hindrance from glycosylation (Nguyen et al., 2021). However, Rizzuti et al. (2021) noted that rutin's sugar moiety improved solubility and bioavailability, enhancing its binding within the Mpro catalytic pocket (His-41/Cys-145) (Rizzuti et al.,

2021). These findings are supported by studies highlighting rutin's high potency against SARS-CoV-2 Mpro (Agrawal et al., 2021; Cherrak et al., 2020; Ibrahim et al., 2021). Collectively, these results underscore the potential of sugar-conjugated flavonoids in WF-MLCE as effective Mpro inhibitors, with structural features contributing to their superior antiviral properties.

To our knowledge, compounds such as myricetin-3-O-β-D-galactopyranoside, maragrol B, and quercetin-3-O-robinobioside have not been previously investigated for their interactions with SARS-CoV-2 proteins or evaluated for anti-SARS-CoV-2 activity in vitro or in vivo. Our findings suggest that the sugar moiety in these flavonoid conjugates enhances their antiviral efficacy by improving solubility and accessibility to the active site of viral proteins. However, the larger molecular size of glycosylated flavonoid conjugates may pose challenges for drug delivery, despite their improved solubility compared to aglycone counterparts.

5.2 Possible Interpretation on Anti-SARS-CoV-2 activity of WF-MLCE

The flavonoid/phenolic-rich extract (WF-MLCE) demonstrated potent anti-SARS-CoV-2 efficacy in both pre-entry (viricidal) and post-infection treatment modes, achieving about 3 log reduction value (LRV), equivalent to 99.9% efficacy, at a concentration of 250 µg/mL. This suggests that WF-MLCE targets multiple stages of the viral life cycle, making it a promising candidate for both prophylactic and therapeutic applications.

5.2.1 Pre-entry treatment (virucidal efficacy)

In the pre-entry mode, the virus was treated with WF-MLCE for 1 h before infecting Calu-3 cells. The significant reduction in viral titer indicates that WF-MLCE likely acts as a viricidal agent, directly inactivating the virus. Flavonoids and phenolic compounds are known to interact with viral envelopes and proteins, disrupting their structure and preventing viral entry into host cells (Gligorijevic et al., 2021; Rakshit et al., 2022; Sopjani et al., 2024). For example, flavonoids can bind to the spike (S) protein, blocking its interaction with the host cell receptor ACE2 (Dinda et al., 2024; Meng et al., 2023). Additionally, phenolic compounds may generate reactive oxygen species (ROS), causing oxidative damage to viral RNA or proteins

(Hussain et al., 2016; Rudrapal et al., 2022). The 1-h incubation period is sufficient for WF-MLCE to exert its virucidal effects, allowing adequate time for interaction with viral components while minimizing potential cytotoxicity to host cells.st cells.

5.2.2 Post-infection treatment (viral replication inhibition efficacy)

In the post-infection mode, Calu-3 cells were infected with SARS-CoV-2 for 2 h, followed by treatment with WF-MLCE for 48 h. The significant reduction in viral titer suggests that WF-MLCE inhibits viral replication and viral spread within the host cells. Flavonoids are known to target key viral enzymes, such as the RNA-dependent RNA polymerase (RdRp) and proteases (Mpro and PLpro), which are essential for viral replication and protein processing (Gligorijevic et al., 2021; Rakshit et al., 2022). WF-MLCE may also modulate host cell metabolism, such as lipid and carbohydrate pathways, depriving the virus of resources needed for replication (Miron et al., 2017; Shahzad et al., 2024). Furthermore, flavonoids can enhance host innate immune responses, such as the production of interferons (IFNs), which play a critical role in antiviral defense (Dinda et al., 2024; Meng et al., 2023). The 48-h treatment period is appropriate for capturing multiple rounds of viral replication and assessing WF-MLCE's ability to inhibit viral spread. However, shorter time points (e.g., 6 h, 12 h, and 24 h) could provide additional insights into the kinetics of viral inhibition and the specific stages of the viral life cycle targeted by WF-MLCE.

5.2.3 Considerations for experimental timing

The timing of treatment is critical for interpreting the results and understanding WF-MLCE's mechanisms of action. In the **pre-entry mode**, the 1-h incubation period allows WF-MLCE to interact with the virus without significantly affecting host cells. In the **post-infection mode**, the 2-h absorption period ensures sufficient time for viral attachment and entry, while the 48-h treatment period captures the full extent of viral replication and spread. However, monitoring cytopathic effects (CPE) and measuring viral titers at multiple time points (e.g., 6 h, 12 h, 24 h) could help identify the specific stages of the viral life cycle targeted by WF-MLCE. For example, early time points (6–12 h) may reveal effects on viral replication and transcription, while later time points (24–48 h) may reveal effects on viral assembly, budding, and release (Lou & Rao, 2022). The timing of treatment is critical for optimizing WF-MLCE's efficacy and understanding its mechanisms of

action. These findings highlight the potential of WF-MLCE as a broad-spectrum antiviral agent for preventing and treating SARS-CoV-2 infection.

5.3 Modification of Mulberry Leaf Extraction Method: Chemical Profile and Anti-SARS-CoV-2 Efficacy of Resulting Extracts

5.3.1 Chemical profiles of resulting mulberry leaf extracts

In Phase 2, modifications were made to refine the extraction of the water-soluble fraction of mulberry leaf crude extract (WF-MLCE), aiming to isolate components with the highest antiviral efficacy identified in Phase 1. The modified extracts (WF-W and WCE) were compared with the original WF-MLCE (WF-EtAct) using FTIR, LC-HRMS, TPC, and TFC assays. FTIR analysis revealed key functional groups, particularly flavonoids and phenolics, in the water-soluble extracts (**Figure 16**). Notably, WF-W exhibited a more complex chemical profile than WCE, correlating with higher polyphenolic content. The similarity in chemical composition between WF-EtAct and WF-W was further confirmed by principal component analysis (PCA) and log2 fold change (log2FC) analysis of metabolite mass spectral data (**Figures 17 & 18**).

5.3.2 Anti-SARS-CoV-2 efficacy of resulting mulberry leaf extracts

Beyond chemical characterization, the selection of WF-W over WF-EtAct was supported by its superior antiviral efficacy. Both extracts demonstrated similar safety profiles (CC_{50} > 0.5 mg/mL), but WF-W exhibited higher antiviral activity. At 100 µg/mL, WF-W displayed the highest viral inhibition (LRV = 2.448) with the lowest IC_{50} value (0.0011 µg/mL), surpassing molnupiravir, rutin, and WF-EtAct in pre-entry mode (**Figure 21**). These results suggest that WF-W effectively inhibits SARS-CoV-2 before viral entry into host cells, positioning it as a promising preventive or virucidal agent. Its enhanced antiviral activity may be attributed to phytocomponents interfering with viral proteins, such as the SARS-CoV-2 spike protein, thereby preventing ACE2 receptor binding. Similar mechanisms have been observed with flavonoids such as luteolin, quercetin, and apigenin, which bind viral proteins, inhibit replication, and modulate host immune responses to prevent infection. Additionally, some phytocompounds in WF-W may exert direct virucidal effects, inactivating the virus before host cell invasion (Abubakar et al., 2021; De Pellegrin et al., 2021). This

mechanism aligns with findings from elderberry (*Sambucus nigra*), which inhibited SARS-CoV-2 entry by binding to the receptor-binding domain (RBD) of the spike protein, thereby blocking ACE2 receptor engagement (Boroduske et al., 2021).

The post-infection antiviral assay (**Table 12**) further confirmed WF-W's efficacy. At 100 µg/mL, WF-W exhibited the highest viral inhibition (LRV = 2.458, 99.6% inhibition), outperforming WF-EtAct, molnupiravir, and rutin. While both mulberry leaf extracts demonstrated greater efficacy than molnupiravir and rutin at high concentrations, their IC_{50} values—WF-W (0.0100 µg/mL) and WF-EtAct (0.0117 µg/mL) were notably higher than those of rutin (0.0008 µg/mL) and molnupiravir (0.0025 µg/mL) (**Figure 22**). This suggests that although mulberry leaf extracts exhibit strong antiviral activity at higher concentrations, their potency declines more rapidly at lower doses (< 0.1 µg/mL), whereas rutin and molnupiravir maintain more stable efficacy over a broader concentration range. The difference in stability may be attributed to molnupiravir's synthetic design, which ensures chemical stability and sustained efficacy under physiological conditions (Reçber et al., 2022). In contrast, herbal extracts may degrade over time due to factors such as compound instability, metabolic degradation, and lower concentrations of active ingredients (Mukhtar et al., 2008; Perera et al., 2021). Since mulberry leaf extract contains multiple bioactive compounds with varying stability, its antiviral potency may fluctuate more than single-compound drugs like rutin and molnupiravir. These findings underscore the importance of optimizing the dosage of mulberry leaf extract to maintain therapeutic efficacy. Further studies should focus on compound stability, bioavailability, and potential formulation strategies to enhance efficacy at lower concentrations.

5.4 Mechanism of Anti-SARS-CoV-2 Activity of WF-W Extract: SR-FTIR of Cellular Responses

To investigate the mechanism of action of WF-W in post-infection treatment mode, Synchrotron radiation Fourier-transform infrared (SR-FTIR) spectroscopy was employed. This advanced analytical technique enables precise molecular-level characterization of biochemical alterations in infected host cells upon WF-W treatment. By examining specific spectral changes, we aimed to identify key

biochemical pathways and molecular targets modulated by the extract, which may contribute to its anti-SARS-CoV-2 activity. The data provide insights into how WF-W interferes with viral replication, alters cellular metabolism, or disrupts viral-host interactions, reinforcing its potential as an antiviral agent against SARS-CoV-2. Additionally, WF-W's impact on uninfected Calu-3 cells was examined to assess its role in metabolic priming, potentially enhancing cellular defense against future viral infections.

5.4.1 Potential antiviral mechanisms of WF-W in SARS-CoV-2-infected Calu-3 cells and their implications

The FTIR analysis of SARS-CoV-2-infected Calu-3 cells treated with WF-W (**Figure 27**) revealed significant metabolic changes in lipid, protein, and carbohydrate content, suggesting that WF-W counteracts viral-induced metabolic dysregulation, potentially through multi-mechanistic actions.

Lipid metabolism: SARS-CoV-2 infection induced lipid accumulation, as indicated by increased CH_2/CH_3 stretching (3000–2800 cm^{-1}) and C=O lipid head (1740 cm^{-1}). This aligns with the virus's ability to hijack host lipid metabolism, particularly lipid droplets (LDs) and extracellular vesicles (EVs), to support viral replication and assembly. (Baek et al., 2022; Cesar-Silva et al., 2023; Sumbria et al., 2020). After treatment with WF-W, CH_3/CH_2 groups stabilized, while the C=O lipid head groups decreased significantly. This suggests that WF-W may interfere with viral-induced lipid accumulation, potentially by modulating lipid droplet dynamics or promoting lipid oxidation. Flavonoids are known to stabilize membranes and inhibit lipid biosynthesis enzymes, which could explain the observed reduction in C=O groups after treatment (Gligorijevic et al., 2021; Shahzad et al., 2024; Sopjani et al., 2024). Another possible mechanism, WF-W may promotes lipid oxidation rather than storage, possibly mediated by adenosine monophosphate-activated protein kinase (AMPK) activation (Ganjayi et al., 2023). The lipid metabolic change after cell infection agreed with the clinical study from Cesar-Silva et al. The study found that COVID-19 patients often present with dysregulated lipid profiles linked to severe disease outcomes (Cesar-Silva et al., 2023). Since LDs serve as viral replication platforms, targeting lipid metabolism could provide therapeutic benefits (Baek et al., 2022).

Protein Homeostasis: Infection led to a significant decrease in protein content, likely due to viral hijacking of host translation machinery and activation of proteasomal degradation pathways (Tsiambas et al., 2021; Wei & Hui, 2022). WF-W stabilized protein levels, possibly by inhibiting viral proteases (e.g., Mpro and PLpro) or modulating host stress responses, such as the unfolded protein response (UPR) (Gligorijevic et al., 2021; Rudrapal et al., 2022; Sopjani et al., 2024). Flavonoids are known to protect host proteins from degradation and restore protein synthesis, which may contribute to the observed stabilization (Montenegro-Landívar et al., 2021; Tabari et al., 2021).

Carbohydrate Metabolism: Carbohydrate content increased significantly after infection, likely due to viral manipulation of host glycosylation pathways to facilitate viral entry and immune evasion (Martínez-Gómez et al., 2022). WF-W reduced carbohydrate levels, though they remained slightly higher than basal levels. This suggests that WF-W may inhibit viral-induced glycosylation or modulate carbohydrate metabolism pathways, such as the hexosamine biosynthesis pathway (Tang et al., 2025). Flavonoids in WF-MLCE are known to interfere with glycosylation enzymes, which could explain the observed decrease in carbohydrate content (Xu et al., 2024).

5.4.2 Possible implications of WF-W treatment on metabolism in uninfected Calu-3 cells

The treatment of uninfected Calu-3 cells with WF-W induced dynamic metabolic changes over time, as revealed by FTIR analysis (**Figure 23 & 24**). These changes suggest that the extract triggers a transient stress response followed by cellular adaptation, potentially priming the cells for future challenges such as viral infection.

Lipid metabolism: At 1 h post-treatment, the levels of CH3/CH2 and C=O lipid head groups increased significantly, indicating a rapid interaction between WF-W and cellular membranes or an upregulation of lipid biosynthesis. By 24 and 48 h, lipid levels returned to basal levels, suggesting cellular adaptation and restoration of lipid homeostasis, possibly through lipid oxidation or lipolysis (Baek et al., 2022; Miron et al., 2017). Flavonoids are known to integrate into lipid bilayers, altering membrane fluidity and signaling (Hendrich, 2006; Oteiza et al., 2005). This transient

lipid remodeling could strengthen cell membranes, making them more resistant to future stressors such as viral infection.

Protein homeostasis: Protein content decreased significantly at 1-h post-treatment, likely due to the activation of stress responses such as proteasomal degradation or the inhibition of protein synthesis. By 24 and 48 h, protein levels increased slightly above basal levels, indicating cellular adaptation and the upregulation of protective proteins, such as heat shock proteins or antioxidant enzymes(Bhutta et al., 2021; Middleton et al., 2000). This recovery phase may enhance the cells' ability to handle future stress, including viral infection

Carbohydrate metabolism: Carbohydrate content decreased significantly at 1 h post-treatment, likely reflecting a shift in energy metabolism to meet the demands of the stress response. By 24 and 48 hours, carbohydrate levels stabilized, suggesting the restoration of metabolic balance This transient mobilization of carbohydrates could optimize energy utilization and resource allocation for defense mechanisms. Flavonoids may transiently inhibit carbohydrate storage pathways (e.g., glycogenesis) or promote carbohydrate utilization (Shahzad et al., 2024).

The 48-h experimental period is likely too long to capture the direct effects of WF-W on SARS-CoV-2 replication, as multiple rounds of the viral life cycle would have occurred, and cells may already be heavily damaged. However, the data from this time point can still provide valuable insights into long-term cellular changes, such as metabolic stabilization (e.g., lipids, proteins, carbohydrates), cellular stress responses, and viral clearance. These findings suggest that WF-W may protect cells from viral-induced damage over time. However, shorter time points (e.g., 6 h, 12 h, 24 h) are recommended to study direct antiviral effects and viral replication dynamics. Future experiments should focus on mechanistic studies, viral titer measurement, and cellular viability to fully elucidate the antiviral potential of WF-W extract. These steps will help optimize its efficacy and provide a deeper understanding of its mechanisms of action. Additionally, future research should explore the long-term metabolic impacts of WF-W, its broad-spectrum antiviral properties, and clinical applications as a dietary supplement or adjunct therapy for COVID-19 and emerging coronaviruses.

CHAPTER VI
CONCLUSIONS

This study successfully identified and optimized the water-soluble fraction of mulberry leaf extract (WF-MLCE) as a potent anti-SARS-CoV-2 agent. The modified extraction method yielded WF-W, a solvent-free formulation with enhanced antiviral efficacy and a favorable chemical profile rich in phenolics and flavonoids. SR-FTIR analysis revealed that WF-W influences host metabolism, likely through AMPK activation, shifting lipid metabolism towards oxidation while preventing protein degradation. These metabolic modulations contribute to both antiviral activity and cellular priming against future infections. Additionally, WF-W appears to support both metabolic and immune modulation, potentially enhancing cellular defense. Given its dual role in infected and uninfected cells, WF-W could serve as both a preventive supplement and a therapeutic agent for COVID-19 and other viral infections. However, further in vivo studies and clinical trials are essential to validate its efficacy, optimize dosing, and explore broader applications, including transcriptomic analysis to uncover deeper molecular mechanisms.

REFERENCES

Abbas, O., Compère, G., Larondelle, Y., et al. (2017). Phenolic Compound Explorer: A Mid-Infrared Spectroscopy Database. *Vibrational Spectroscopy, 92*, 111-118. https://doi.org/https://doi.org/10.1016/j.vibspec.2017.05.008.

Abd-Alla, H. I., Kutkat, O., Sweelam, H.-t. M., et al. (2022). Investigating the Potential Anti-Sars-Cov-2 and Anti-Mers-Cov Activities of Yellow Necklacepod among Three Selected Medicinal Plants: Extraction, Isolation, Identification, in Vitro, Modes of Action, and Molecular Docking Studies. *Metabolites, 12*(11), 1109. https://www.mdpi.com/2218-1989/12/11/1109.

Abubakar, A. R., & Haque, M. (2020). Preparation of Medicinal Plants: Basic Extraction and Fractionation Procedures for Experimental Purposes. *Journal of Pharmacy & Bioallied Sciences, 12*(1), 1-10. https://doi.org/10.4103/jpbs.JPBS_175_19.

Abubakar, M. B., Usman, D., El-Saber Batiha, G., et al. (2021). Natural Products Modulating Angiotensin Converting Enzyme 2 (Ace2) as Potential Covid-19 Therapies [Review]. *Frontiers in Pharmacology, 12*. https://doi.org/10.3389/fphar.2021.629935.

Agatonovic-Kustrin, S., Doyle, E., Gegechkori, V., & Morton, D. W. (2020). High-Performance Thin-Layer Chromatography Linked with (Bio)Assays and Ftir-Atr Spectroscopy as a Method for Discovery and Quantification of Bioactive Components in Native Australian Plants. *Journal of Pharmaceutical and Biomedical Analysis, 184*, 113208. https://doi.org/https://doi.org/10.1016/j.jpba.2020.113208.

Agrawal, P. K., Agrawal, C., & Blunden, G. (2021). Rutin: A Potential Antiviral for Repurposing as a Sars-Cov-2 Main Protease (Mpro) Inhibitor. *Natural Product Communications, 16*..

Ali, A., Wu, H., Ponnampalam, E. N., et al. (2021). Comprehensive Profiling of Most Widely Used Spices for Their Phenolic Compounds through Lc-Esi-Qtof-Ms^2

and Their Antioxidant Potential. *Antioxidants (Basel), 10*(5). https://doi.org/10.3390/antiox10050721.

Amirfakhryan, H., & safari, F. (2021). Outbreak of Sars-Cov2: Pathogenesis of Infection and Cardiovascular Involvement. *Hellenic Journal of Cardiology, 62*(1), 13-23. https://doi.org/https://doi.org/10.1016/j.hjc.2020.05.007.

Arfan, M., Amin, H., Karamać, M., et al. (2007). Antioxidant Activity of Extracts of *Mallotus Philippinensis* Fruit and Bark. *Journal of Food Lipids, 14*(3), 280-297. https://doi.org/https://doi.org/10.1111/j.1745-4522.2007.00086.x.

Astiti, M. A., Jittmittraphap, A., Leaungwutiwong, P., et al. (2021). Lc-Qtof-Ms/Ms Based Molecular Networking Approach for the Isolation of α-Glucosidase Inhibitors and Virucidal Agents from *Coccinia Grandis* (L.) Voigt. *Foods, 10*(12), 3041. https://www.mdpi.com/2304-8158/10/12/3041.

ASTM. (2020). *Astm E1053–20, Standard Practice to Assess Virucidal Activity of Chemicals Intended for Disinfection of Inanimate, Nonporous Environmental Surfaces*. https://doi.org/ https://www.astm.org/Standards/E1053.htm.

Baek, Y.-B., Kwon, H.-J., Sharif, M., et al. (2022). Therapeutic Strategy Targeting Host Lipolysis Limits Infection by Sars-Cov-2 and Influenza a Virus. *Signal Transduction and Targeted Therapy, 7*(1), 367. https://doi.org/10.1038/s41392-022-01223-4.

Baeshen, M. N., Attar, R., Bouback, T. A., et al. (2022). Assaying for Antiviral Activity of the Folkloric Medicinal Desert Plant *Rhazya Stricta* on Coronavirus Sars-Cov-2. *Biotechnology & Biotechnological Equipment, 36*(1), 68-74. https://doi.org/10.1080/13102818.2022.2047107.

Bajrai, L. H., El-Kafrawy, S. A., Alnahas, R. S., & Azhar, E. I. (2021). In Vitro Screening of Anti-Viral and Virucidal Effects against Sars-Cov-2 by *Hypericum Perforatum* and *Echinacea*. *Scientific Reports, 12*.

Baker, M. J., Trevisan, J., Bassan, P., et al. (2014). Using Fourier Transform Ir Spectroscopy to Analyze Biological Materials. *Nature Protocols, 9*(8), 1771-1791. https://doi.org/10.1038/nprot.2014.110.

Bangkokbiznews. (2022, July 12th). กรมการแพทย์ออกแนวทางรักษาโควิด-19 ฉบับใหม่ ปรับยากลุ่มมีปัจจัยเสี่ยง. กรุงเทพธุรกิจ.

Benjaponpitak, A., Sawaengtham, T., Thaneerat, T., et al. (2023). Effect of *Andrographis Paniculata* Treatment for Nonimmune Patients with Early-Stage Covid-19 on the Prevention of Pneumonia: A Retrospective Cohort Study. *Archives of Internal Medicine Research, 6*, 35-43.

Berman, H. M., Westbrook, J., Feng, Z., et al. (2000). The Protein Data Bank. *Nucleic Acids Research, 28*(1), 235-242. https://doi.org/10.1093/nar/28.1.235.

Bhutta, M. S., Gallo, E. S., & Borenstein, R. (2021). Multifaceted Role of Ampk in Viral Infections. *Cells, 10*(5). https://doi.org/10.3390/cells10051118.

Boroduske, A., Jekabsons, K., Riekstina, U., et al. (2021). Wild *Sambucus Nigra* L. From North-East Edge of the Species Range: A Valuable Germplasm with Inhibitory Capacity against Sars-Cov2 S-Protein Rbd and Hace2 Binding in Vitro. *Industrial Crops & Products, 165*, 113438. https://doi.org/10.1016/j.indcrop.2021.113438.

Bullen, C. K., Davis, S. L., & Looney, M. M. (2022). Quantification of Infectious Sars-Cov-2 by the 50% Tissue Culture Infectious Dose Endpoint Dilution Assay. In J. J. H. Chu, B. A. Ahidjo, & C. K. Mok (Eds.), *Sars-Cov-2: Methods and Protocols* (pp. 131-146). Springer US. https://doi.org/10.1007/978-1-0716-2111-0_9.

Burmer, G., Burmer, M., & Pabuwal, V. (2021). Sars-Cov-2 and Covid-19 Pathogenesis: A Review. LifeSpan BioSciences, Inc. Retrieved 14 July 2024 from https://www.lsbio.com/.

Cesar-Silva, D., Pereira-Dutra, F. S., Giannini, A. L. M., Maya-Monteiro, C. M., & de Almeida, C. J. G. (2023). Lipid Compartments and Lipid Metabolism as Therapeutic Targets against Coronavirus. *Frontiers in Immunology, 14*, 1268854. https://doi.org/10.3389/fimmu.2023.1268854.

Chan, J. F., Kok, K. H., Zhu, Z., et al. (2020). Genomic Characterization of the 2019 Novel Human-Pathogenic Coronavirus Isolated from a Patient with Atypical Pneumonia after Visiting Wuhan. *Emerging in Microbes & Infections, 9*(1), 221-236. https://doi.org/10.1080/22221751.2020.1719902.

Chang, C.-k., Hou, M.-H., Chang, C.-F., Hsiao, C.-D., & Huang, T.-h. (2014). The Sars Coronavirus Nucleocapsid Protein – Forms and Functions. *Antiviral Research, 103*, 39-50. https://doi.org/https://doi.org/10.1016/j.antiviral.2013.12.009.

Chen, C. C., Chuang, W.-T., Lin, A.-H., et al. (2016). Andrographolide Inhibits Adipogenesis of 3t3-L1 Cells by Suppressing C/Ebpbeta Expression and Activation. *Toxicology and Applied Pharmacology, 307*, 115-122. https://doi.org/doi: 10.1016/j.taap.2016.07.021.

Cherrak, S. A., Merzouk, H., & Mokhtari-Soulimane, N. (2020). Potential Bioactive Glycosylated Flavonoids as Sars-Cov-2 Main Protease Inhibitors: A Molecular Docking and Simulation Studies. *PLoS One, 15*(10), e0240653. https://doi.org/10.1371/journal.pone.0240653.

Chiow, K. H., Phoon, M. C., Putti, T., Tan, B. K. H., & Chow, V. T. (2016). Evaluation of Antiviral Activities of *Houttuynia Cordata* Thunb. Extract, Quercetin, Quercetrin and Cinanserin on Murine Coronavirus and Dengue Virus Infection. *Asian Pacific Journal of Tropical Medicine, 9*(1), 1-7. https://doi.org/https://doi.org/10.1016/j.apjtm.2015.12.002

Churiyah, Pongtuluran, O. B., Rofaani, E., & April, T. (2015). Antiviral and Immunostimulant Activities of *Andrographis Paniculata Journal of Biosciences, 22*(2), 67-72. https://doi.org/DOI: 10.4308/hjb.22.2.67.

De Pellegrin, M. L., Rohrhofer, A., Schuster, P., et al. (2021). The Potential of Herbal Extracts to Inhibit Sars-Cov-2: A Pilot Study. *Clinical Phytoscience, 7*(1), 29. https://doi.org/10.1186/s40816-021-00264-6.

Derenne, A., Van Hemelryck, V., Lamoral-Theys, D., Kiss, R., & Goormaghtigh, E. (2013). Ftir Spectroscopy: A New Valuable Tool to Classify the Effects of Polyphenolic Compounds on Cancer Cells. *Biochimica et Biophysica Acta (BBA) - Molecular Basis of Disease, 1832*(1), 46-56. https://doi.org/https://doi.org/10.1016/j.bbadis.2012.10.010.

Dinda, B., Dinda, M., Dinda, S., Ghosh, P. S., & Das, S. K. (2024). Anti-Sars-Cov-2, Antioxidant and Immunomodulatory Potential of Dietary Flavonol Quercetin: Focus on Molecular Targets and Clinical Efficacy. *European Journal of Medicinal Chemistry Reports, 10*, 100125. https://doi.org/https://doi.org/10.1016/j.ejmcr.2023.100125.

El Gizawy, H. A., Boshra, S. A., Mostafa, A., et al. (2021). *Pimenta Dioica* (L.) Merr. Bioactive Constituents Exert Anti-Sars-Cov-2 and Anti-Inflammatory Activities:

Molecular Docking and Dynamics, in Vitro, and in Vivo Studies. *Molecules, 26*(19), 5844. https://www.mdpi.com/1420-3049/26/19/5844.

Emrani, J., Ahmed, M., Jeffers-Francis, L., et al. (2021). Sars-Cov-2, Infection, Transmission, Transcription, Translation, Proteins, and Treatment: A Review. *International Journal of Biological Macromolecules, 193*, 1249-1273. https://doi.org/https://doi.org/10.1016/j.ijbiomac.2021.10.172.

Essalmani, R., Jain, J., Susan-Resiga, D., et al. (2022). Distinctive Roles of Furin and Tmprss2 in Sars-Cov-2 Infectivity. *Journal of Virology, 96*(8), e0012822. https://doi.org/10.1128/jvi.00128-22.

Félix, M. M., Tavares, M. V., Santos, I. P., et al. (2024). Cervical Squamous Cell Carcinoma Diagnosis by Ftir Microspectroscopy. *Molecules, 29*(5), 922. https://www.mdpi.com/1420-3049/29/5/922.

Ganjayi, M. S., Karunakaran, R. S., Gandham, S., & Meriga, B. (2023). Quercetin-3-O-Rutinoside from *Moringa Oleifera* Downregulates Adipogenesis and Lipid Accumulation and Improves Glucose Uptake by Activation of Ampk/Glut-4 in 3t3-L1 Cells. *Revista Brasileira de Farmacognosia, 33*(2), 334-343. https://doi.org/10.1007/s43450-022-00352-9.

Gao, Y., Huo, X., Dong, L., et al. (2015). Fourier Transform Infrared Microspectroscopy Monitoring of 5-Fluorouracil-Induced Apoptosis in Sw620 Colon Cancer Cells. *Molecular Medicine Reports, 11*(4), 2585-2591. https://doi.org/10.3892/mmr.2014.3088.

Gligorijevic, N., Radomirovic, M., Nedic, O., et al. (2021). Molecular Mechanisms of Possible Action of Phenolic Compounds in Covid-19 Protection and Prevention. *International Journal of Molecular Sciences, 22*(22), 12385. https://www.mdpi.com/1422-0067/22/22/12385.

Gordon, C. J., Tchesnokov, E. P., Woolner, E., et al. (2020). Remdesivir Is a Direct-Acting Antiviral That Inhibits Rna-Dependent Rna Polymerase from Severe Acute Respiratory Syndrome Coronavirus 2 with High Potency. *Journal of Biological Chemistry, 295*(20), 6785-6797. https://doi.org/10.1074/jbc.RA120.013679.

Greenblatt, W., Gupta, C., & Kao, J. (2023). Drug Repurposing During the Covid-19 Pandemic: Lessons for Expediting Drug Development and Access. *Health Affairs, 42*(3), 424-432. https://doi.org/10.1377/hlthaff.2022.01083.

Guo, Z., Lai, J., Wu, Y., Fang, S., & Liang, X. (2023). Investigation on Antioxidant Activity and Different Metabolites of Mulberry (*Morus* Spp.) Leaves Depending on the Harvest Months by Uplc–Q-Tof-Ms with Multivariate Tools. *Molecules, 28*(4).

Hafez Ghoran, S., El-Shazly, M., Sekeroglu, N., & Kijjoa, A. (2021). Natural Products from Medicinal Plants with Anti-Human Coronavirus Activities. *Molecules, 26*(6). https://doi.org/10.3390/molecules26061754.

Hendrich, A. B. (2006). Flavonoid-Membrane Interactions: Possible Consequences for Biological Effects of Some Polyphenolic Compounds. *Acta Pharmacologica Sinica, 27*(1), 27-40. https://doi.org/10.1111/j.1745-7254.2006.00238.x.

Hileman, C. O., Malakooti, S. K., Patil, N., Singer, N. G., & McComsey, G. A. (2024). New-Onset Autoimmune Disease after Covid-19 [Original Research]. *Frontiers in Immunology, 15*. https://doi.org/10.3389/fimmu.2024.1337406.

Ho, T.-Y., Wu, S.-L., Chen, J.-C., Li, C.-C., & Hsiang, C.-Y. (2007). Emodin Blocks the Sars Coronavirus Spike Protein and Angiotensin-Converting Enzyme 2 Interaction. *Antiviral Research, 74*(2), 92-101. https://doi.org/https://doi.org/10.1016/j.antiviral.2006.04.014

Hong, E., Lee, S. Y., Jeong, J. Y., et al. (2017). Modern Analytical Methods for the Detection of Food Fraud and Adulteration by Food Category. *Journal of the Science of Food and Agriculture, 97*(12), 3877-3896. https://doi.org/10.1002/jsfa.8364.

Hssaini, L., Razouk, R., & Bouslihim, Y. (2022). Rapid Prediction of Fig Phenolic Acids and Flavonoids Using Mid-Infrared Spectroscopy Combined with Partial Least Square Regression [Original Research]. *Frontiers in Plant Science, 13*. https://doi.org/10.3389/fpls.2022.782159.

Huang, C., Wang, Y., Li, X., et al. (2020). Clinical Features of Patients Infected with 2019 Novel Coronavirus in Wuhan, China. *The Lancet, 395*(10223), 497-506. https://doi.org/10.1016/S0140-6736(20)30183-5.

Hussain, T., Tan, B., Yin, Y., et al. (2016). Oxidative Stress and Inflammation: What Polyphenols Can Do for Us? *Oxidative Medicine and Cellular Longevity, 2016*, 7432797. https://doi.org/10.1155/2016/7432797.

Hussain, W., Haleem, K., Khan, I., et al. (2017). Medicinal Plants: A Repository of Antiviral Metabolites. *Future Virology, 12*, 299-308..

Ibrahim, M. A. A., Mohamed, E. A. R., Abdelrahman, A. H. M., et al. (2021). Rutin and Flavone Analogs as Prospective Sars-Cov-2 Main Protease Inhibitors: In Silico Drug Discovery Study. *Journal of Molecular Graphics and Modelling, 105*, 107904. https://doi.org/10.1016/j.jmgm.2021.107904.

Islam, M. T., Sarkar, C., El-Kersh, D. M., et al. (2020). Natural Products and Their Derivatives against Coronavirus: A Review of the Non-Clinical and Pre-Clinical Data. *Phytotherapy Research, 34*(10), 2471-2492. https://doi.org/10.1002/ptr.6700.

Jin, Z., Du, X., Xu, Y., et al. (2020). Structure of Mpro from Sars-Cov-2 and Discovery of Its Inhibitors. *Nature, 582*(7811), 289-293. https://doi.org/10.1038/s41586-020-2223-y.

Kandanur, S. G. S., Tamang, N., Golakoti, N. R., & Nanduri, S. (2019). Andrographolide: A Natural Product Template for the Generation of Structurally and Biologically Diverse Diterpenes. *European Journal of Medicinal Chemistry, 176*, 513-533. https://doi.org/10.1016/j.ejmech.2019.05.022.

Kanjanasirirat, P., Suksatu, A., Manopwisedjaroen, S., et al. (2020). High-Content Screening of Thai Medicinal Plants Reveals *Boesenbergia Rotunda* Extract and Its Component Panduratin a as Anti-Sars-Cov-2 Agents. *Scientific Reports, 10*(1), 19963. https://doi.org/10.1038/s41598-020-77003-3.

Kassem, A., Abbas, L., Coutinho, O., et al. (2023). Applications of Fourier Transform-Infrared Spectroscopy in Microbial Cell Biology and Environmental Microbiology: Advances, Challenges, and Future Perspectives. *Frontiers in Microbiology, 14*, 1304081. https://doi.org/10.3389/fmicb.2023.1304081.

Kim, C.-H. (2021). Anti–Sars-Cov-2 Natural Products as Potentially Therapeutic Agents [Review]. *Frontiers in Pharmacology, 12*. https://doi.org/10.3389/fphar.2021.590509.

Kim, S., Chen, J., Cheng, T., et al. (2022). Pubchem 2023 Update. *Nucleic Acids Research, 51*(D1), D1373-D1380. https://doi.org/10.1093/nar/gkac956.

Kimberlin, D. W. (2008). Chapter 295 - Antiviral Agents. In S. S. Long (Ed.), *Principles and Practice of Pediatric Infectious Disease (Third Edition)* (pp. 1470-1488). W.B. Saunders. https://doi.org/https://doi.org/10.1016/B978-0-7020-3468-8.50301-1.

Krysa, M., Szymańska-Chargot, M., & Zdunek, A. (2022). Ft-Ir and Ft-Raman Fingerprints of Flavonoids – a Review. *Food Chemistry, 393*, 133430. https://doi.org/https://doi.org/10.1016/j.foodchem.2022.133430.

Kushwaha, P. P., Singh, A. K., Bansal, T., et al. (2021). Identification of Natural Inhibitors against Sars-Cov-2 Drugable Targets Using Molecular Docking, Molecular Dynamics Simulation, and Mm-Pbsa Approach [Original Research]. *Frontiers in Cellular and Infection Microbiology, 11*. https://doi.org/10.3389/fcimb.2021.730288.

Li, L., Ma, L., Hu, Y., et al. (2022). Natural Biflavones Are Potent Inhibitors against Sars-Cov-2 Papain-Like Protease. *Phytochemistry, 193*, 112984. https://doi.org/https://doi.org/10.1016/j.phytochem.2021.112984.

Li, S. Y., Chen, C., Zhang, H. Q., et al. (2005). Identification of Natural Compounds with Antiviral Activities against Sars-Associated Coronavirus. *Antiviral Research, 67*(1), 18-23. https://doi.org/10.1016/j.antiviral.2005.02.007.

Liang, J., Pitsillou, E., Karagiannis, C., et al. (2020). Interaction of the Prototypical A-Ketoamide Inhibitor with the Sars-Cov-2 Main Protease Active Site in Silico: Molecular Dynamic Simulations Highlight the Stability of the Ligand-Protein Complex. *Computational Biology and Chemistry, 87*, 107292. https://doi.org/https://doi.org/10.1016/j.compbiolchem.2020.107292.

Lill, M. A., & Danielson, M. L. (2011). Computer-Aided Drug Design Platform Using Pymol. *Journal of Computer-Aided Molecular Design, 25*(1), 13-19. https://doi.org/10.1007/s10822-010-9395-8.

Lin, F., Zhang, H., Li, L., et al. (2022). Pedv: Insights and Advances into Types, Function, Structure, and Receptor Recognition. *Viruses, 14*(8). https://doi.org/10.3390/v14081744.

Lou, Z., & Rao, Z. (2022). The Life of Sars-Cov-2 inside Cells: Replication-Transcription Complex Assembly and Function. *Annual Review of Biochemistry, 91*, 381-401. https://doi.org/10.1146/annurev-biochem-052521-115653.

Luo, Y., Wang, C.-Z., Hesse-Fong, J., Lin, J.-G., & Yuan, C.-S. (2019). Application of Chinese Medicine in Acute and Critical Medical Conditions. *The American Journal of Chinese Medicine, 47*(06), 1223-1235. https://doi.org/10.1142/s0192415x19500629.

Mahmud, S., Uddin, M. A. R., Paul, G. K., et al. (2021). Virtual Screening and Molecular Dynamics Simulation Study of Plant-Derived Compounds to Identify Potential Inhibitors of Main Protease from Sars-Cov-2. *Briefings in Bioinformatics, 22*(2), 1402-1414. https://doi.org/10.1093/bib/bbaa428.

Martínez-Gómez, L. E., Ibarra-González, I., Fernández-Lainez, C., et al. (2022). Metabolic Reprogramming in Sars-Cov-2 Infection Impacts the Outcome of Covid-19 Patients [Original Research]. *Frontiers in Immunology, 13*. https://doi.org/10.3389/fimmu.2022.936106.

Matveeva, T., Khafizova, G., & Sokornova, S. (2020). In Search of Herbal Anti-Sars-Cov2 Compounds [Mini Review]. *Frontiers in Plant Science, 11*. https://doi.org/10.3389/fpls.2020.589998.

Maya, P. G., Mahayasih, W., Herman, H., & Ahmad, I. (2021). *In Silico* Identification of Natural Products from *Centella Asiatica* as Severe Acute Respiratory Syndromecoronavirus 2 Main Protease Inhibitor [Original Article]. *Journal of Advanced Pharmaceutical Technology & Research, 12*(3), 261-266. https://doi.org/10.4103/japtr.JAPTR_297_20.

Medthai. (2024). รายชื่อสมุนไพร. Medthai.com. Retrieved Feb 21, 2025 from https://medthai.com/.

Meng, J. R., Liu, J., Fu, L., et al. (2023). Anti-Entry Activity of Natural Flavonoids against Sars-Cov-2 by Targeting Spike Rbd. *Viruses, 15*(1). https://doi.org/10.3390/v15010160.

Middleton, E., Jr., Kandaswami, C., & Theoharides, T. C. (2000). The Effects of Plant Flavonoids on Mammalian Cells:Implications for Inflammation, Heart Disease, and Cancer. *Pharmacological Reviews, 52*(4), 673-751. https://doi.org/10.1016/S0031-6997(24)01472-8.

Minh, T. N., Xuan, T. D., Tran, H.-D., et al. (2019). Isolation and Purification of Bioactive Compounds from the Stem Bark of *Jatropha Podagrica*. *Molecules (Basel, Switzerland), 24*(5), 889. https://doi.org/10.3390/molecules24050889.

Miron, A., Aprotosoaie, A. C., Trifan, A., & Xiao, J. (2017). Flavonoids as Modulators of Metabolic Enzymes and Drug Transporters. *Annals of the New York Academy of Sciences, 1398*(1), 152-167. https://doi.org/https://doi.org/10.1111/nyas.13384.

Montenegro-Landívar, M. F., Tapia-Quirós, P., Vecino, X., et al. (2021). Polyphenols and Their Potential Role to Fight Viral Diseases: An Overview. *Science of The Total Environment, 801*, 149719. https://doi.org/https://doi.org/10.1016/j.scitotenv.2021.149719.

Morris, G. M., Huey, R., Lindstrom, W., et al. (2009). Autodock4 and Autodocktools4: Automated Docking with Selective Receptor Flexibility. *Journal of Computational Chemistry, 30*(16), 2785-2791. https://doi.org/10.1002/jcc.21256.

Morris, G. M., & Lim-Wilby, M. (2008). Molecular Docking. *Methods in Molecular Biology, 443*, 365-382. https://doi.org/10.1007/978-1-59745-177-2_19.

Mottaghipisheh, J., & Iriti, M. (2020). Sephadex(®) Lh-20, Isolation, and Purification of Flavonoids from Plant Species: A Comprehensive Review. *Molecules (Basel, Switzerland), 25*(18), 4146. https://doi.org/10.3390/molecules25184146.

Mukhtar, M., Arshad, M., Ahmad, M., et al. (2008). Antiviral Potentials of Medicinal Plants. *Virus Research, 131*(2), 111-120. https://doi.org/10.1016/j.virusres.2007.09.008.

Nainu, F., Abidin, R. S., Bahar, M. A., et al. (2020). Sars-Cov-2 Reinfection and Implications for Vaccine Development. *Human Vaccines & Immunotherapeutics, 16*(12), 3061-3073. https://doi.org/10.1080/21645515.2020.1830683.

Nair, M. S., Huang, Y., Fidock, D. A., et al. (2021). *Artemisia Annua* L. Extracts Inhibit the *in Vitro* Replication of Sars-Cov-2 and Two of Its Variants. *Journal of Ethnopharmacology, 274*, 114016. https://doi.org/10.1016/j.jep.2021.114016.

Nangare, S., Bhatane, D., Mali, R., & Shitole, M. (2021). Development of a Novel Freeze-Dried Mulberry Leaf Extract-Based Transfersome Gel. *Turkish Journal of Pharmaceutical Sciences, 18*(1), 44-55. https://doi.org/10.4274/tjps.galenos.2019.98624.

Nguyen, T. T. H., Jung, J.-H., Kim, M.-K., et al. (2021). The Inhibitory Effects of Plant Derivate Polyphenols on the Main Protease of Sars Coronavirus 2 and Their Structure–Activity Relationship. *Molecules, 26*(7), 1924. https://www.mdpi.com/1420-3049/26/7/1924.

Ni, L., Zhou, L., Zhou, M., Zhao, J., & Wang, D. W. (2020). Combination of Western Medicine and Chinese Traditional Patent Medicine in Treating a Family Case of Covid-19. *Frontiers of Medicine, 14*(2), 210-214. https://doi.org/10.1007/s11684-020-0757-x.

Nie, C., Trimpert, J., Moon, S., et al. (2021). *In Vitro* Efficacy of Artemisia Extracts against Sars-Cov-2. *Virology Journal, 18*(1), 182. https://doi.org/10.1186/s12985-021-01651-8.

NIH. (2022, 8 August 2022). Table 4d. Characteristics of Antiviral Agents. National Institutes of Health. Retrieved 7 September from https://www.covid19treatmentguidelines.nih.gov/tables/antiviral-characteristics/.

O'Boyle, N. M., Banck, M., James, C. A., et al. (2011). Open Babel: An Open Chemical Toolbox. *Journal of Cheminformatics, 3*(1), 33. https://doi.org/10.1186/1758-2946-3-33.

Orege, J. I., Adeyemi, S. B., Tiamiyu, B. B., et al. (2023). *Artemisia* and Artemisia-Based Products for Covid-19 Management: Current State and Future Perspective. *Advances in Traditional Medicine, 23*(1), 85-96. https://doi.org/10.1007/s13596-021-00576-5.

Orhan, I. E., & Senol Deniz, F. S. (2020). Natural Products as Potential Leads against Coronaviruses: Could They Be Encouraging Structural Models against Sars-Cov-2? *Natural Products and Bioprospecting, 10*(4), 171-186. https://doi.org/10.1007/s13659-020-00250-4.

Oteiza, P. I., Erlejman, A. G., Verstraeten, S. V., Keen, C. L., & Fraga, C. G. (2005). Flavonoid-Membrane Interactions: A Protective Role of Flavonoids at the

Membrane Surface? *Journal of Immunology Research, 12*(1), 592035. https://doi.org/https://doi.org/10.1080/10446670410001722168.

Paje, L. A., Choi, J., Lee, H.-D., et al. (2022). Phenolic Acids and Flavonoids from *Salvia Plebeia* and Hplc-Uv Profiling of Four *Salvia* Species. *Heliyon, 8*(3). https://doi.org/10.1016/j.heliyon.2022.e09046.

Paltiel, A. D., Schwartz, J. L., Zheng, A., & Walensky, R. P. (2021). Clinical Outcomes of a Covid-19 Vaccine: Implementation over Efficacy. *Health Aff (Millwood), 40*(1), 42-52. https://doi.org/10.1377/hlthaff.2020.02054.

Perera, W., Liyanage, J. A., Dissanayake, K. G. C., et al. (2021). Antiviral Potential of Selected Medicinal Herbs and Their Isolated Natural Products. *BioMed Research International, 2021*, 7872406. https://doi.org/10.1155/2021/7872406.

Portaccio, M., Faramarzi, B., & Lepore, M. (2023). Probing Biochemical Differences in Lipid Components of Human Cells by Means of Atr-Ftir Spectroscopy. *Biophysica, 3*(3), 524-538. https://www.mdpi.com/2673-4125/3/3/35.

Rabaan, A. A., Al-Ahmed, S. H., Garout, M. A., et al. (2021). Diverse Immunological Factors Influencing Pathogenesis in Patients with Covid-19: A Review on Viral Dissemination, Immunotherapeutic Options to Counter Cytokine Storm and Inflammatory Responses. *Pathogens, 10*(5). https://doi.org/10.3390/pathogens10050565.

Rafi, M. O., Bhattacharje, G., Al-Khafaji, K., et al. (2022). Combination of Qsar, Molecular Docking, Molecular Dynamic Simulation and Mm-Pbsa: Analogues of Lopinavir and Favipiravir as Potential Drug Candidates against Covid-19. *Journal of Biomolecular Structure and Dynamics, 40*(8), 3711-3730. https://doi.org/10.1080/07391102.2020.1850355.

Raghav, P. K., Mann, Z., Ahluwalia, S. K., & Rajalingam, R. (2023). Potential Treatments of Covid-19: Drug Repurposing and Therapeutic Interventions. *Journal of Pharmacological Sciences, 152*(1), 1-21. https://doi.org/https://doi.org/10.1016/j.jphs.2023.02.004.

Rakshit, G., Dagur, P., Satpathy, S., et al. (2022). Flavonoids as Potential Therapeutics against Novel Coronavirus Disease-2019 (Ncovid-19). *Journal of Biomolecular Structure and Dynamics, 40*(15), 6989-7001. https://doi.org/10.1080/07391102.2021.1892529.

Ramos-Casals, M., Brito-Zerón, P., & Mariette, X. (2021). Systemic and Organ-Specific Immune-Related Manifestations of Covid-19. *Nature Reviews Rheumatology, 17*(6), 315-332. https://doi.org/10.1038/s41584-021-00608-z.

Rattanamaneerusmee, A., Thirapanmethee, K., Nakamura, Y., Bongcheewin, B., & Chomnawang, M. T. (2018). Chemopreventive and Biological Activities of *Helicteres Isora* L. Fruit Extracts. *Research in Pharmaceutical Sciences, 13*(6), 484-492. https://doi.org/10.4103/1735-5362.245960.

Reçber, T., Timur, S. S., Erdoğan Kablan, S., et al. (2022). A Stability Indicating Rp-Hplc Method for Determination of the Covid-19 Drug Molnupiravir Applied Using Nanoformulations in Permeability Studies. *Journal of Pharmaceutical and Biomedical Analysis, 214*, 114693. https://doi.org/10.1016/j.jpba.2022.114693.

Reed, L. J., & Muench, H. (1938). A Simple Method of Estimating Fifty Per Cent Endpoints. *American Journal of Epidemiology, 27*(3), 493-497. https://doi.org/10.1093/oxfordjournals.aje.a118408 (American Journal of Epidemiology).

Rehman, S. u., Shafique, L., Ihsan, A., & Liu, Q. (2020). Evolutionary Trajectory for the Emergence of Novel Coronavirus Sars-Cov-2. *Pathogens, 9*(3), 240. https://www.mdpi.com/2076-0817/9/3/240.

Riihinen, K. R., Gödecke, T., & Pauli, G. F. (2012). Purification of Berry Flavonol Glycosides by Long-Bed Gel Permeation Chromatography. *Journal of Chromatography A, 1244*, 20-27. https://doi.org/10.1016/j.chroma.2012.04.060.

Rizzuti, B., Grande, F., Conforti, F., et al. (2021). Rutin Is a Low Micromolar Inhibitor of Sars-Cov-2 Main Protease 3clpro: Implications for Drug Design of Quercetin Analogs. *Biomedicines, 9*(4). https://doi.org/10.3390/biomedicines9040375.

Rodrigues, L., Bento Cunha, R., Vassilevskaia, T., Viveiros, M., & Cunha, C. (2022). Drug Repurposing for Covid-19: A Review and a Novel Strategy to Identify New Targets and Potential Drug Candidates. *Molecules, 27*(9). https://doi.org/10.3390/molecules27092723.

Ruan, J., Yan, J., Zheng, D., et al. (2019). Comprehensive Chemical Profiling in the Ethanol Extract of *Pluchea Indica* Aerial Parts by Liquid Chromatography/Mass Spectrometry Analysis of Its Silica Gel Column Chromatography Fractions. *Molecules, 24*(15), 2784. https://doi.org/10.3390/molecules24152784.

Rudrapal, M., Khairnar, S. J., Khan, J., et al. (2022). Dietary Polyphenols and Their Role in Oxidative Stress-Induced Human Diseases: Insights into Protective Effects, Antioxidant Potentials and Mechanism(S) of Action. *Frontiers in Pharmacology, 13*, 806470. https://doi.org/10.3389/fphar.2022.806470.

Sa-ngiamsuntorn, K., Suksatu, A., Pewkliang, Y., et al. (2021). Anti-Sars-Cov-2 Activity of *Andrographis Paniculata* Extract and Its Major Component Andrographolide in Human Lung Epithelial Cells and Cytotoxicity Evaluation in Major Organ Cell Representatives. *Journal of Natural Products, 84*, 1261-1270. https://doi.org/10.1021/acs.jnatprod.0c01324.

Scudellari, M. (2021). How the Coronavirus Infects Cells - and Why Delta Is So Dangerous. *Nature, 595*(7869), 640-644. https://doi.org/10.1038/d41586-021-02039-y.

Shahzad, A., Liu, W., Sun, Y., et al. (2024). Flavonoids as Modulators of Metabolic Reprogramming in Renal Cell Carcinoma (Review). *Oncology Reports, 52*(6), 167. https://doi.org/10.3892/or.2024.8826.

Sher, E. K., Ćosović, A., Džidić-Krivić, A., et al. (2023). Covid-19 a Triggering Factor of Autoimmune and Multi-Inflammatory Diseases. *Life Sciences, 319*, 121531. https://doi.org/https://doi.org/10.1016/j.lfs.2023.121531.

Şimşek Yavuz, S., & Ünal, S. (2020). Antiviral Treatment of Covid-19. *Turkish Journal of Medical Sciences, 50*(Si-1), 611-619. https://doi.org/10.3906/sag-2004-145.

Sindhuphak, R., Issaravanich, S., Udomprasertgul, V., et al. (2003). A New Approach for the Detection of Cervical Cancer in Thai Women. *Gynecologic Oncology, 90*(1), 10-14. https://doi.org/https://doi.org/10.1016/S0090-8258(03)00196-3.

Singh, G., Jorgenson, J., Pringle, T., Nelson, T., & Ramamoorthy, S. (2021). Monitoring Sars-Cov-2 Decontamination by Dry Heat and Ultraviolet Treatment with a Swine Coronavirus as a Surrogate. *Infection Prevention in Practice, 3*(1), 100103. https://doi.org/https://doi.org/10.1016/j.infpip.2020.100103.

SLRI. (2023). Beamline 4.1: Ir Spectroscopy and Imaging. Synchrotron Light Research Institute (Public Organization), THAILAND. Retrieved 7 July 2024 from https://irbeamline.wixsite.com/home.

Solnier, J., & Fladerer, J.-P. (2021). Flavonoids: A Complementary Approach to Conventional Therapy of Covid-19? *Phytochemistry Reviews, 20*(4), 773-795. https://doi.org/10.1007/s11101-020-09720-6.

Soltane, R., Chrouda, A., Mostafa, A., et al. (2021). Strong Inhibitory Activity and Action Modes of Synthetic Maslinic Acid Derivative on Highly Pathogenic Coronaviruses: Covid-19 Drug Candidate. *Pathogens, 10*(5), 623. https://doi.org/10.3390/pathogens10050623.

Song, Y., Singh, P., Nelson, E., & Ramamoorthy, S. (2016). A Computationally Designed Serological Assay for Porcine Epidemic Diarrhea Virus. *Journal of Clinical Microbiology, 54*(8), 2039-2046. https://doi.org/10.1128/jcm.00460-16.

Sopjani, M., Falco, F., Impellitteri, F., et al. (2024). Flavonoids Derived from Medicinal Plants as a Covid-19 Treatment. *Phytotherapy Research, 38*(3), 1589-1609. https://doi.org/https://doi.org/10.1002/ptr.8123.

Sornpet, B., Potha, T., Tragoolpua, Y., & Pringproa, K. (2017). Antiviral Activity of Five Asian Medicinal Pant Crude Extracts against Highly Pathogenic H5n1 Avian Influenza Virus. *Asian Pacific Journal of Tropical Medicine, 10*(9), 871-876.

Stefaniu, A. (2019). Introductory Chapter: Molecular Docking and Molecular Dynamics Techniques to Achieve Rational Drug Design. In S. Amalia (Ed.), *Molecular Docking and Molecular Dynamics* (pp. Ch. 1). IntechOpen. https://doi.org/ 10.5772/intechopen.84200.

Su, M., Shi, D., Xing, X., et al. (2021). Coronavirus Porcine Epidemic Diarrhea Virus Nucleocapsid Protein Interacts with P53 to Induce Cell Cycle Arrest in S-Phase and Promotes Viral Replication. *Journal of Virology, 95*(16), e00187-00121. https://doi.org/doi:10.1128/JVI.00187-21.

Sulé-Suso, J., Skingsley, D., Sockalingum, G. D., et al. (2005). Ft-Ir Microspectroscopy as a Tool to Assess Lung Cancer Cells Response to Chemotherapy. *Vibrational Spectroscopy, 38*(1), 179-184. https://doi.org/https://doi.org/ 10.1016/j. vibspec.2005.02.010.

Sumbria, D., Berber, E., Mathayan, M., & Rouse, B. T. (2020). Virus Infections and Host Metabolism-Can We Manage the Interactions? *Frontiers in Immunology, 11*, 594963. https://doi.org/10.3389/fimmu.2020.594963.

Tabari, K., Amin, M., Iranpanah, A., Bahramsoltani, R., & Rahimi, R. (2021). Flavonoids as Promising Antiviral Agents against Sars-Cov-2 Infection: A Mechanistic Review. *Molecules, 26*(13), 3900. https://www.mdpi.com/1420-3049/26/13/3900.

Tang, J., Dunshea, F. R., & Suleria, H. A. R. (2020). Lc-Esi-Qtof/Ms Characterization of Phenolic Compounds from Medicinal Plants (Hops and Juniper Berries) and Their Antioxidant Activity. *Foods, 9*(7). https://doi.org/10.3390/foods9010007.

Tang, S., Wang, B., Liu, X., et al. (2025). Structural Insights and Biological Activities of Flavonoids: Implications for Novel Applications. *Food Frontiers, 6*(1), 218-247. https://doi.org/https://doi.org/10.1002/fft2.494.

Tanveer, A., Akhtar, B., Sharif, A., et al. (2022). Pathogenic Role of Cytokines in Covid-19, Its Association with Contributing Co-Morbidities and Possible Therapeutic Regimens. *Inflammopharmacology, 30*(5), 1503-1516. https://doi.org/10.1007/s10787-022-01040-9.

Tanwettiyanont, J., Piriyachananusorn, N., Sangsoi, L., et al. (2022). Use of *Andrographis Paniculata* (Burm.F.) Wall. Ex Nees and Risk of Pneumonia in Hospitalised Patients with Mild Coronavirus Disease 2019: A Retrospective Cohort Study [Original Research]. *Frontiers in Medicine, 9*. https://doi.org/10.3389/fmed.2022.947373.

Trougakos, I. P., Stamatelopoulos, K., Terpos, E., et al. (2021). Insights to Sars-Cov-2 Life Cycle, Pathophysiology, and Rationalized Treatments That Target Covid-19 Clinical Complications. *Journal of Biomedical Science, 28*(1), 9. https://doi.org/10.1186/s12929-020-00703-5.

Tsiambas, E., Chrysovergis, A., Papanikolaou, V., et al. (2021). Impact of Ribosome Activity on Sars-Cov-2 Lnp – Based Mrna Vaccines [Mini Review]. *Frontiers in Molecular Biosciences, 8*. https://doi.org/10.3389/fmolb.2021.654866.

Verma, S., Twilley, D., Esmear, T., et al. (2020). Anti-Sars-Cov Natural Products with the Potential to Inhibit Sars-Cov-2 (Covid-19) [Review]. *Frontiers in Pharmacology, 11*(1514). https://doi.org/10.3389/fphar.2020.561334.

Vichaivej-Nongkhaem. (2022). ยารักษาโควิด-19 แยกตามอาการหรือกลุ่มสี โรงพยาบาลวิชัยเวช อินเตอร์เนชั่นแนล หนองแขม. Retrieved 7 กันยายน 2565 from https://vichaivej-nongkhaem.com/health-info/.

Vincent, S., Arokiyaraj, S., Saravanan, M., & Dhanraj, M. (2020). Molecular Docking Studies on the Anti-Viral Effects of Compounds from Kabasura Kudineer on Sars-Cov-2 $3cl^{pro}$ [Original Research]. *Frontiers in Molecular Biosciences, 7*, 613401. https://doi.org/10.3389/fmolb.2020.613401.

Vlietinck, A. J., Pieters, L. A. C., & Vander Berghe, D. A. (1995). Chapter 6-Bioassay-Guided Isolation and Structure Elucidation of Pharmacologically Active Plant Substances. In J. T. Arnason, R. Mata, & J. T. Romeo (Eds.), *Phytochemistry of Medicinal Plants* (pp. 113-135). Springer US. https://doi.org/10.1007/978-1-4899-1778-2_6.

Walkowiak-Bródka, A., Pieku**Ś**-Słomka, N., Wnuk, K., & Kupcewicz, B. (2022). Analysis of White Mulberry Leaves and Dietary Supplements, Atr-Ftir Combined with Chemometrics for the Rapid Determination of 1-Deoxynojirimycin. *Nutrients, 14*(24). https://doi.org/10.3390/nu14245276.

Wanaratna, K., Leethong, P., Inchai, N., et al. (2022). Efficacy and Safety of Andrographis Paniculata Extract in Patients with Mild Covid-19: A Randomized Controlled Trial. *Archives of Internal Medicine Research, 5*, 423-427.

Wang, S., Sakhatskyy, P., Chou, T.-H. W., & Lu, S. (2005). Assays for the Assessment of Neutralizing Antibody Activities against Severe Acute Respiratory Syndrome (Sars) Associated Coronavirus (Scv). *Journal of immunological methods, 301*(1-2), 21-30. https://doi.org/10.1016/j.jim.2005.03.008.

Wei, J., & Hui, A. (2022). Review of Ribosome Interactions with Sars-Cov-2 and Covid-19 Mrna Vaccine. *Life (Basel), 12*(1). https://doi.org/10.3390/life12010057.

Whitehead, C. L., & Walker, S. P. (2020). Consider Pregnancy in Covid-19 Therapeutic Drug and Vaccine Trials. *The Lancet, 395*(10237), e92. https://doi.org/https://doi.org/10.1016/S0140-6736(20)31029-1.

WHO. (2025a). Coronavirus Disease (Covid-19) Pandemic: Overview. Retrieved 5 January from https://www.who.int/europe/emergencies/situations/covid-19.

WHO. (2025b). Who Coronavirus Dashboard. World Health Organization. Retrieved 29 December 2024 from https://data.who.int/dashboards/covid19/deaths.

Widyawaruyanti, A., Asrory M, Ekasari W, et al. (2014). *In Vivo* Antimalarial Activity of *Andrographis Paniculata* Tablets. *Procedia Chemistry, 13*, 101-104.

Wongsa, P., Phatikulrungsun, P., & Prathumthong, S. (2022). Ft-Ir Characteristics, Phenolic Profiles and Inhibitory Potential against Digestive Enzymes of 25 Herbal Infusions. *Scientific Reports, 12*(1), 6631. https://doi.org/10.1038/s41598-022-10669-z.

Wu, B.-B., Gong, Y.-P., Wu, X.-H., et al. (2015). Fourier Transform Infrared Spectroscopy for the Distinction of Mcf-7 Cells Treated with Different Concentrations of 5-Fluorouracil. *Journal of Translational Medicine, 13*(1), 108. https://doi.org/10.1186/s12967-015-0468-2.

Wu, Y. C., Chen, C. S., & Chan, Y. J. (2020). The Outbreak of Covid-19: An Overview. *Journal of the Chinese Medical Association, 83*(3), 217-220. https://doi.org/10.1097/jcma.0000000000000270.

Xu, Y., Bai, L., Yang, X., et al. (2024). Recent Advances in Anti-Inflammation Via Ampk Activation. *Heliyon, 10*(13), e33670. https://doi.org/https://doi.org/10.1016/j.heliyon.2024.e33670.

Xu, Z., Peng, C., Shi, Y., et al. (2020). Nelfinavir Was Predicted to Be a Potential Inhibitor of 2019-Ncov Main Protease by an Integrative Approach Combining Homology Modelling, Molecular Docking and Binding Free Energy Calculation. *bioRxiv*, 2020.2001.2027.921627. https://doi.org/10.1101/2020.01.27.921627.

Ye, X. T., Luo, Y. L., Xia, S. C., et al. (2020). Clinical Efficacy of Lopinavir/Ritonavir in the Treatment of Coronavirus Disease 2019. *European Review for Medical and Pharmacological Sciences, 24*(6), 3390-3396. https://doi.org/10.26355/eurrev_202003_20706.

Zhang, L., Lin, D., Sun, X., et al. (2020). Crystal Structure of Sars-Cov-2 Main Protease Provides a Basis for Design of Improved A-Ketoamide Inhibitors. *Science, 368*(6489), 409-412. https://doi.org/doi:10.1126/science.abb3405.

Zhu, N., Zhang, D., Wang, W., et al. (2020). A Novel Coronavirus from Patients with Pneumonia in China, 2019. *New England Journal of Medicine, 382*(8), 727-733. https://doi.org/10.1056/NEJMoa2001017.

Zolkefali, P. T. M. Z. b., & Noh, C. H. C. (2017). Algorithm for Rapid Identification of Flavonoids Classes. *International Food Research Journal, 24*, S410-S415. http://www.myjurnal.my/public/article-view.php?id=111440.

คณะเภสัชศาสตร์มหาวิทยาลัยมหิดล. (2025). [อุทยานธรรมชาติวิทยาสิรีรุกขชาติ]. Retrieved Feb 23, 2025 from www.pharmacy.mahidol.ac.th/siri/.

คณะเภสัชศาสตร์มหาวิทยาลัยอุบลราชธานี. (2025). ฐานข้อมูลเครื่องยาไทย Retrieved Feb 23, 2025 from https://phar.ubu.ac.th/herb-DetailThaicrudedrug/.

APPENDIX

APPENDIX

ADDITIONAL FIGURES AND TABLES

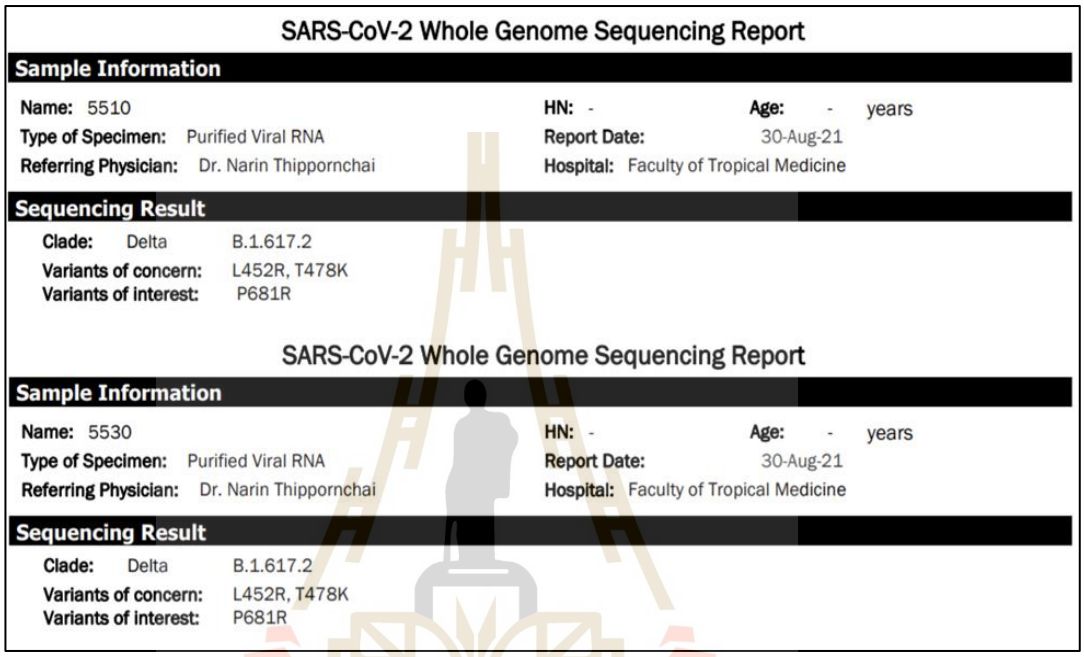

SARS-CoV-2 Whole Genome Sequencing Report

Sample Information

Name: 5510 **HN:** - **Age:** - years
Type of Specimen: Purified Viral RNA **Report Date:** 30-Aug-21
Referring Physician: Dr. Narin Thippornchai **Hospital:** Faculty of Tropical Medicine

Sequencing Result

Clade: Delta B.1.617.2
Variants of concern: L452R, T478K
Variants of interest: P681R

SARS-CoV-2 Whole Genome Sequencing Report

Sample Information

Name: 5530 **HN:** - **Age:** - years
Type of Specimen: Purified Viral RNA **Report Date:** 30-Aug-21
Referring Physician: Dr. Narin Thippornchai **Hospital:** Faculty of Tropical Medicine

Sequencing Result

Clade: Delta B.1.617.2
Variants of concern: L452R, T478K
Variants of interest: P681R

Figure A1 The SARS-CoV-2 strain results from whole genome sequencing of two samples, no. 5510 and 5530. The samples were collected from COVID-19 patients at the Tropical Diseases Reference Laboratory, Faculty of Tropical Medicine, Mahidol University. Both samples were identified as the B.1.617.2 strain, also known as the Delta variant, which was widely circulated in Thailand.

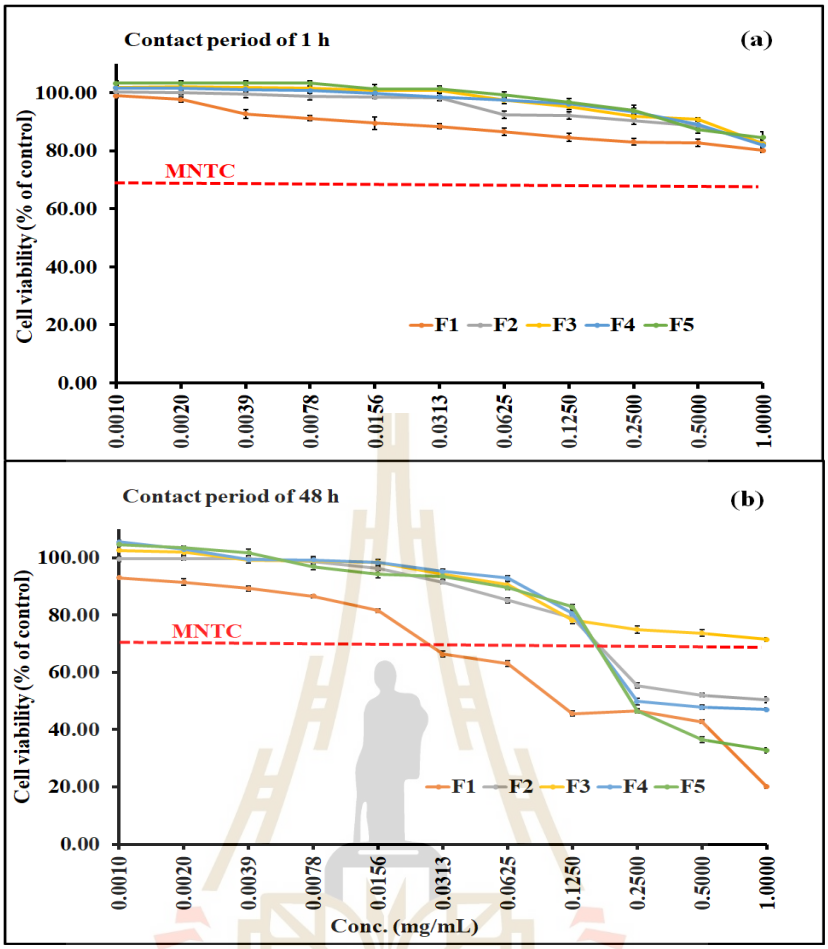

Figure A2 Cytotoxicity of the five fractions from WF-MLCE column chromatography, assessed on Vero E6 cells using the MTT assay. Results are presented as % cell viability (mean ± SD). (a) Cytotoxicity after a 1-h contact period and (b) cytotoxicity after a 48-h contact period. The red dotted line indicates the minimum non-toxic concentration (MNTC), defined as 70% cell viability for each crude extract.

Table A1 Review of traditional herbal candidates for potential COVID-19 therapeutic agent screening.

Scientific Name	Common name	Traditional & Modern Medical Applications
Colubrina asiatica (L.) Brongn.	Khan Song	-Used for fever, detoxification, skin irritation, and pain relief. - Anti-inflammatory, supports immune function, potential antimicrobial properties. - **Traditional Formulation**: Root is often mixed with *Tiliacora triandra* and *Sauropus androgynus* in fever remedies.
Morus alba Linn.	-Mulberry -Mon	- Used for fever, sore throat, flu, and antioxidant effects. - Anti-diabetic, regulates blood sugar, supports cardiovascular health. - **Traditional Formulation**: Dried leaves brewed as tea for sore throat and cooling effect.
Gynostemma pentaphyllum (Thunb) Makino	Jiaogulan	-Anti-aging, immune modulation, bronchitis treatment. - Regulates cholesterol, potential anti-cancer and hepatoprotective effects. - **Active Compounds**: Saponins. - **Traditional Formulation**: Brewed into tea for longevity and detoxification.
Artemisia annua L.	Sweet Wormwood, Kot Chula Lampha	- Used for malaria, fever, asthma, and respiratory diseases. - **Modern Use**: Contains artemisinin, widely used as an anti-malarial drug; investigated for antiviral properties against SARS-CoV-2. - **Active Compounds**: Flavonoids, Artemisinin. - **Traditional Formulation**: Found in at least 13 Thai traditional medicine formulations for fever and lung infections.

Table A1 (Continued)

Scientific Name	Common name	Traditional & Modern Medical Applications
Centella asiatica (L.)	Gotu Kola, Bua bok	- Used for headache, stress relief, fever, and wound healing - Enhances cognitive function, promotes skin repair, neuroprotective and anti-inflammatory properties. - **Active Compounds**: Triterpenoids. - **Traditional Formulation**: Combined with *Pluchea indica* and *Aegle marmelos* in herbal detox remedies.
Justicia gendarussa Burm.f.	San Phra Mon	- Fever relief, antibacterial, anti-inflammatory, pain relief - Found to inhibit HIV protease enzyme; antiviral potential - **Active Compounds**: Flavonoids (Vitexin, Apigenin), Juaticin.
Helicteres isora L.	Indian Screw Tree, Po bid	- Used for fever, cough, diarrhea, and gastrointestinal disorders - Antiviral against hepatitis viruses; antimicrobial properties. - **Active Compounds**: Flavonoid (Isoscutellarein). - **Traditional Formulation**: Dried fruit included in digestive and respiratory tonic preparations
Phyllanthus niruri L.	Chanca Piedra, Look Tai Bai	- Used for fever, anti-inflammatory, and liver protection - Antiviral activity against Hepatitis B (HBV); supports liver detoxification. - **Traditional Formulation**: Common in Thai herbal mixtures for jaundice treatment

Table A1 (Continued)

Scientific Name	Common name	Traditional & modern medical applications and biological properties
Oldenlandia corymbosa L.	Ya Lin Ngu	- Used for fever, malaria, anti-inflammatory, antimicrobial - Investigated for anti-cancer properties and immunomodulatory effects. - **Traditional Formulation**: Boiled with *Andrographis paniculata* for fever relief.
Garcinia atroviridis	Asam Gelugur, Som Khaek	- Used for cough, expectorant, blood pressure regulation. - Hydroxycitric Acid (HCA) aids in weight loss and metabolism regulation. - **Active Compounds**: Hydroxycitric Acid (HCA). - **Traditional Formulation**: Dried fruit commonly brewed into tea for weight loss.
Canna indica L.	Indian Shot, Phutha Raksa	- Used for tuberculosis, cough, and hepatitis treatment. - Hepatoprotective properties; anti-inflammatory effects. - **Traditional Formulation**: Rhizome sometimes combined with *Curcuma longa* for liver health.
Acanthus ebracteatus Vahl	Ngueak Pla Mo	- Anti-cancer, immune booster, fever relief. - Found to exhibit cytotoxic effects against cancer cells; anti-inflammatory. - **Active Compounds**: Carotenoids, Hexadecenoic Acid, Sterols. - **Traditional Formulation**: Used with *Zingiber officinale* for immune enhancement.

Table A1 (Continued)

Scientific Name	Common name	Traditional & modern medical applications and biological properties
Clinacanthus nutans (Burm.f) Lindua	Snake Grass, Phaya Plong Thong	- Used for fever, sore throat, anti-inflammatory, herpes treatment. - Antiviral against herpes simplex virus (HSV-1). - **Active Compounds**: Betulin, Lupeol, Flavonoids. - **Traditional Formulation**: Applied as a fresh leaf poultice for skin infections and herpes sores.
Momordica charantia L.	Bitter Melon, Mara Kee Nok	- Anti-diabetic, anti-cancer, fever relief. - Contains compounds that lower blood sugar -Potential HIV-inhibitory effects. - **Active Compounds**: Charantin, Polypeptide-p. - **Traditional Formulation**: Often included in herbal formulations for diabetes management.
Hymenocallis littoralis (Jacq.) Salisb.	Spider Lily, Plub Plueng Tin Pade	- Used for mucus expulsion, wound healing, postpartum recovery. - Contains lycorine, known for its antiviral properties (including inhibition of poliovirus and measles virus). - **Active Compounds**: Lycorine. - **Traditional Formulation**: Leaves roasted and applied to bruises; bulbs boiled for postpartum care.

Table A2 Information on plants utilized in this research includes their assigned voucher specimen numbers (TTM no.), and used plant parts for extraction and harvesting areas.

Sample Code	Scientific name [part of use]	Common Thai name	TTM no.	Harvesting area
S1	*Colubrina asiatica* (L.) Brongn. [leaves]	Khan song	0005480	Nakhon Ratchasima
S2	*Morus alba* Linn. [leaves]	Mon	0005481	Nakhon Ratchasima
S3	*Gynostemma pentaphyllum* (Thunb) Makino [leaves]	Jiaogulan	0005482	Chiang Mai
S4	*Artemisia annua* L. [leaves]	Kot chula lampha	0005483	Kanchanaburi
S5	*Centella asiatica* (L.) [leaves]	Bua bok	0005484	Mahasarakham
S6	*Justicia gendarussa* Burm.f. [leaves and stems]	San phra mon	1000745	Sing Buri
S7	*Helicteres isora* L. [fruits]	Po bid	0005485	Nakhonpathom
S8	*Phyllanthus niruri* L. [leaves, fruits, and stems]	Lok tai bai	0005486	Burirum
S9	*Orthosiphon aristatus* [leaves and stem]	Ya nuat maew	0005487	Nakhonpathom
S10	*Oldenlandia corymbosa* L. [leaves, flowers, and stems]	Ya lin ngu	0005488	Chai Nat
S11	*Garcinia atroviridis* [leaves]	Som khaek	0005489	Nakhonpathom
S12	*Canna indica* L. [stems]	Phutha raksa	1000746	Sing Buri
S13	*Euphorbia thymifolia* L. [leaves and stems]	Nam nom ratchasi lek	0005490	Nakhon ratchasima

Table A2 (continued).

Sample Code	Scientific name [part of use]	Common Thai name	TTM no.	Harvesting area
S14	*Acanthus ebracteatus* Vahl [leaves and stems]	Ngueak pla mo	1000747	Sing Buri
S15	*Clinacanthus nutans* (Burm.f) Lindua [leaves and stems]	Phaya plong thong	1000748	Sing Buri
S16	*Jatropha integerrima* [flowers]	Pattawia	0005491	Nakhon ratchasima
S17	*Jatropha integerrima* [leaves]	Pattawia	0005491	Nakhon ratchasima
S18	*Jatropha integerrima* [stems]	Pattawia	0005491	Nakhon ratchasima
S19	*Punica granatum* L. [leaves]	Thapthim	0005492	Nakhon ratchasima
S20	*Momordica charantia* L. [fruits]	Mara kee nok	0005493	Nakhon ratchasima
S21	*Hymenocallis littoralis* (Jacq.) Salisb. [Root]	Plub plueng tin pade	0005494	Nakhon ratchasima
S22	*Hymenocallis littoralis* (Jacq.) Salisb [Leaves]	Plub plueng tin pade	0005494	Nakhon ratchasima

A1. Calculation of anti-SARS-CoV-2 efficacy and percentage of viral reduction

In this study, the anti-SARS-CoV-2 activity of the extracts was quantified as efficacy (percentage of viral reduction) and log reduction value (LRV), with their relationship shown in Table A2.

Table A3 Relationship between LRV and % viral reduction, as an expression of antiviral efficacy.

Number of viruses (TCID50/ml)	Log reduction	Efficacy/ % viral reduction
100,000 (10^5)	0 log (Log0)	0%
10,000 (10^4)	1 log (Log1)	90%
1,000 (10^3)	2 log (Log2)	99%
100 (10^2)	3 log (Log3)	99.9%
10 (10)	4 log (Log4)	99.99%
1 (1)	5 log (Log5)	99.999%

Equations:

$$\text{Efficacy or \% viral reduction} = \frac{(A-B)\times 100}{A}$$

$$\text{Log Reduction Value} = \log_{10} A - \log_{10} B$$

where A = The starting viral titer subjected to the test

B = The remaining viral number after testing

Example of calculation

The starting viral number for the pre-entry study was 100,000 TCID50/mL. After testing, the remaining viral number was 100 TCID50/mL.

$$\text{Efficacy or \% Reduction} = \frac{(100{,}0000-100)\text{x } 100}{100{,}000}$$

= 99.9%

Log Reduction $= \log_{10} 100{,}000 - \log_{10} 100$

= 3 Log reduction (or LRV = 3)

Table A4 FTIR spectral band assignment for water fraction of mulberry-leaf crude extract (Abbas et al., 2017; Hssaini et al., 2022; Krysa et al., 2022; Wongsa et al., 2022; Zolkefali & Noh, 2017).

Region	Wave number (cm^{-1})	Functional group assignment	Possible predicted phytochemical class
1	3500-3000 (broaden)	H-bonded, O-H, N-H	alcohols, polyphenolics, carbohydrates
2	3000-2800	C-H of CH_2 & CH_3	polysaccharides, fatty acids, lipids
3	1750-1650	C=O of carboxylic group	lipids, phenolics
	1650-1550 (distinct) &1500-1455 (small	C=C-C and C-H of aromatic rings	flavonoids
4	1500-1150	O-H deformation, C-O, C=C of phenols	flavonoids (flavonols), phenols
	1499-1452	-C-OH and C-H of aromatic rings	Flavonoids (flavones & flavonols), phenolics
	1450-1200	O-H deformation of aromatic rings	flavonoids, phenolics
5	1100-1075	C-H & C-H out-of-plane of Ring B-flavonoids	flavonoids
	1041 (distinct) & 1103 (small)	C-O of aromatic rings, C-O-C of heterocyclic ring, O-H in-plane	phenolics saccharides/ carbohydrates

Table A4 (continued).

Region	Wave number (cm^{-1})	Functional group assignment	Possible predicted phytochemical class
5 (continued).	990 (distinct)	C-H out-of-plane of pyranosyl rings	sugars (if appeared with peaks at 1140-1120, suggested the sugar molecules conjugated with aromatic structure)
	925	C-H & C-H out-of-plane of Ring B-flavonoids	flavonoids
6	800-400	C-C-O deformation, C-C-C of aromatics, C-H deformation of polyphenols	flavonoids

Table A5 LC–HRMS analysis of tentative phytochemical contents of Fraction 2 (F2) fractionated of WF-MLCE (S2-WF).

No.	Tentative phytochemical	Formula	Theoretical MW	Reference ion	Average Peak Area (Most Common Adduct)
1	Trigonelline	$C_7H_7NO_2$	137.04768	$[M+H]^+$	3.95E+09
2	γ-Aminobutyric acid (GABA)	$C_4H_9NO_2$	103.06333	$[M+H]^+$	1.95E+09
3	L-Norleucine	$C_6H_{13}NO_2$	131.09463	$[M+H]^+$	1.06E+09
4	L-Glutamic acid	$C_5H_9NO_4$	147.05316	$[M+H]^+$	9.28E+08
5	Proline	$C_5H_9NO_2$	115.06333	$[M+H]^+$	9.05E+08
6	Prolylleucine	$C_{11}H_{20}N_2O_3$	228.14739	$[M+H]^+$	8.46E+08
7	Isoleucine	$C_6H_{13}NO_2$	131.09463	$[M+H]^+$	5.86E+08
8	Valine	$C_5H_{11}NO_2$	117.07898	$[M+H]^+$	5.42E+08
9	1-deoxymannojirimycin or 1-deoxynorijimycin	$C_6H_{13}NO_4$	163.08446	$[M+H]^+$	4.70E+08
10	Pantothenic acid	$C_9H_{17}NO_5$	219.11067	$[M-H]^-$	4.17E+08
11	DL-Carnitine	$C_7H_{15}NO_3$	161.10519	$[M+H]^+$	3.29E+08
12	3-Methoxybenzaldehyde	$C_8H_8O_2$	136.05243	$[M+H]^+$	2.66E+08
13	D-(-)-Glutamine	$C_5H_{10}N_2O_3$	146.06914	$[M+H]^+$	2.50E+08

Table A5 (continued). Fraction 2

No.	Tentative phytochemical	Formula	Theoretical MW	Reference ion	Average Peak Area (Most Common Adduct)
14	Asparagine	$C_4H_8N_2O_3$	132.05349	$[M+H]^+$	2.48E+08
15	Acetylcholine	$C_7H_{15}NO_2$	145.11028	$[M+H]^+$	2.10E+08
16	DL-Stachydrine	$C_7H_{13}NO_2$	143.09463	$[M+H]^+$	1.88E+08
17	D-(-)-Quinic acid	$C_7H_{12}O_6$	192.06339	$[M+H]^+$	1.77E+08
18	D-(+)-Pyroglutamic Acid	$C_5H_7NO_3$	129.04259	$[M+H]^+$	1.73E+08
19	Nicotinic acid	$C_6H_5NO_2$	123.03203	$[M+H]^+$	1.70E+08
20	L-Threonine	$C_4H_9NO_3$	119.05824	$[M+H]^+$	1.65E+08
21	Muramic acid	$C_9H_{17}NO_7$	251.1005	$[M+H]^+$	1.39E+08
22	Acetyl-L-carnitine	$C_9H_{17}NO_4$	203.11576	$[M+H]^+$	1.12E+08
23	N-Acetylornithine	$C_7H_{14}N_2O_3$	174.10044	[M+H]+	8.37E+07
24	3,8,9-trihydroxy-10-propyl-3,4,5,8,9,10-hexahydro-2H-oxecin-2-one	$C_{12}H_{20}O_5$	244.1311	$[M-H]^-$	9.29E+07
25	4-Hydroxybenzaldehyde	$C_7H_6O_2$	122.0368	$[M+H]^+$	6.93E+07

Table A5 (continued) Fraction 2.

No.	Tentative phytochemical	Formula	Theoretical MW	Reference ion	Average Peak Area (Most Common Adduct)
26	N-Acetylneuraminic acid	$C_{11}H_{19}NO_9$	309.1060	$[M+H]^+$	6.56E+07
27	(-)-Caryophyllene oxide	$C_{15}H_{24}O$	220.1827	$[M+H]^+$	5.17E+07
28	Apocynin	$C_9H_{10}O_3$	166.0630	$[M+H]^+$	4.11E+07
29	Salsolinol	$C_{10}H_{13}NO_2$	179.0946	$[M+H]^+$	3.72E+07
30	L-Phenylalanine	$C_9H_{11}NO_2$	165.0790	$[M+H]^+$	3.52E+07
31	Sinapinic acid	$C_{11}H_{12}O_5$	224.0685	$[M-H]^-$	2.25E+07
32	4-Hydroxy-3-(3-methyl-2-buten-1-yl) phenyl 6-O-[(2R,3R,4R)-3,4-dihydroxy-4-(hydroxymethyl)tetrahydro-2-furanyl]-beta-D-glucopyranoside	$C_{22}H_{32}O_{11}$	472.1945	$[M-H]^-$	1.99E+07
33	5-O-Caffeoylquinic acid (Chlorogenic acid isomer)	$C_{16}H_{18}O_9$	354.0951	$[M-H]^-$	1.49E+07
34	3-[3-(beta-D-Glucopyranosyloxy)-2-hydroxyphenyl] propanoic acid	$C_{15}H_{20}O_9$	344.1107	$[M-H]^-$	1.07E+07

Table A5 (continued). Fraction 2

No.	Tentative phytochemical	Formula	Theoretical MW	Reference ion	Average Peak Area (Most Common Adduct)
35	Coumarin	$C_9H_6O_2$	146.0368	$[M+H]^+$	1.84E+07
36	4-Coumaric acid	$C_9H_8O_3$	164.0473	$[M+H]^+$	1.43E+07
37	L-Tyrosine	$C_9H_{11}NO_3$	181.0739	$[M+H]^+$	1.29E+07
38	α-Aspartylphenylalanine	$C_{13}H_{16}N_2O_5$	280.1059	$[M+H]^+$	1.10E+07
39	3-[3-(beta-D-Glucopyranosyloxy)-2-methoxyphenyl] propanoic acid	$C_{16}H_{22}O_9$	358.1264	$[M-H]^-$	5.99E+06
40	4-O-Caffeoylquinic acid (Chlorogenic acid isomer)	$C_{16}H_{18}O_9$	354.0951	$[M-H]^-$	3.81E+06
41	4-(beta-D-Glucopyranosyloxy)-2-methylenebutanoic acid	$C_{11}H_{18}O_8$	278.1002	$[M-H]^-$	2.91E+06
42	Gentisic acid 5-O-β-D-glucoside	$C_{13}H_{16}O_9$	316.0794	$[M-H]^-$	2.77E+06
43	D-(-)-Salicin	$C_{13}H_{18}O_7$	286.1053	$[M-H]^-$	1.52E+06

Table A6 LC–HRMS analysis of tentative phytochemical contents of Fraction 3 (F3) fractionated of WF-MLCE (S2-WF).

No.	Tentative phytochemical	Formula	Theoretical MW	Reference ion	Average Peak Area (Most Common Adduct)
1	Trigonelline	$C_7H_7NO_2$	137.0477	$[M+H]^+$	6.91E+09
2	L-Norleucine	$C_6H_{13}NO_2$	131.0946	$[M+H]^+$	2.43E+09
3	Pipecolic acid	$C_6H_{11}NO_2$	129.0790	$[M+H]^+$	2.12E+09
4	3,8,9-trihydroxy-10-propyl-3,4,5,8,9,10-hexahydro-2H-oxecin-2-one (isomer 1)	$C_{12}H_{20}O_5$	244.1311	$[M-H]^-$	1.71E+09
5	Proline	$C_5H_9NO_2$	115.0633	$[M+H]^+$	1.56E+09
6	Gentisic acid 5-O-β-D-glucoside (isomer 1)	$C_{13}H_{16}O_9$	316.0794	$[M-H]^-$	1.06E+09
7	1-deoxymannojirimycin or 1-deoxynorijimycin	$C_6H_{13}NO_4$	163.0845	$[M+H]^+$	9.21E+08
8	4-Guanidinobutyric acid	$C_5H_{11}N_3O_2$	145.0851	$[M+H]^+$	8.48E+08
9	L-Valine	$C_5H_{11}NO_2$	117.0790	$[M+H]^+$	8.44E+08
10	3,8,9-trihydroxy-10-propyl-3,4,5,8,9,10-hexahydro-2H-oxecin-2-one (isomer 2)	$C_{12}H_{20}O_5$	244.1311	$[M-H]^-$	6.88E+08
11	Gentisic acid 5-O-β-D-glucoside (isomer 2)	$C_{13}H_{16}O_9$	316.0794	$[M-H]^-$	4.93E+08

Table A6 (continued) Fraction 3

No.	Tentative phytochemical	Formula	Theoretical MW	Reference ion	Average Peak Area (Most Common Adduct)
12	Nicotinic acid	$C_6H_5NO_2$	123.0320	$[M+H]^+$	4.57E+08
13	3-[3-(beta-D-Glucopyranosyloxy)-2-hydroxyphenyl] propanoic acid (isomer 1)	$C_{15}H_{20}O_9$	344.1107	$[M-H]^-$	3.85E+08
14	Tropine	$C_8H_{15}NO$	141.1154	$[M+H]^+$	3.53E+08
15	4-Hydroxybenzaldehyde	$C_7H_6O_2$	122.0368	$[M+H]^+$	3.42E+08
16	DL-Stachydrine	$C_7H_{13}NO_2$	143.0946	$[M+H]^+$	2.85E+08
17	Prolylleucine	$C_{11}H_{20}N_2O_3$	228.1474	$[M+H]^+$	2.82E+08
18	Nicotinic acid	$C_6H_5NO_2$	123.0320	$[M+H]^+$	2.51E+08
19	Pantothenic acid	$C_9H_{17}NO_5$	219.1107	$[M-H]^-$	2.33E+08
20	5-hydroxy-4-methoxy-5,6-dihydro-2H-pyran-2-one	C6H8O4	144.0423	[M+H]+	1.85E+08
21	DL-Carnitine	$C_7H_{15}NO_3$	161.1052	$[M+H]^+$	1.12E+08
22	4-(4-hydroxy-2,6,6-trimethyl-3-([(2R,3R,4S,5S,6R)-3,4,5-trihydroxy-6-(hydroxymethyl)oxan-2-yl]oxy) cyclohex-1-en-1-yl) butan-2-one (isomer 1)	$C_{19}H_{32}O_8$	388.2097	$[M+H]^+$	1.03E+08

Table A6 (continued) Fraction 3

No.	Tentative phytochemical	Formula	Theoretical MW	Reference ion	Average Peak Area (Most Common Adduct)
23	Threonine	$C_4 H_9 N O_3$	119.0582	$[M+H]^+$	7.46E+07
24	N-Acetylornithine	$C_7 H_{14} N_2 O_3$	174.1004	$[M+H]^+$	6.43E+07
25	3-[3-(beta-D-Glucopyranosyloxy)-2-hydroxyphenyl] propanoic acid (isomer 2)	$C_{15} H_{20} O_9$	344.1107	$[M-H]^-$	5.62E+07
26	(-)-Caryophyllene oxide (isomer 1)	$C_{15}H_{24}O$	220.1827	$[M+H]^+$	4.70E+07
27	Gentisic acid 5-O-β-D-glucoside (isomer 3)	$C_{13}H_{16}O_9$	316.0794	$[M-H]^-$	4.61E+07
28	(-)-Caryophyllene oxide (isomer 2)	$C_{15}H_{24}O$	220.1827	$[M+H]^+$	3.98E+07
29	N-Acetyl-DL-tryptophan	$C_{13}H_{14}N_2O_3$	246.1004	$[M-H]^-$	3.84E+07
30	3-[3-(beta-D-Glucopyranosyloxy)-2-methoxyphenyl] propanoic acid (isomer 3)	$C_{16}H_{22}O_9$	358.1264	$[M-H]^-$	3.75E+07
31	Gentisic acid 5-O-β-D-glucoside (isomer 4)	$C_{13}H_{16}O_9$	316.0794	$[M-H]^-$	3.21E+07
32	2-Hexyl-3-methylenesuccinic acid	$C_{11}H_{18}O_4$	214.1205	$[M+H]^+$	3.06E+07
33	Sinapinic acid	$C_{11}H_{12}O_5$	224.0685	$[M+H]^+$	2.88E+07

Table A6 (continued) Fraction 3

No.	Tentative phytochemical	Formula	Theoretical MW	Reference ion	Average Peak Area (Most Common Adduct)
34	4-(4-hydroxy-2,6,6-trimethyl-3-([(2R,3R,4S,5S,6R)-3,4,5-trihydroxy-6-(hydroxymethyl) oxan-2-yl] oxy) cyclohex-1-en-1-yl) butan-2-one (isomer 2)	$C_{19}H_{32}O_8$	388.2097	$[M+H]^+$	2.67E+07
35	3-[3-(beta-D-Glucopyranosyloxy)-2-hydroxyphenyl] propanoic acid (isomer 4)	$C_{15}H_{20}O_9$	344.1107	$[M-H]^-$	2.57E+07
36	NP-008952	$C_{12}H_{20}O_4$	228.1362	$[M+H]^+$	2.26E+07
37	Coumarin	$C_9H_6O_2$	146.0368	$[M+H]^+$	2.01E+07
38	4'-Methoxyacetophenone	$C_9H_{10}O_2$	150.0681	$[M+H]^+$	1.95E+07
39	Curcolonol	$C_{15}H_{20}O_4$	264.1362	$[M+H]^+$	1.84E+07
40	7-Hydroxycoumarine	$C_9H_6O_3$	162.0317	$[M+H]^+$	1.74E+07
41	Chlorogenic acid	$C_{16}H_{18}O_9$	354.0951	$[M+H]^+$	1.58E+07
42	4-Coumaric acid	$C_9H_8O_3$	164.0473	$[M+H]^+$	1.46E+07
43	dihydrophaseic acid	$C_{15}H_{22}O_5$	282.1467	$[M-H]^-$	1.31E+07

Table A6 (continued) Fraction 3

No.	Tentative phytochemical	Formula	Theoretical MW	Reference ion	Average Peak Area (Most Common Adduct)
44	((1S,5R,9R,13R)-1,5,9-trimethyl-11,14,15,16-tetraoxatetracyclo [10.3.1.04,13.08,13] hexadecan-10-one or epi-Artemisinin	$C_{15}H_{22}O_5$	282.1467	$[M+H]^+$	1.14E+07
45	Thapsic acid	$C_{16}H_{30}O_4$	286.2144	$[M+H]^+$	1.05E+07
46	Jasmone	$C_{11}H_{16}O$	164.1201	$[M+H]^+$	1.04E+07
47	(1aR,1bR,2R,3R,7R,7aS)-1b,2-dimethyl-7a-(prop-1-en-2-yl)-1aH,1bH,2H,3H,4H,5H,7H,7aH-naphtho[1,2-b] oxirene-3,7-diol	$C_{15}H_{22}O_3$	250.1569	$[M+H]^+$	9.87E+06
48	L-Tyrosine	$C_9H_{11}NO_3$	181.0739	$[M+H]^+$	9.82E+06
49	4-oxododecanedioic acid	$C_{12}H_{20}O_5$	244.1311	$[M+H]^+$	9.35E+06
50	2-Hydroxy-2-methyl-3-buten-1-yl beta-D-glucopyranoside	$C_{11}H_{20}O_7$	264.1209	$[M-H]^-$	8.70E+06
51	Verrucarol	$C_{15}H_{22}O_4$	266.1518	$[M+H]^+$	8.52E+06
52	5-(6-hydroxy-6-methyloctyl)-2,5-dihydrofuran-2-one	$C_{13}H_{22}O_3$	226.1569	$[M+H]^+$	8.07E+06

Table A6 (continued) Fraction 3

No.	Tentative phytochemical	Formula	Theoretical MW	Reference ion	Average Peak Area (Most Common Adduct)
53	Sinapinic acid	$C_{11}H_{12}O_5$	224.0685	$[M-H]^-$	7.76E+06
54	6-Pentyl-2H-pyran-2-one	$C_{10}H_{14}O_2$	166.0994	$[M+H]^+$	7.76E+06
55	12-oxo Phytodienoic Acid	$C_{18}H_{28}O_3$	292.2038	$[M+H]^+$	7.66E+06
56	(1r,3R,4s,5S)-4-([(2E)-3-(3,4-dihydroxyphenyl) prop-2-enoyl] oxy)-1,3,5-trihydroxycyclohexane-1-carboxylic acid	$C_{16}H_{18}O_9$	354.0951	$[M+H]^+$	7.24E+06
57	(1S,3R,4S,5R)-3,5-bis(([(2E)-3-(3,4-dihydroxyphenyl) prop-2-enoyl]oxy))-1,4-dihydroxycyclohexane-1-carboxylic acid	$C_{25}H_{24}O_{12}$	516.1268	$[M+H]^+$	6.75E+06
58	4-O-Caffeoylquinic acid (Chlorogenic acid isomer)	$C_{16}H_{18}O_9$	354.0951	$[M-H]^-$	6.64E+06
59	Coumarin	$C_9H_6O_2$	146.0368	$[M+H]^+$	6.58E+06

Table A6 (continued) Fraction 3

No.	Tentative phytochemical	Formula	Theoretical MW	Reference ion	Average Peak Area (Most Common Adduct)
60	(4S)-4-hydroxy-3,5,5-trimethyl-4-[(1E)-3-([(2R,3R,4S,5S,6R)-3,4,5-trihydroxy-6-(hydroxymethyl) oxan-2-yl] oxy) but-1-en-1-yl] cyclohex-2-en-1-one	$C_{19}H_{30}O_8$	386.1941	$[M+H]^+$	5.83E+06
61	alpha-D-Glucopyranosyl 2-O-(2-methylbutanoyl)-alpha-D-glucopyranoside	$C_{17}H_{30}O_{12}$	426.1737	$[M-H]^-$	5.70E+06
62	Syringic acid	$C_9H_{10}O_5$	198.0528	$[M-H]^-$	4.72E+06
63	D-(-)-Salicin	$C_{13}H_{18}O_7$	286.1053	$[M-H]^-$	4.53E+06

Table A7 LC–HRMS analysis of tentative phytochemical contents of Fraction 4 (F4) fractionated of WF-MLCE (S2-WF).

No.	Tentative phytochemical	Formula	Theoretical MW	Reference ion	Average Peak Area (Most Common Adduct)
1	*trans*-5-O-Caffeoylquinic acid (Chlorogenic acid isomer)	$C_{16}H_{18}O_9$	354.0951	$[M+H]^+$	6.80E+09
2	*cis*-3-O-Caffeoylquinic acid (Chlorogenic acid isomer)	$C_{16}H_{18}O_9$	354.0951	$[M-H]^-$	5.57E+09
3	Gentisic acid 5-O-β-D-glucoside (isomer **1**)	$C_{13}H_{16}O_9$	316.0794	$[M-H]^-$	5.39E+09
4	*cis*-4-O-Caffeoylquinic acid (Chlorogenic acid isomer)	$C_{16}H_{18}O_9$	354.0951	$[M-H]^-$	4.88E+09
5	Trigonelline	$C_7H_7NO_2$	137.0477	$[M+H]^+$	4.03E+09
6	*cis*-5-O-Caffeoylquinic acid (Chlorogenic acid isomer)	$C_{16}H_{18}O_9$	354.0951	$[M-H]^-$	2.09E+09
7	Gentisic acid 5-O-β-D-glucoside (isomer **2**)	$C_{13}H_{16}O_9$	316.0794	$[M-H]^-$	1.07E+09
8	Proline	$C_5H_9NO_2$	122.0368	$[M+H]^+$	1.03E+09
9	1-deoxymannojirimycin	$C_6H_{13}NO_4$	115.0633	$[M+H]^+$	1.00E+09
10	4-Hydroxybenzaldehyde	$C_7H_6O_2$	163.0845	$[M+H]^+$	9.76E+08
11	3-([(2R,3S,4S,5R,6S)-6-([2-(3,4-dihydroxyphenyl)-5,7-dihydroxy-4-oxo-4H-chromen-3-yl] ox)-3,4,5-trihydroxyoxan-2-yl] methoxy)-3-oxopropanoic acid	$C_{24}H_{22}O_{15}$	550.0959	$[M+H]^+$	8.33E+08

Table A7 (continued) Fraction 4

No.	Tentative phytochemical	Formula	Theoretical MW	Reference ion	Average Peak Area (Most Common Adduct)
12	4-Guanidinobutyric acid	$C_5H_{11}N_3O_2$	135.0545	$[M+H]^+$	7.07E+08
13	Uridine	$C_9H_{12}N_2O_6$	316.0794	$[M-H]^-$	6.97E+08
14	Adenine	$C_5H_5N_5$	145.0851	$[M+H]^+$	6.80E+08
15	Gentisic acid 5-O-β-D-glucoside (isomer 3)	$C_{13}H_{16}O_9$	244.0695	$[M-H]^-$	6.03E+08
16	*trans*-4-O-Caffeoylquinic acid (Chlorogenic acid isomer)	$C_{16}H_{18}O_9$	354.0951	$[M-H]^-$	5.66E+08
17	7-Hydroxycoumarine	$C_9H_6O_3$	162.0317	$[M+H]^+$	4.37E+08
18	*trans*-3-O-Caffeoylquinic acid (Chlorogenic acid isomer)	$C_{16}H_{18}O_9$	354.0951	$[M-H]^-$	4.22E+08
19	12-oxo Phytodienoic Acid	$C_{18}H_{28}O_3$	292.2038	$[M+H]^+$	4.19E+08
20	Scopoletin	$C_{10}H_8O_4$	192.0423	$[M+H]^+$	3.25E+08
21	Caffeic acid	$C_9H_8O_4$	180.0423	$[M+H]^+$	2.93E+08
22	Esculetin	$C_9H_6O_4$	178.0266	$[M+H]^+$	2.48E+08

Table A7 (continued) Fraction 4.

No.	Tentative phytochemical	Formula	Theoretical MW	Reference ion	Average Peak Area (Most Common Adduct)
23	4-(4-hydroxy-2,6,6-trimethyl-3-([(2R,3R,4S,5S,6R)-3,4,5-trihydroxy-6-(hydroxymethyl) oxan-2-yl]oxy) cyclohex-1-en-1-yl) butan-2-one	$C_{19}H_{32}O_8$	164.0473	$[M+H]^+$	2.27E+08
24	2-Hydroxycinnamic acid	$C_9H_8O_3$	354.0951	$[M+H]^+$	2.01E+08
25	(1S,3R,4R,5R)-1,3,4-trihydroxy-5-([(2E)-3-(4-hydroxy-3-methoxyphenyl) prop-2-enoyl]oxy) cyclohexane-1-carboxylic acid	$C_{17}H_{20}O_9$	368.1107	$[M-H]^-$	1.85E+08
26	(1r,3R,4s,5S)-4-([(2E)-3-(3,4-dihydroxyphenyl) prop-2-enoyl]oxy)-1,3,5-trihydroxycyclohexane-1-carboxylic acid	$C_{16}H_{18}O_9$	388.2097	$[M+H]^+$	1.82E+08
27	5-hydroxy-4-methoxy-5,6-dihydro-2H-pyran-2-one	$C_6H_8O_4$	144.0423	$[M+H]^+$	1.43E+08
28	Nicotinic acid	$C_6H_5NO_2$	123.0320	$[M+H]^+$	1.37E+08
29	Dodecanedioic acid	$C_{12}H_{22}O_4$	230.1518	$[M-H]^-$	1.27E+08
30	Esculin	$C_{15}H_{16}O_9$	340.0794	$[M-H]^-$	1.26E+08

Table A7 (continued) Fraction 4

No.	Tentative phytochemical	Formula	Theoretical MW	Reference ion	Average Peak Area (Most Common Adduct)
31	Apocynin	$C_9H_{10}O_3$	166.0630	$[M+H]^+$	1.08E+08
32	2-Hydroxyphenylalanine	$C_9H_{11}NO_3$	181.0739	$[M+H]^+$	1.03E+08
33	Coumarin	$C_9H_6O_2$	146.0368	$[M+H]^+$	1.01E+08
34	2-Methoxybenzaldehyde	$C_8H_8O_2$	368.1107	$[M+H]^+$	8.52E+07
35	(4S)-4-hydroxy-3,5,5-trimethyl-4-[(1E)-3-([(2R,3R,4S,5S,6R)-3,4,5-trihydroxy-6-(hydroxymethyl) oxan-2-yl]oxy)but-1-en-1-yl]cyclohex-2-en-1-one	$C_{19}H_{30}O_8$	136.0524	$[M+H]^+$	8.51E+07
36	2-(4-Hydroxyphenyl) ethyl 6-O-[(2R,3R,4R)-3,4-dihydroxy-4-(hydroxymethyl) tetrahydro-2-furanyl]-beta-D-glucopyranoside	$C_{19}H_{28}O_{11}$	204.0899	$[M-H]^-$	8.25E+07
37	(1S,3R,4R,5R)-1,3,4-trihydroxy-5-([(2E)-3-(4-hydroxy-3-methoxyphenyl) prop-2-enoyl] oxy}cyclohexane-1-carboxylic acid	$C_{17}H_{20}O_9$	386.1941	$[M+H]^+$	7.58E+07

Table A7 (continued) Fraction 4.

No.	Tentative phytochemical	Formula	Theoretical MW	Reference ion	Average Peak Area (Most Common Adduct)
38	DL-Tryptophan	$C_{11}H_{12}N_2O_2$	432.1632	$[M-H]^-$	7.34E+07
39	5,7-dihydroxy-2-(3-hydroxy-4-([(2S,3R,4S,5S,6R)-3,4,5-trihydroxy-6-(hydroxymethyl) oxan-2-yl]oxy) phenyl)-4H-chromen-4-one	$C_{21}H_{20}O_{11}$	448.1006	$[M+H]^+$	7.23E+07
40	2,3-Dihydroxybenzoic acid	$C_7H_6O_4$	902.2692	$[M+H]^+$	6.20E+07
41	(-)-Caryophyllene oxide	$C_{15}H_{24}O$	150.1045	$[M+H]^+$	5.98E+07
42	L-(-)-Carvone	$C_{10}H_{14}O$	154.0266	$[M+H]^+$	5.95E+07
43	7-([(2S,3R,4S,5S,6R)-4,5-dihydroxy-6-(hydroxymethyl)-3-([(2S,3R,4R,5R,6S)-3,4,5-trihydroxy-6-methyloxan-2-yl]oxy)oxan-2-yl]oxy)-5-hydroxy-2-(4-hydroxyphenyl)-3-([(2S,3R,4S,5S,6R)-3,4,5-trihydroxy-6-(([(2R,3R,4R,5R,6S)-3,4,5-trihydroxy-6-methyloxan-2-yl]oxy)methyl)oxan-2-yl]oxy)-4H-chromen-4-one	$C_{39}H_{50}O_{24}$	154.0266	$[M+H]^+$	6.82E+07

Table A7 (continued) Fraction 4.

No.	Tentative phytochemical	Formula	Theoretical MW	Reference ion	Average Peak Area (Most Common Adduct)
44	3-([(2R,3S,4S,5R,6S)-6-([2-(3,4-dihydroxyphenyl)-5,7-dihydroxy-4-oxo-4H-chromen-3-yl]oxy)-3,4,5-trihydroxyoxan-2-yl]methoxy)-3-oxopropanoic acid	$C_{24}H_{22}O_{15}$	220.1827	$[M+H]^+$	5.85E+07
45	2,4-Dihydroxybenzoic acid	$C_7H_6O_4$	550.0959	$[M+H]^+$	5.62E+07
46	5-O-(4-coumaroyl)-D-quinic acid (isomer 1)	$C_{16}H_{18}O_8$	358.1264	$[M-H]^-$	5.07E+07
47	5-O-(4-coumaroyl)-D-quinic acid (isomer 2)	$C_{16}H_{18}O_8$	338.1002	$[M-H]^-$	4.88E+07
48	3-[3-(beta-D-Glucopyranosyloxy)-2-methoxyphenyl]propanoic acid	$C_{16}H_{22}O_9$	338.1002	$[M-H]^-$	4.57E+07
49	3-[3-(beta-D-Glucopyranosyloxy)-2-hydroxyphenyl]propanoic acid	$C_{15}H_{20}O_9$	344.1107	$[M-H]^-$	3.66E+07
50	(1S,3R,4R,5R)-1,3,4-trihydroxy-5-([(2E)-3-(4-hydroxy-3-methoxyphenyl)prop-2-enoyl]oxy)cyclohexane-1-carboxylic acid	$C_{17}H_{20}O_9$	368.1107	$[M-H]^-$	3.03E+07
51	N-Acetyl-DL-tryptophan	$C_{13}H_{14}N_2O_3$	368.1107	$[M-H]^-$	2.60E+07
52	Riboflavin	$C_{17}H_{20}N_4O_6$	246.1004	$[M-H]^-$	2.59E+07

Table A7 (continued) Fraction 4.

No.	Tentative phytochemical	Formula	Theoretical MW	Reference ion	Average Peak Area (Most Common Adduct)
53	1,3,5-trihydroxy-4-([(2E)-3-(3-hydroxy-4-methoxyphenyl)prop-2-enoyl]oxy)cyclohexane-1-carboxylic acid	$C_{17}H_{20}O_9$	286.1053	$[M-H]^-$	2.58E+07
54	D-(-)-Salicin	$C_{13}H_{18}O_7$	376.1383	$[M-H]^-$	2.31E+07
55	Benzyl 6-O-beta-D-glucopyranosyl-beta-D-glucopyranoside	$C_{19}H_{28}O_{11}$	432.1632	$[M-H]^-$	2.29E+07
56	(±)-Abscisic acid	$C_{15}H_{20}O_4$	264.1362	$[M-H]^-$	1.35E+07
57	D-(-)-Salicin	$C_{13}H_{18}O_7$	286.1053	$[M-H]^-$	1.27E+07
58	5-Hydroxytryptophan	$C_{11}H_{12}N_2O_3$	220.0848	$[M-H]^-$	9.43E+06
59	2-(4-Hydroxyphenyl)ethyl 6-O-[(2R,3R,4R)-3,4-dihydroxy-4-(hydroxymethyl)tetrahydro-2-furanyl]-beta-D-glucopyranoside	$C_{19}H_{28}O_{11}$	432.1632	$[M-H]^-$	6.84E+06
60	1,3,5-trihydroxy-4-([(2E)-3-(3-hydroxy-4-methoxyphenyl)prop-2-enoyl]oxy) cyclohexane-1-carboxylic acid	$C_{17}H_{20}O_9$	368.1107	$[M-H]^-$	5.20E+06

Table A8 Polyphenol contents and antioxidant activities of the fractions obtained from column chromatography of WF-MLCE.

Fraction	TPC (mg GAE/g)	TFC (mg QE/g)	FRAP value		$DPPH^{\bullet}$ scavenging activity		$ABTS^{\bullet+}$ scavenging activity	
			μmol TE/g	μmol $Fe2^{+}$/g	μmol TE/g	EC_{50} (mg/mL)	μmol TE/g	EC_{50} (mg/mL)
F1	16.90^{c} ± 0.74	54.50^{c} ± 5.56	43.48^{c} ± 2.11	79.40^{c} ± 3.91	33.11^{c} ± 3.48	5.45^{b} ± 0.26	131.03^{c} ± 5.53	2.91^{b} ± 0.30
F2	6.73^{d} ± 0.70	8.20^{d} ± 1.22	24.23^{c} ± 1.63	44.38^{c} ± 3.02	12.24^{d} ± 0.65	9.45^{c} ± 1.49	53.97^{c} ± 3.54	7.51^{c} ± 0.99
F3	8.53^{cd} ± 0.78	11.28^{d} ± 1.23	39.81^{c} ± 3.62	72.79^{c} ± 6.70	22.29^{cd} ± 2.21	6.81^{b} ± 1.21	83.90^{c} ± 9.76	6.07^{c} ± 0.81
F4	76.88^{b} ± 9.16	131.45^{b} ± 9.81	399.64^{b} ± 23.35	730.79^{b} ± 43.11	259.49^{b} ± 22.95	0.54^{a} ± 0.08	640.24^{b} ± 5.75	0.67^{a} ± 0.08
F5	158.10^{a} ± 12.08	565.88^{a} ± 19.71	1269.38^{a} ± 179.24	2322.42^{a} ± 323.25	532.58^{a} ± 18.90	0.23^{a} ± 0.02	2475.63^{a} ± 182.40	0.13^{a} ± 0.03

Results are expressed as mean ± SD on a dry weight basis in triplicate experiment. The values with significant differences ($p \leq 0.05$) are indicated within the same column by
different superscript letters. F1-F5, Fraction 1-5; TPC, total phenolic content; TFC, total flavonoid content; FRAP, ferric reducing antioxidant power assay; EC50, effective
concentration that performed 50% antioxidant activity; GAE, gallic acid equivalents; QE, quercetin equivalents; and TE, Trolox equivalents.

BIOGRAPHY

Miss Bussyarat Maikhunthod was born on December 17, 1977, in Nakhon Ratchasima, Thailand. She earned her Master of Science degree from the School of Food Technology, Suranaree University of Technology, Thailand, in 2004. She then pursued her Doctoral Degree in Biotechnology at the School of Biotechnology, Suranaree University of Technology, from 2019 to 2025, supported by a One Research One Graduate (OROG) scholarship from the university. Her research received additional funding from the Synchrotron Light Research Institute (Public Organization) and the National Research Council of Thailand (NTRC) (Project No. 109704). Part of her findings has been published in the BMC Complementary Medicine and Therapies journal (2024; 24:274, https://doi.org/10.1186/s12906-024-04586-z) under the title *"Exploring the Therapeutic Potential of Thai Medicinal Plants: In Vitro Screening and In Silico Docking of Phytoconstituents for Novel Anti-SARS-CoV-2 Agents"*. Additionally, she presented some of her research at the 8th SUT International Colloquium on Agricultural Technology at the Institute of Agricultural Technology, Suranaree University of Technology, Thailand, on February 7, 2025, under the title *"The Potential of Mulberry Leaf Extract as an Anti-SARS-CoV-2 Candidate: Anti-SARS-CoV-2 Efficacy and Mechanism of Action."*